

CHARLES UNIVERSITY

1st Faculty of Medicine

Department of Medical Biochemistry

The Role of Uncoupling in Down-regulation of Reactive Oxygen Species



DOCTORAL THESIS

Supervisors:

RNDr. Markéta Žáčková, Ph.D.

RNDr. Petr Ježek, DrSc.

Institute of Physiology ASCR

Author:

RNDr. Jan Ježek

PRAGUE 2009



ACKNOWLEDGMENTS

I would like to express my gratitude and appreciation to my supervisor, RNDr. Markéta Žáčková, Ph.D. and to my father RNDr. Petr Ježek, DrSc. A special thanks goes to my colleagues Mgr. Martin Jabůrek, Ph.D., Ing. Tomáš Špaček, RNDr. Lydie Plecítá-Hlavatá, Ph.D., and Ing. Andrea Dlasková, Ph.D. for their help and fruitful cooperation. Mitochondria were isolated with the excellent technical assistance of Jitka Smíková with the participation of Mgr. Michal Růžička, Ph.D. and RNDr. Miloš Nekvasil. Cell tissue culture was taken well care of by Lenka Josková. Many thanks to all, as well as to Mgr. Katarína Smolková, Mgr. Jitka Šantorová, Ph.D., Ludmila Šimečková, Jana Košařová, Mgr. Lukáš Alán, Ing. Jan Tabuer, and Ing. Jaroslav Zelenka, Ph.D., the great staff from the Department No. 75, Membrane Transport Biophysics. Thanks goes also to my ex-coworkers Jana Brucknerová, Mgr. Ludmila Tahotná, and Mgr. Kateřina Janouchová, we were all one team. The professional work of all the administration, human resources, animal house, and storeroom people, technicians, librarians, cooks, cleaners and security guards from the Institute of Physiology (www.biomed.cas.cz/fgu) and the associated institutes was highly acknowledged.

I certify that I worked out this doctoral thesis single-handedly under the supervision of RNDr. Markéta Žáčková, Ph.D. and RNDr. Petr Ježek, DrSc. and I certify that I have properly cited all used sources.

Prague, June 15, 2009

.....



LIST OF AUTHOR'S PUBLICATIONS

Plecitá-Hlavatá, L., Ježek, J., Ježek, P.: Pro-oxidant mitochondrial matrix-targeted ubiquinone MitoQ₁₀ acts as anti-oxidant at retarded electron transport or proton pumping within Complex I. *Int. J. Biochem. Cell Biol.* 41, 1697–1707 (2009)

<http://dx.doi.org/10.1016/j.biocel.2009.02.015> IF (2007) = **4.009**

Dlasková, A., Hlavatá, L., Ježek, J., Ježek, P.: Mitochondrial Complex I superoxide production is attenuated by uncoupling. *Int. J. Biochem. Cell Biol.* 40, 2098–2109 (2008)

<http://dx.doi.org/10.1016/j.biocel.2008.02.007> IF (2007) = **4.009**

Raju, N., Špaček, T., Ježek, J., Caminiti, I.M., Leinisch, F., Hideg, K., Ježek, P., Trommer, W.E.: Fatty acid binding site of mitochondrial uncoupling protein UCP2 as probed by EPR spectroscopy of spin-labeled fatty acids. *Appl. Magn. Reson.* 30, 373–383 (2006)

IF = 0.692

Ježek, P., Ježek, J.: Sequence anatomy of mitochondrial anion carriers. *FEBS Lett.* 534, 15–25 (2003) [http://dx.doi.org/10.1016/S0014-5793\(02\)03779-1](http://dx.doi.org/10.1016/S0014-5793(02)03779-1) IF = **3.609**

Total IF = 12.319

All publications are downloadable in PDF format from www.mitonet.cz free of charge.



ABBREVIATIONS

AACOCF ₃	arachidonyltrifluoromethyl ketone
ADP	adenosine 5'-diphosphate
Amplex Red	<i>N</i> -acetyl-3,7-dihydroxyphenoxazine
Anti	antimycin A
ATP	adenosine 5'-triphosphate
BAX	Bcl-2-associated X protein
BCA	2,2'-bicinchoninic acid
BCECF, AM	2',7'-bis-(2-carboxyethyl)-5-(and-6)-carboxyfluorescein, acetoxymethyl ester
BCIP/NBT	5-bromo-4-chloro-3-indolyl phosphate/nitro blue tetrazolium chloride
BEL	bromo-enol lactone
BLM	bilayer lipid membrane
BSA	bovine serum albumin
cAMP	adenosine-3',5'-cyclic monophosphate
CoQ	coenzyme Q (ubiquinone)
cPLA ₂	cytosolic phospholipase A ₂
CREB	cAMP response element-binding protein
Ctrl	control
CuZnSOD	copper-zinc superoxide dismutase
DecylTPP	decyltriphenylphosphonium bromide
DMEM	Dulbecco's modified Eagle's medium
DMSO	dimethyl sulfoxide
EDTA	ethylenediaminetetraacetic acid
EGTA	ethylene glycol-bis(2-aminoethylether)- <i>N,N,N',N'</i> -tetraacetic acid
EIPA	5-(<i>N</i> -ethyl- <i>N</i> -isopropyl)amiloride
EPR	electron paramagnetic resonance
ETF	electron-transfer flavoprotein
FA	fatty acid
FapyG	2,6-diamino-4-hydroxy-5-formamidopyrimidine
FCCP	carbonyl cyanide 4-(trifluoromethoxy)phenylhydrazone

FIH	factor inhibiting HIF
FMN	flavin mononucleotide
GAPDH	glyceraldehyde-3-phosphate dehydrogenase
GDP	guanosine 5'-diphosphate
GLC5	5 mM glucose-cultivated HepG2 cells
GLC25	25 mM glucose-cultivated HepG2 cells
GLUT	glucose transporter
GM	glutamate plus malate
GPX	glutathione peroxidase
GSH	reduced glutathione
GSIS	glucose-stimulated insulin secretion
GSSG	oxidized glutathione
GTP	guanosine 5'-triphosphate
HEPES	4-(2-hydroxyethyl)piperazine-1-ethanesulfonic acid
HepG2	human hepatocellular carcinoma cells
HIF	hypoxia-inducible factor
HNE	4-hydroxynonenal
HRE	hypoxia-responsive element
HRP	horseradish peroxidase
IGF	insulin-like growth factor
IMAC	inner membrane anion channel
IMS	intermembrane space
iNOS	inducible nitric oxide synthase
iPLA ₂	calcium-independent phospholipase A ₂
ISP	iron-sulfur protein (Fe-S protein)
αKGDH	α-ketoglutarate dehydrogenase
KP _i	potassium phosphate
Lac	lactate
LDHA	lactate dehydrogenase A
MACP	mitochondrial anion carrier protein
MAFP	methyl arachidonyl fluorophosphonate
MAO	monoamine oxidase
MAPK	mitogen-activated protein kinase

MCT4	plasma membrane monocarboxylate transporter 4
MELAS	mitochondrial encephalopathy lactic acidosis stroke-like episodes
MitoQ ₁₀	10-(6'-ubiquinonyl)decyltriphenylphosphonium methanesulfonate
MLuM	mouse lung mitochondria
MnSOD	manganese superoxide dismutase
MOPS	3-(<i>N</i> -morpholino)propanesulfonic acid
mtDNA	mitochondrial DNA
mtPLA ₂	mitochondrial phospholipase A ₂
Myxo	myxothiazol
NAD ⁺	β-nicotinamide adenine dinucleotide
NADH	reduced form of NAD ⁺
NCR	non-coding region
NOS	nitric oxide synthase
ODDD	O ₂ -dependent degradation domain
Oligo	oligomycin
OXPHOS	galactose/glutamine-cultivated HepG2 cells
PBS	phosphate buffered saline
PDGF	platelet-derived growth factor
PHD	prolyl hydroxylase domain enzyme
PI3K	phosphoinositide 3-kinase
PLA ₂	phospholipase A ₂
PMSF	phenylmethanesulfonyl fluoride
PTEN	phosphatase and tensin homolog
PUFA	polyunsaturated fatty acid
PUMP	plant uncoupling mitochondrial protein
PVDF	polyvinylidene fluoride
Q	coenzyme Q (ubiquinone)
Q-cycle	coenzyme Q cycle
Q-pool	quinone pool
Q-site	quinone-binding site
Ras/Raf/MAPK	Ras/Raf/mitogen-activated protein kinase pathway
RET	reverse electron transport
RLM	rat liver mitochondria

RLuM	rat lung mitochondria
RNS	reactive nitrogen species
ROS	reactive oxygen species
Rot	rotenone
RT-PCR	reverse transcription polymerase chain reaction
SDS-PAGE	sodium dodecyl sulfate polyacrylamide gel electrophoresis
SkQ1	10-(6'-plastoquinonyl)decyltriphenylphosphonium
sPLA ₂	secretory phospholipase A ₂
Stig	stigmatellin
Succ	succinate
SUMO	small ubiquitin-like modifier
TBHP	<i>tert</i> -butyl hydroperoxide
tBID	truncated BH3 interacting domain death agonist
Tris	2-amino-2-hydroxymethyl-1,3-propanediol
TTFA	2-thenoyltrifluoroacetone
UCP	uncoupling protein
UCP2-KO	UCP2 knockout mice
UCP2-WT	UCP2 wild-type mice
UV	ultraviolet
VDAC	voltage-dependent anion channel (or porin)
VHL	von Hippel-Landau tumor-suppressor protein

Remainder of ROS and RNS nomenclature

FAOOH	fatty acid hydroperoxide
H ₂ O ₂	hydrogen peroxide
HO ₂ [•]	hydroperoxyl radical
•NO	nitric oxide
O ₂ ^{•-}	superoxide
•OH	hydroxyl radical
ONOO ⁻	peroxynitrite
PLOOH	phospholipid hydroperoxide
PUFAOOH	polyunsaturated fatty acid hydroperoxide
RC [•] R	carbon-centered radical
RO [•]	alkoxyradical
ROO [•]	peroxyl radical

Notation for biophysical quantities







$\Delta\Psi_m$	membrane potential
Δp	proton motive force
ΔpH	pH gradient
$p\text{O}_2$	partial pressure of oxygen
















CONTENTS

1 INTRODUCTION 4

2 BACKGROUND 6

- 2.1  Mitochondria and Reactive Oxygen Species 6
- 2.2  NADH:ubiquinone Oxidoreductase 14
- 2.3  Mitochondrial Matrix-targeted Ubiquinone MitoQ₁₀ 18
- 2.4  Mitochondrial Phospholipase A₂ 21
- 2.5  Mitochondrial Uncoupling Protein 2 26
- 2.6  Physiological Hypoxia 28

3 MATERIALS AND METHODS 33

- 3.1  Isolation of Intact Mitochondria by Differential Centrifugation 33
 -  3.1.1 Isolation of Rat Liver Mitochondria 33
 -  3.1.2 Isolation of Mitochondria from Hepatocellular Carcinoma Cells 34
 -  3.1.3 Isolation of Rat Lung Mitochondria 34
 -  3.1.4 Isolation of Mouse Lung Mitochondria 35
- 3.2  Assay Media and Chemicals 35
- 3.3  Assay for Mitochondrial H₂O₂ Generation *In Vitro* 37
- 3.4  Assay for Polarographic Detection of Oxygen Consumption 38
 -  3.4.1 High-Resolution Respiration Measurements 38
 -  3.4.2 Respiration Measurements of Cells at Physiological Oxygen Levels 38
- 3.5  Assay for Complex I Proton Pumping 39
- 3.6  Cell Cultures 39
- 3.7  Statistical Analysis 40

4 **RESULTS 41**

4.1 **The Inhibition of Mitochondrial Complex I Proton Pumping 41**

4.1.1 EIPA Inhibits Complex I Proton Pumping in Isolated Rat Liver Mitochondria Respiring in State 4 **41**

4.1.2 EIPA Inhibits Complex I Proton Pumping in Isolated Rat Liver Mitochondria Respiring in State 3 **49**

4.1.3 EIPA Exerts No Significant Effects on Respiration of Isolated Rat Liver Mitochondria **50**

4.2 **The Mechanism of Action of Mitochondrial Matrix-targeted Ubiquinone MitoQ₁₀ 52**

4.2.1 MitoQ₁₀ Accelerates Respiration of HepG2 Cells **52**

4.2.2 Respiration Increase Induced by MitoQ₁₀ Requires Complexes II and III **61**

4.2.3 MitoQ₁₀ Effects on Total H₂O₂ Formation in Isolated Rat Liver Mitochondria **64**

4.2.4 MitoQ₁₀ Effects on Respiration of Mitochondria Isolated from HepG2 Cells **68**

4.3 **Mitochondrial Phospholipase iPLA₂-Dependent Regulation of Uncoupling Protein 2 70**

4.3.1 TBHP Induces Increase in Respiration of Isolated Rat Lung Mitochondria **70**

4.3.2 Mitochondrial iPLA₂ Promotes UCP2-dependent Uncoupling **72**

4.3.3 The Effect of TBHP and GDP on Lung Mitochondria Isolated from UCP2-WT and UCP2-KO Mice – the Effect is Absent in KO **77**

4.3.4 H₂O₂ Production Monitored with Amplex Red during TBHP-induced Oxidative Stress and its Acceleration by BEL **78**


4.4 **The Elevation of State 4 Respiration upon Adaptation to Physiological Normoxia 80**

4.4.1 Glycolytic Cells Reduce Respiration at 5% Oxygen in Parallel with Eliciting Less Efficient Oxidative Phosphorylation than OXPHOS Cells **80**

4.4.2 Glycolytic Normoglycemic Cells Adapt to 5% Oxygen by Elevated State 4 Respiration **86**

4.4.3 Dependence of Cellular Respiration Rate on Oxygen Concentration 86

5 DISCUSSION 88

5.1  Mechanism of Attenuation of Mitochondrial Complex I Superoxide Production by Uncoupling 88

5.2  Targeting of MitoQ₁₀-related Therapeutics to Oxidative Stress 93


5.3  The Role of Mitochondrial Phospholipases in Concert with Uncoupling in Feedback Down-regulation of Oxidative Stress 98

5.4  Implementation of Physiological Normoxia Conditions as a Real Experimental Model 102

6 SUMMARY OF FINDINGS 105

6.1  Characterization of a Novel Inhibitor of Proton Pumping by Mitochondrial Complex I 105

6.2  The Mechanism of Action of Mitochondrial Matrix-targeted Ubiquinone MitoQ₁₀ 106

6.3  Mitochondrial Phospholipase iPLA₂-Dependent Regulation of Uncoupling Protein 2 108

6.4  The Elevation of State 4 Respiration upon Adaptation to Physiological Normoxia 109

7 CONCLUSIONS 111

8 REFERENCES 112

1 INTRODUCTION





Mitochondria are essential organelles for eukaryotic aerobic metabolism, involving respiratory chain, citric acid cycle and β -oxidation pathways. The principal function of mitochondria is to generate energy by coupling respiration to the synthesis of ATP during a process called oxidative phosphorylation (average daily turnover of ATP in human body exceeds 50 kg), but they are also involved in apoptosis, thermogenesis, homeostasis of reactive oxygen species and calcium. Mitochondria participate in information signaling, aging, regulation of body weight, glucose sensing by pancreatic beta cells and oxygen sensing (nearly in all cells *via* hypoxia-inducible factor activated through prolyl hydroxylase inhibition by mitochondrial H_2O_2). No doubt mitochondria play a central role in molecular physiology of the cell and their dysfunction is implicated in numerous pathophysiological states: atherosclerosis, hypertension, ischemia-reperfusion injury, inflammation, cystic fibrosis, cancer, diabetes mellitus II, Parkinson's disease, Alzheimer's disease, and other neurodegenerative diseases.

Reactive oxygen species evolve as a by-product of oxidative metabolism, and mitochondria represent the major source of reactive oxygen species for the cell. Oxidative stress arises from surplus production of reactive oxygen species above the levels which are required for normal ROS homeostasis and signaling. As their name implies, reactive oxygen species readily attack ambient biomolecules including DNA, proteins, and lipids. In healthy cells, excessive harmful ROS are decomposed by protective antioxidant systems. Nevertheless, oxidative damage slowly but steadily accumulates over the years in a process known as aging, eventually resulting in a pathological condition.

The significance of mitochondrial uncoupling proteins (UCPs) lies in their ability to affect energetic status of mitochondria and as was shown in our laboratory, to attenuate mitochondrial production of reactive oxygen species even those generated by Complex I. Fatty acid hydroperoxides may be the key elements of ROS-sensing signal pathways, acting as cycling substrates of uncoupling proteins during the feedback inhibition of lipoperoxidation.

The purpose of this work was to study the relationship between the mechanisms of reactive oxygen species homeostasis and uncoupling in the context of mitochondrially related physiology and pathology.

The thesis encompasses four different selected aims in order to elucidate:

-  The Inhibition of Mitochondrial Complex I Proton Pumping
-  The Mechanism of Action of Mitochondrial Matrix-targeted Ubiquinone MitoQ₁₀
-  Mitochondrial Phospholipase iPLA₂-Dependent Regulation of Uncoupling Protein UCP2
-  The Elevation of State 4 Respiration upon Adaptation to Physiological Normoxia

The above color coding will be used throughout the text for better orientation.

2 BACKGROUND

2.1 Mitochondria and Reactive Oxygen Species

Reactive oxygen species (ROS) are an inevitable by-product of aerobic metabolism in living organisms. The major source of ROS in cells are ultimately mitochondria [4]. Complex I and Complex III of the mitochondrial respiratory chain (Fig. 1, page 7, Table 1) are considered by some authors to be the main sources of superoxide ($O_2^{\bullet-}$) and other downstream ROS in most cells [5–7]. *In vitro* assays have determined that up to 2% (it could be less *in vivo*) of oxygen consumed by the mitochondrial respiratory chain undergoes successive monoelectronic reduction by the quinonoid or flavonoid electron carriers leading to constitutive production of reactive intermediates with odd electrons, such as superoxide anion radicals $O_2^{\bullet-}$ (Eq. 1) [4, 8–9].



TABLE 1 Main sources of mitochondrially-located superoxide production.^a

Enzyme	location	orientation
Complex I	inner membrane	matrix
Complex II	inner membrane	matrix
Complex III	inner membrane	matrix and IMS
Dihydroorotate dehydrogenase	matrix	matrix
Electron-transfer flavoprotein	matrix	matrix
ETF:ubiquinone oxidoreductase	matrix	matrix
Glycerol-3-phosphate dehydrogenase	inner membrane	intermembrane space
α -Ketoglutarate dehydrogenase	matrix	matrix
Monoamine oxidase	outer membrane	intermembrane space

^aCompiled from [4, 10].

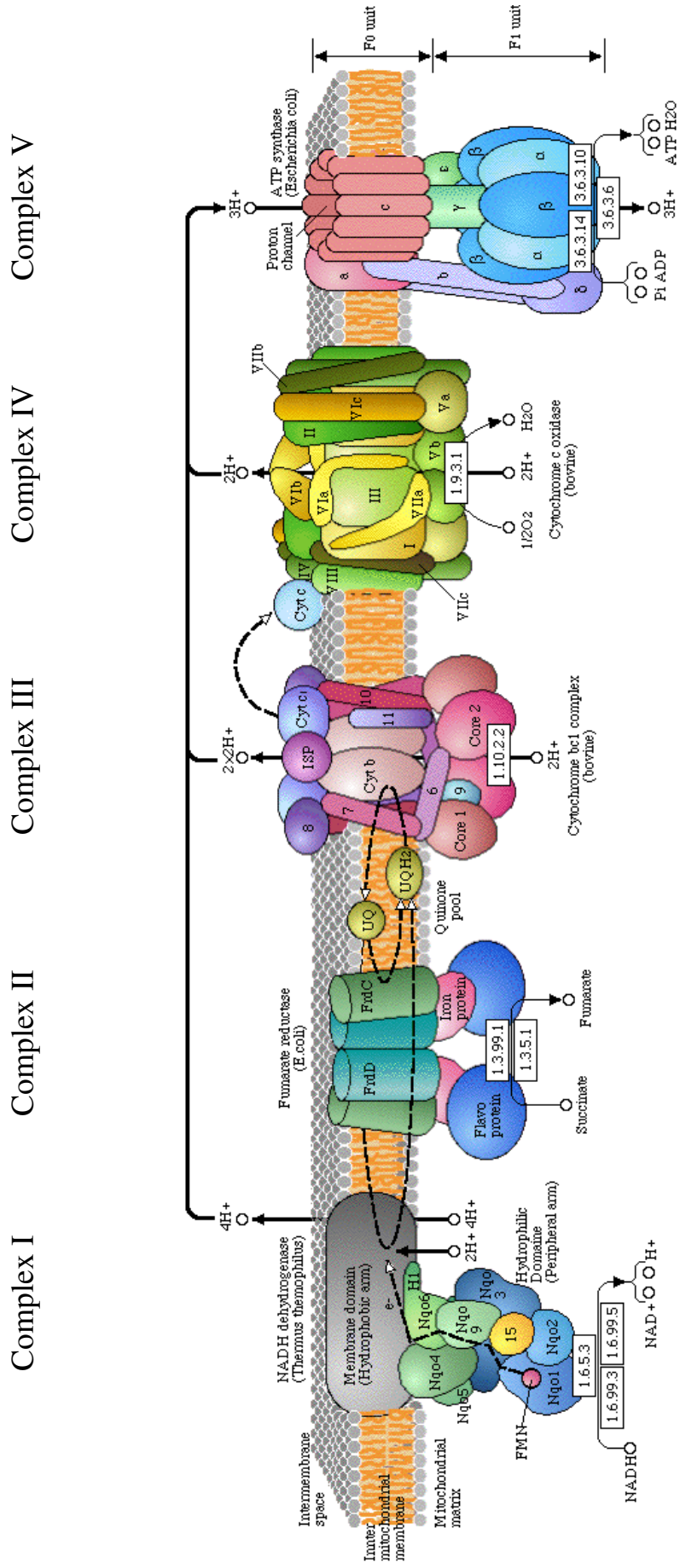
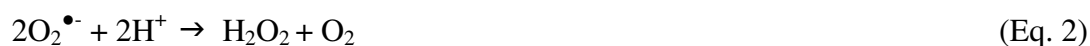


FIGURE 1 Oxidative phosphorylation and the involved complexes. Adopted from [11].

Superoxide is not reactive *per se*, but its conjugated acid, arising in ~ 1% from $O_2^{\bullet-}$, the hydroperoxyl radical (HO_2^{\bullet}) causes mitochondrial DNA mutations, protein damage, and initiates lipid peroxidation [4, 12], see Fig. 2 (*page 9*). Oxidative damage can be prevented by the protective action of various enzymatic antioxidant mechanisms. Superoxide dismutase (MnSOD in the matrix, CuZnSOD in the cytosol and the mitochondrial intramembrane space) converts superoxide into hydrogen peroxide (H_2O_2), see Eq. 2.



Superoxide dismutation product, H_2O_2 can be decomposed to H_2O in a reaction that converts reduced glutathione (GSH) to oxidized glutathione (GSSG), catalyzed by glutathione peroxidase (GPX) in the mitochondrial matrix (Fig. 2, *page 9*) as well as in the cytosol [5, 13–14], see Eq. 3.



Alternatively, H_2O_2 can be disproportionated to H_2O by the action of catalase in peroxisomes or in heart mitochondria [5]. By means of these detoxifying systems, ROS are maintained at optimum physiological levels, but also elevated in pulses, to fulfil specific signaling roles [15–16]. An important example of signaling involving ROS is apoptosis [17]. Another example is HIF1 α stabilization *via* H_2O_2 -mediated inhibition of prolyl hydroxylases (converting their cofactor Fe^{2+} to Fe^{3+}) when oxygen sensing proceeds within the electron transport on the respiratory chain Complex III and burst of superoxide is released at Q_0 site of Complex III [18]. However, under severe oxidative or xenobiotic stress, certain fraction of H_2O_2 escapes the above-mentioned guarding mechanisms, by undergoing Fenton reaction with free Fe^{2+} (or other transient metals), and forms the most reactive species, the hydroxyl radical ($\bullet OH$) [19], see Eq. 4.



Hydroxyl radical evokes additional mtDNA damage, protein modifications and lipid peroxidation in the very proximal sites (Fig. 2, *page 9*).

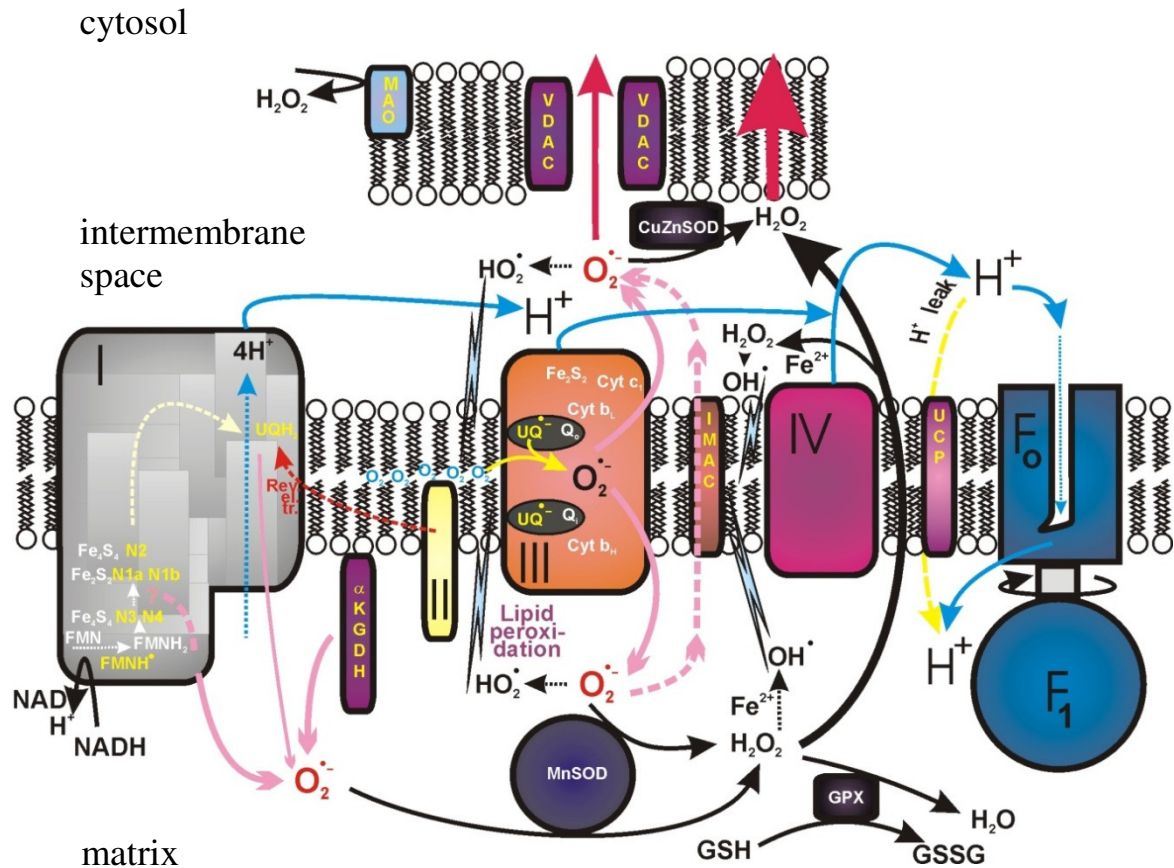


FIGURE 2 Proposed sources of superoxide and its immediate distribution in downstream reactions of mitochondria and respiratory chain. *Adopted from [4].*

Oxidative stress is a consequence of dysbalance of ROS homeostasis given either by their overproduction or by dysfunction of detoxifying antioxidant defense mechanisms, or by both. Oxidative damage may be caused to electron transfer components, or their encoding mtDNA segments, resulting in higher O₂^{•-} leak. In this way, oxidative stress is propagated in new rounds of vicious cycle [4, 20–22]. Perpetual accumulation of cellular oxidative damage is linked with aging [23–25] and oxidative stress-related diseases such as atherosclerosis [26], hypertension, inflammation, cystic fibrosis, cancer, diabetes mellitus II [27], cardiovascular [28] and liver [29] diseases, or Parkinson's and Alzheimer's neurodegenerative diseases, *etc.* [30–34].

Oxidized mtDNA bases, such as 8-oxoguanine and FapyG (the two most frequent ones), are formed with the frequency of 100 – 500 per day and in spite of the mtDNA repair mechanisms, a pool ends up as mtDNA mutations [35]. This is due to the poor

proof-reading activity of mitochondrial DNA polymerase γ which inserts adenine instead of guanine with the frequency of 27%. Accumulation of either inherited mutations (carried over through the purifying bottleneck effect during the maturation of mother's egg cells) or those superimposed due to the mtDNA oxidative modifications over a certain threshold is indeed lethal, as proven by numerous mitopathies [36–37]. Mutations in the tRNA and rRNA mitochondrial genes cause the overall impairment of mtDNA expression, while mutations in the mitochondria-coded protein subunits are even more deleterious, leading to diseases and cell death [36], see Fig. 3.

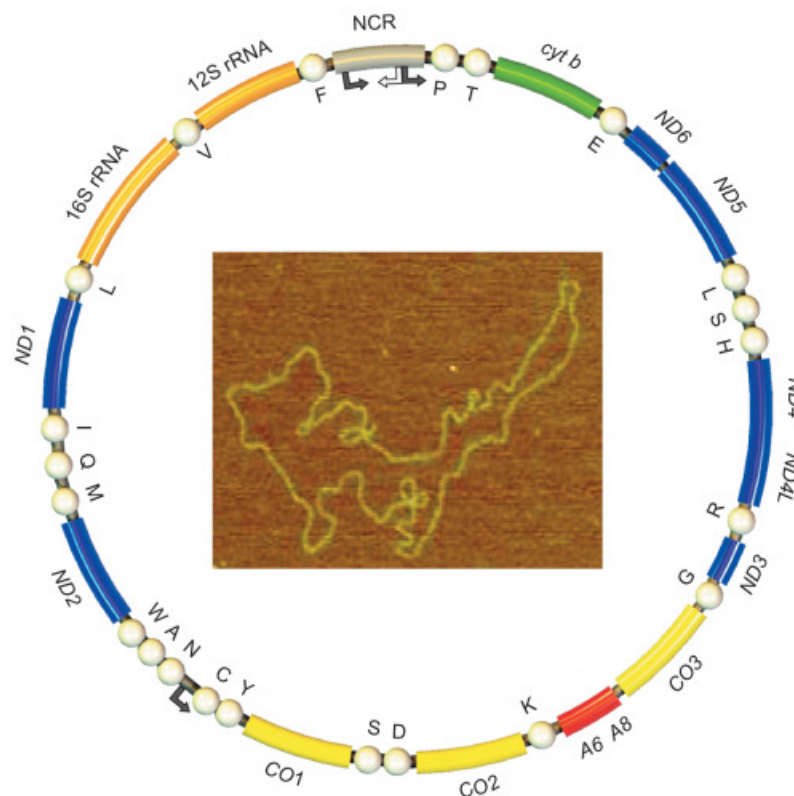


FIGURE 3 The human mitochondrial genome. Mitochondrial genome consists of numerous copies of small circular DNA molecules, each encoding 13 proteins of respiratory chain and oxidative phosphorylation complexes, **blue**: 7 subunits (ND1–6, ND4L) of Complex I; **green**: cytochrome *b* (cyt *b*) subunit of Complex III; **yellow**: 3 subunits (CO1–3) of Complex IV (cytochrome *c* oxidase); **red**: 2 subunits (A6 and A8) of Complex V (ATP-synthase). In addition, mtDNA contains genes for 22 tRNAs (indicated by letter symbols) and **orange**: 2 rRNAs (12S, 16S), **gray**: non-coding region (NCR). *Adopted from [38].*

It is generally accepted that slow electron transport leads to prolonged half-life of ubisemiquinone species which are in turn more prone to donate electron to O₂ in the reaction of O₂^{•-} formation [4, 39–42], see Eq. 1 (*page 6*). The rate of electron transport through the respiratory chain is influenced by the proton motive force Δp (electrochemical membrane proton gradient expressed in mV), which is postulated in general bioenergetics as the sum of electrical potential difference $\Delta\Psi_m$ (membrane potential) and chemical concentration difference ΔpH (pH gradient) connected with the spatial distribution of protons (H⁺) across the inner mitochondrial membrane, see Eq. 5.

$$\Delta p = \Delta\Psi_m - 60\Delta\text{pH} \quad \text{at } 30^\circ\text{C (in mV)} \quad (\text{Eq. 5})$$

Therefore, superoxide production can be limited by attenuating the magnitude of the membrane potential ($\Delta\Psi_m$) so that the accelerated electron flow does not allow superoxide to be generated [43]. Uncoupling, defined as the dissipation of Δp , can be achieved by the action of uncoupling protein or ATP synthase (Complex V) [4]. However, in coupled mitochondria, the rate of ATP synthase activity is subject to feedback inhibition exerted by the ATP produced, slowing down electron flow within the mitochondrial respiratory chain in a process called respiratory control [50–51]. In this view, uncoupling virtually represents a shortcircuit in the respiratory control [4, 52]. A mild uncoupling of oxidative phosphorylation, during which ATP synthesis is largely unaffected, may be accomplished by the action of UCP2 which reportedly plays a role in the suppression of ROS production [43–49]. On the contrary, high number of non-phosphorylating and coupled mitochondria means increased generation of O₂^{•-} for the cell [4]. Other sources report attenuation of Complex I-derived O₂^{•-} production with the decreasing ΔpH component of the proton motive force in skeletal muscle mitochondria [40, 53].

Complex III (ubiquinol:cytochrome *c* oxidoreductase, also termed cytochrome *bc*₁ complex) is an efficient producer of O₂^{•-} as well. In contrast to Complex I, which delivers its entire O₂^{•-} production into the matrix side of the inner mitochondrial membrane [43, 54], Complex III-mediated O₂^{•-} production arising from so-called Q_i site and Q_o site is targeted to both matrix and cytosolic sides, respectively [55]. ROS coming from Complex III are subject to modulation by membrane potential as well, as can be

documented by a 55% H_2O_2 production decrease upon a 10% $\Delta\Psi_m$ drop in rat heart mitochondria [56–57].

It has been reported that significant fraction of $\text{O}_2^{\bullet-}$ produced by Complex I may originate from Complex II-linked substrates (in the absence of rotenone) through the increased intensity of reverse electron transport (RET) slowing down the net electron flux within the respiratory chain [4, 49, 58–59], especially under conditions when oxygen O_2 levels become low [60]. It has been shown that involvement of RET in generation of $\text{O}_2^{\bullet-}$ by Complex I is amenable to down-regulation by uncoupling or ATP synthase as in the case of forward electron transport [4, 43]. Nevertheless, the existence of RET *in vivo* is a matter of ongoing scientific debate [4].

Despite the fact that oxidative stress of mitochondrial origin, *e.g.* elevated mitochondrial superoxide ($\text{O}_2^{\bullet-}$) production, exceeds other ROS sources, such as NADPH oxidase, xanthine oxidase, lipoxygenase, cyclooxygenase, or cytochrome P450 enzymes [4], one must not forget about reactive nitrogen species (RNS) and nitrosative stress. The major sources of RNS are three types of NO synthases (neuronal, inducible, and endothelial) giving rise to nitric oxide ($\bullet\text{NO}$) [61]. The most invasive types of ROS and RNS are membrane permeable, particularly H_2O_2 , nitric oxide ($\bullet\text{NO}$), hydroperoxyl radical (HO_2^{\bullet}), and hydroxyl radical ($\bullet\text{OH}$) [62]. The latter two and peroxynitrite (ONOO^-) are able to initiate lipoperoxidation, see below [45]. Peroxynitrite is formed from nitric oxide in reaction with $\text{O}_2^{\bullet-}$ and has been implicated in various signaling pathways and related diseases, prominently of cardiovascular origin [63]. Nitric oxide inhibits mitochondrial cytochrome *c* oxidase (Complex IV) in an oxygen-dependent manner [64–65]. This can lead to increased $\text{O}_2^{\bullet-}$ production because of the obstructed electron transport in the respiratory chain [4]. Inhibition of mitochondrial respiration by nitric oxide was also accounted to have preventing effects in stabilization of hypoxia-inducible transcription factor at low concentrations of O_2 [66]. Recently, a cardinal role of mitochondrial nitric oxide synthase (NOS) initiated by insulin signaling has been ascribed [67], predicting an instant transient respiration inhibition by $\bullet\text{NO}$ upon insulin stimulation in skeletal muscle. Dysfunction of such a signaling, leading to progressive oxidative and nitrosative stress, could lead to type-2 diabetes.

Enzymatic lipoperoxidation involves cyclooxygenases and lipoxygenases, *i.e.* dioxygenases specific for unsaturated fatty acids, which were reportedly implicated in the regulation of many physiological processes including inflammation [68] and apoptosis, respectively [69–70]. Non-enzymatic radical-dependent lipoperoxidation occurs within both, the inner and outer mitochondrial membranes [71–72], preferentially affecting polyunsaturated acids (PUFAs), and proceeding through carbon-centered radical intermediates ($\text{RC}^\bullet\text{R}$) [73], see Fig. 4. Oxidation by O_2 yields reactive peroxy radicals (ROO^\bullet) which propagate peroxidation by reacting with nearby fatty acids (FAs) and phospholipid fatty acyl side chains, producing polyunsaturated fatty acid hydroperoxides (PUFAOOH) and phospholipid hydroperoxides (PLOOH), respectively [74]. Furthermore, in analogy to hydroxyl radicals ($^\bullet\text{OH}$), see Eq. 4 (*page 8*), alkoxyradicals (RO^\bullet) might arise *via* Fe^{2+} -dependent Fenton chemistry [73]. Mitochondrial phospholipase A_2 (mtPLA_2) cleaves fatty acids or fatty acid hydroperoxides (FAOOH) from the corresponding lipid derivatives at any stage of the lipid peroxidation mechanism, thus initiating the signaling function of these bioactive lipid second messengers [75], see chapter 2.4 (*page 21*).

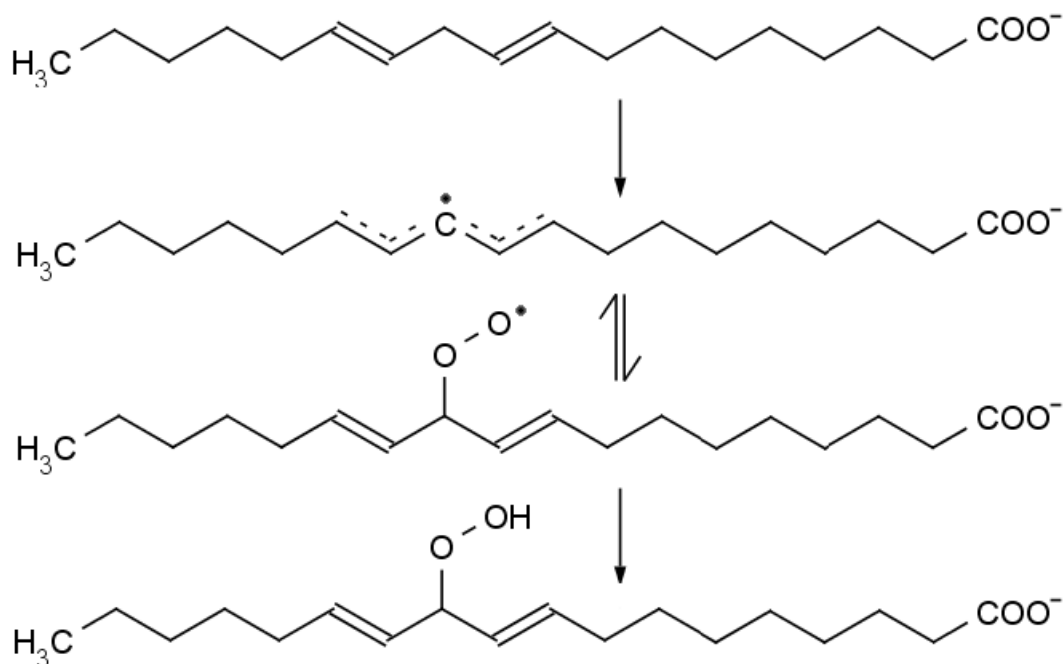


FIGURE 4 Reaction scheme for non-enzymatic lipoperoxidation of linoleic acid.

Adopted from [71].

2.2 NADH:ubiquinone Oxidoreductase

Proton pumping NADH:ubiquinone oxidoreductase, also termed Complex I or NADH dehydrogenase, is the largest enzyme complex of the mitochondrial respiratory chain [76–79]. It belongs to the largest membrane-bound multiprotein assemblies [80]. The principal function of Complex I is to mediate electron transfer from NADH-linked substrates to ubiquinone (oxidized form of coenzyme Q) together with the concomitant vectorial proton transport across the inner mitochondrial membrane from the matrix side into the intermembrane space, see Eq. 6.



Complex I is a massive L-shaped machinery of 46 subunits embedded in the inner mitochondrial membrane, of which 7 most hydrophobic subunits are encoded by the mitochondrial genome (ND1–6, ND4L) [80]. It consists of a matrix-exposed hydrophilic peripheral arm harboring an array of redox active prosthetic groups to promote electron transfer and a hydrophobic membrane arm with a number of sites acting as proton pumps. Electrons transferred during the dehydrogenase reaction between NADH at the distal end of the peripheral domain and ubiquinone in the groove of the connecting region between both the domains provide energy to propel proton translocation with a $4\text{H}^+/2e^-$ stoichiometry [76, 81]. A whole repertoire of Complex I-specific inhibitors have been discovered up to now [82–87]. Byproduct formation of superoxide anion radicals $\text{O}_2^{\bullet-}$ is an inevitable process during the Complex I-dependent oxidative metabolism. Furthermore, retarded electron transport, *e.g.* by means of Complex I inhibitors [40], leads to higher intensity of $\text{O}_2^{\bullet-}$ production [4]. However, the consensus view predicts that in all cases Complex I-derived $\text{O}_2^{\bullet-}$ is exclusively released into the mitochondrial matrix [43, 54].

Electron transfer pathway of the peripheral arm incorporates the NADH⁺-binding site (flavin binding site), noncovalently bound flavin mononucleotide (FMN), eight or nine iron-sulfur clusters (denoted N1a–c, N2–5, N6a–b), and the quinone-binding site (Q-site) [88]. Seven of the Fe-S clusters are predicted to be linearly arranged to constitute an electron transfer chain between NADH and ubiquinone [80], see Fig. 5 (*page 15*).

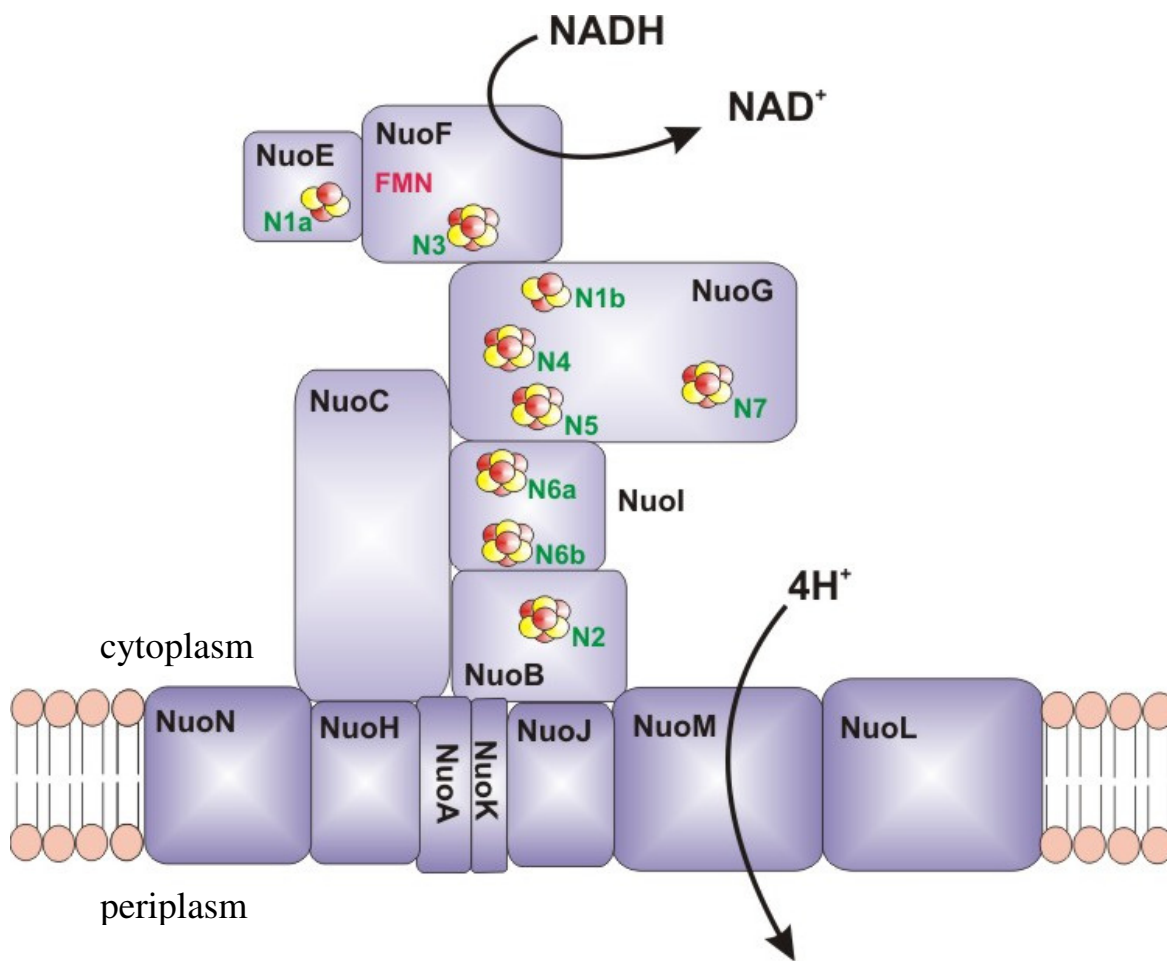


FIGURE 5 The model of Complex I in *E. coli*. The arrangement of iron-sulfur clusters is based on X-ray crystal structure of *T. thermophilus* Complex I peripheral arm. Adopted from [89].

According to the nomenclature for human Complex I the seven peripheral arm central subunits are formed by NDUFS1 (housing N4, N5, N1b, and N1c Fe-S clusters), NDUFS2–3, NDUFV1 (N3 Fe-S cluster and FMN), NDUFV2 (N1a) and NDUFS8/TYKY (N6a and N6b), and NDUFS7/PSST (N2) plus eight accessory subunits [80], see Table 2 (page 16). According to Hirst *et al.*, certain ambiguity exists in assignment of the N4 and N5 Fe-S cluster locations to characteristic signals in EPR spectra analysis [90]. The membrane arm consists of the central subunits ND1 to ND6, and ND4L (mtDNA-coded) and up to 24 accessory subunits. Subunits ND2, ND4, and ND5 are predicted to mediate H⁺-pumping [91], see Table 2 (page 16). Unlike for bacterial NADH:ubiquinone

oxidoreductase peripheral domain [92–94] and membrane domain [95], a high-resolution X-ray crystal structure has not been resolved yet for the mammalian Complex I.

TABLE 2 Nomenclature of selected subunits for mitochondrial and bacterial Complex I.^a

Mitochondria	<i>Paracoccus</i>		Cofactors and/or proposed functions
	<i>Escherichia coli</i> and <i>Rhodobacter capsulatus</i>	<i>denitrificans</i> and <i>Thermus thermophilus</i>	
<i>Peripheral domain</i>			
NDUFS1	NuoG	Nqo3	N1b, N1c, N4, N5
NDUFV1	NuoF	Nqo1	NADH, FMN, N3
NDUFV2	NuoE	Nqo2	N1a
<i>Connecting region</i>			
NDUFS7/PSST	NuoB	Nqo6	N2, Q-site
NDUFS8/TYKY	NuoI	Nqo9	N6a, N6b
NDUFS3	NuoC	Nqo5	–
NDUFS2	NuoD	Nqo4	Q-site
<i>Membrane domain</i>			
ND1	NuoH	Nqo8	–
ND2	NuoN	Nqo14	H ⁺ -pumping
ND3	NuoA	Nqo7	–
ND4	NuoM	Nqo13	H ⁺ -pumping
ND4L	NuoK	Nqo11	–
ND5	NuoL	Nqo12	H ⁺ -pumping
ND6	NuoJ	Nqo10	–

^aCompiled from [96–97].

A conclusive mechanism for $O_2^{\bullet-}$ generation by Complex I is still missing. The following locations were suggested as the potential sources of $O_2^{\bullet-}$ origin: iron-sulfur clusters N1a [98] and N2 [99], the flavin molecule FMN [59, 100–101], and most importantly a semiquinone radical [40, 102–104]. The latter is likely to represent a CoQ-binding site in the immediate vicinity of rotenone-binding site of the peripheral Complex I domain [79–80, 105–106].

Phylogenetic analysis provided a considerable aid in the assignment of H^+ -pumping activity to respective subunits of Complex I. Central subunits ND2, ND4, and ND5 of the membrane arm have probably evolved from subunits of bacterial Na^+/H^+ antiporters [80, 91]. Close sequence identity was shown between the mammalian ND5 subunit of the membrane domain and the MnhA subunit of bacterial Na^+/H^+ antiporters [107–108]. Furthermore, functional Na^+ -pumping activity was linked with the NuoL subunit of *Escherichia coli* NADH dehydrogenase, again pointing to close relationship with the mammalian ND5 subunit (Table 2, page 16) [109]. NuoL-mediated Na^+ -pumping was inhibitable by 5-(*N*-ethyl-*N*-isopropyl)amiloride (EIPA) [109], see Fig 6, which is a hydrophobic compound known as a specific inhibitor of Na^+/H^+ exchangers [108]. The same group has also shown non-competitive inhibition of NADH-quinone reductase activity by EIPA [108] and the prevention of ND5 photoaffinity labeling by fenpyroximate in the presence of EIPA [110]. No direct confirmation for EIPA affecting mammalian Complex I H^+ -pumping has been presented till date.

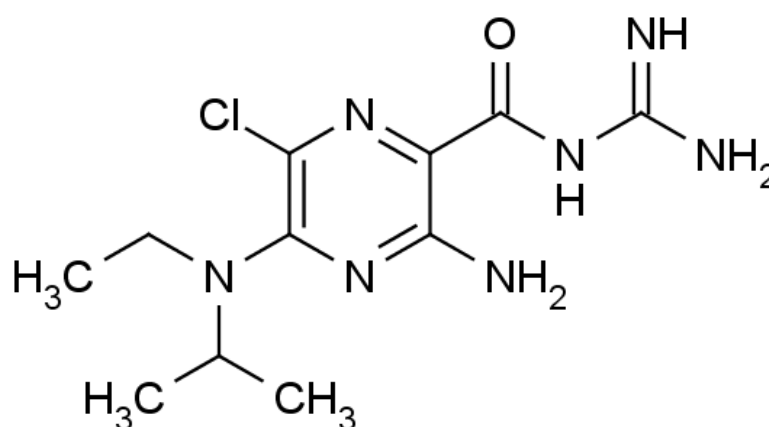


FIGURE 6 Chemical structure of 5-(*N*-ethyl-*N*-isopropyl)amiloride (EIPA).

The mechanism by which electron transfer is coupled to the accompanying H⁺-pumping activity is supposed to utilize long-range redox energy-linked conformational changes [80, 94, 105] arising in the vicinity of NDUFS7/PSST subunit of the connecting region (Table 2, *page 16*). The NDUFS7/PSST subunit shelters redox center N2, which is the terminal Fe-S cluster of the electron transfer sequence (Fig. 5, *page 15*) [80, 106]. Redox energy transfer within the peripheral arm is the driving force for proton pumps at the distal part of the membrane domain, *i.e.* purported H⁺-translocating activity of subunits ND2, ND4, and/or ND5 [80, 94, 105]. In addition to Complex I, H⁺-pumping sites are localized on Complex III and Complex IV of the respiratory chain [111].

Pathophysiology associated with oxidative damage to the *ND5* Complex I mitochondrial gene of the presumed H⁺-pumping subunit, can be illustrated on the following examples: Leber's hereditary optic neuropathy, Leigh syndrome, mitochondrial encephalopathy lactic acidosis stroke-like episodes (MELAS) [112–113], and Parkinson's disease [37]. These mitopathies may be lethal, under conditions of severe and/or chronic oxidative stress, which is accumulated over time in a vicious cycle [37, 112–116].

2.3 Mitochondrial Matrix-targeted Ubiquinone MitoQ₁₀

Oxidative stress can be counteracted by a variety of antioxidants. The best results in preventing or curing pathological states are achieved when there is a means of transporting and/or targeting bioactive compounds to the center of the progressing disease. Due to their directed accumulation, mitochondria-targeted antioxidants derived from MitoQ₁₀ seem to be promising tools in treating oxidative stress and the related pathology of the cell. MitoQ₁₀ resembles coenzyme Q but is conjugated *via* a hydrocarbon chain to a triphenylphosphonium moiety. The lipophilic cation forms an anchor which causes MitoQ₁₀ molecules to gather inside the matrix side of the inner mitochondrial membrane in actively respiring mitochondria when the proton motive force Δp is high [117–122], see Fig. 7 (*page 19*). Oral administration of MitoQ₁₀ is under investigation in connection with hepatitis C virus infection [122].

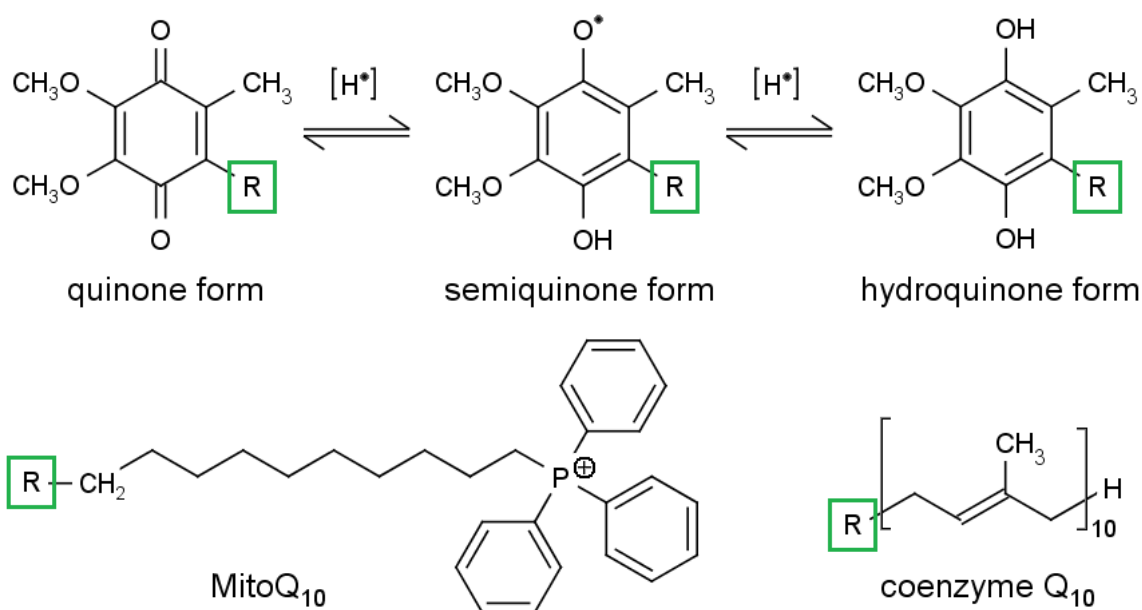


FIGURE 7 Chemical structures of MitoQ₁₀ and coenzyme Q₁₀.

Despite the confirmation of antioxidant MitoQ₁₀ effects *in vivo*, several groups have reported significant pro-oxidant properties of MitoQ₁₀ [118–126]. MitoQ₁₀ was shown to increase H₂O₂ production in mitochondria isolated from endothelial cells [123, 125]. In contrast to coenzyme Q₁₀, MitoQ₁₀ stimulated increase in ROS production by Complex I in isolated mitochondria [123]. The mechanism of pro-oxidant action of MitoQ₁₀ could be explained on the basis of its potential redox cycling effect giving rise to high levels of O₂^{•-}, as was shown *in vitro* experiments with flavin-containing cytochrome P450 reductase [123]. According to the literature, MitoQ₁₀ has a high affinity for binding to ubiquinone-binding site on Complex II [127], whereas binding sites of Complex I and Complex III are not accessible for MitoQ₁₀ [127–131]. The precise mechanism of MitoQ₁₀ action and the conditions for its pro-oxidant and anti-oxidant effects remain to be elucidated. Plecítá-Hlavatá *et al.* have shown that MitoQ₁₀ attenuates rotenone-induced matrix-released surplus O₂^{•-} production of HepG2 cells (means O₂^{•-} production unconsumed by MnSOD) [2]. This attenuation was observed even when H⁺-pumping had been inhibited by EIPA, see Fig. 8 (page 20).

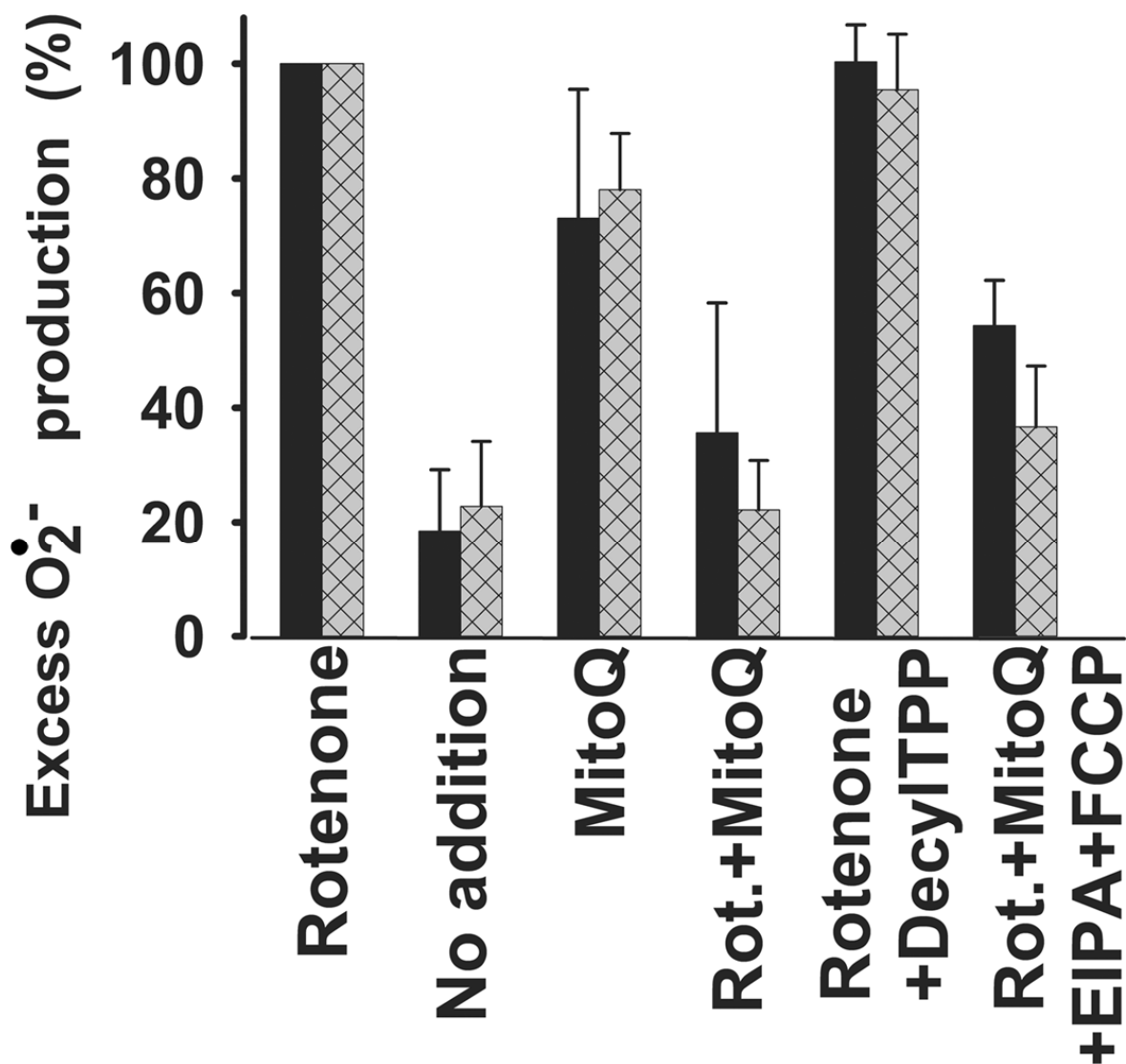


FIGURE 8 Superoxide release to the mitochondrial matrix of GLC25 and OXPPOS HepG2 cells. Superoxide release to mitochondrial matrix, representing the fraction not neutralized by MnSOD, was calculated from MitoSOX Red fluorescence acquired by confocal microscopy for **■** *black bars*: GLC25 cells, relying mostly on glycolysis; **▨** *hatched bars*: OXPPOS cells, forced to oxidative phosphorylation. Rates are normalized to rotenone (taken as 100%). *Adopted from [2].*

2.4 ● Mitochondrial Phospholipase A₂

Mitochondrial phospholipases (mtPLAs) are low-molecular weight enzymes catalyzing the hydrolysis of membrane-anchored glycerophospholipids with specificity similar to their cytosolic counterparts: cleavage of acyl ester bonds between the resulting fatty acyl *sn*-1 (phospholipase A₁) and/or *sn*-2 (phospholipase A₂) side chains and the resulting lysophospholipid moiety, and phosphodiester bonds between diacylglycerol and phosphate-containing alcohol (phospholipase C) or between phosphatidic acid and the resulting alcohol (phospholipase D), see Fig. 9. Unlike the classic pancreatic phospholipase A₂ (PLA₂) [132], which plays a metabolic role in the digestion of dietary lipids, mitochondrial phospholipases act at the beginning of physiologically-relevant signaling pathways releasing lipids as secondary messengers to initiating diverse downstream responses [71–75].

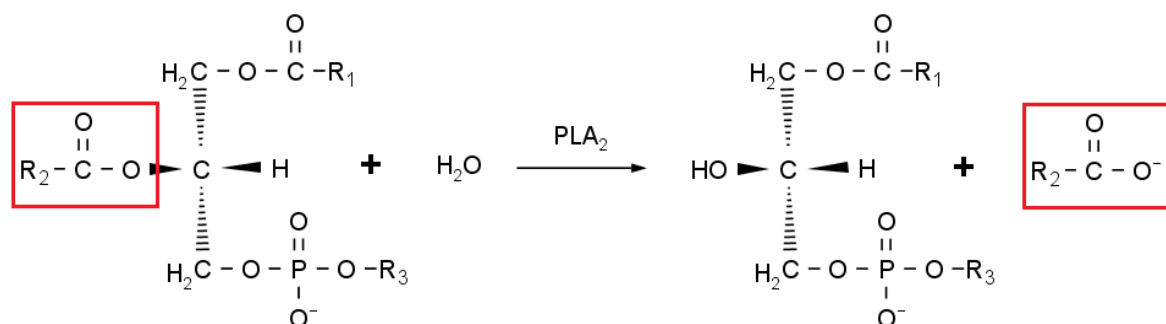


FIGURE 9 Substrate specificity of phospholipase A₂.

In relation to safeguarding mechanisms against oxidative stress, the focus has been drawn to phospholipase A₂ (PLA₂) which preferentially cleaves FAOOH from phospholipid hydroperoxides (PLOOHs) [133]. The significance of protective action of PLA₂ against oxidative damage to mitochondrial membrane lipids is highly recognized since the *sn*-2 position of glycerophospholipids is mainly occupied by unsaturated fatty acids, such as arachidonic or oleic acid, which are more prone to lipid peroxidation initiated namely by hydroperoxyl radical (HO₂•), hydroxyl radical (•OH), nitric oxide (•NO), and peroxynitrite (ONOO⁻) than saturated fatty acids [134].

Phospholipases are supposed to be implicated in lipoperoxidation associated with signaling [45]. Any minute production of the most reactive ROS such as hydroperoxyl radical (HO_2^\bullet), hydroxyl radical ($^\bullet\text{OH}$), or peroxynitrite (ONOO^-) ultimately leads to lipoperoxidation [62]. Since lipid peroxidation is a chain reaction reaching at least up to ~ 15 turns, a single ROS species is propagated into a high number of FAOOH molecules and other lipoperoxidation species [71]. Products of lipid peroxidation, such as phospholipid hydroperoxides (PLOOH), are substrates for phospholipases yielding free fatty acid hydroperoxides (FAOOH). All PLA₂ isoforms have the ability to cleave fatty acid hydroperoxide moieties from the phospholipid backbone. It has been shown in our laboratory that polyunsaturated fatty acids (PUFAs) are potent cycling substrates for UCP2 reconstituted into liposomes [135] or into bilayer lipid membranes (BLMs) [136]. Analogously, fatty acid hydroperoxides (FAOOH) were shown to induce protonophoric UCP2-dependent activity [45]. The appreciation that uncoupling protein may attenuate ROS production completes the mosaic suggesting a potential feedback regulatory loop. Hence, feedback down-regulation circuit to attenuate reactive oxygen species of mitochondrial origin could involve UCP2-mediated uncoupling with FAOOHs acting as the cycling substrates [45, 137–138].

Parallel to their recognized phospholipid membrane repair function, phospholipases A₂ were proposed to participate in lipid homeostasis, signal transduction, [139] and inflammatory response. The latter is mediated by PLA₂ after the cleavage of arachidonic acid which is then available for the synthesis of eicosanoids and platelet-activating factors [140–143]. Examples of clinical manifestations associated with eicosanoid metabolism include inflammation, cancer, allergy, asthma, thrombosis, ischemia-reperfusion, rheumatoid arthritis and autoimmune disorders. [144–145].

The PLA₂ superfamily consist of 15 separate groups [146]. The most general classification used takes into account localization and the requirement for calcium [147]. Secretory phospholipases A₂ (sPLA₂) require millimolar levels of Ca^{2+} for their function, have a low molecular weight (12 – 18 kDa), and are released from cells where they regulate inflammation and other immune responses [148]. Secretory phospholipases A₂ are characterized by the lack of specificity for arachidonic acid-containing phospholipids at the *sn*-2 position. Increased sPLA₂ levels have been correlated with high risk of

cardiovascular diseases. Therefore, secretory phospholipases are being investigated as potential therapeutic targets [149–151]. As a secretory phospholipase A₂ (sPLA₂) has been ascribed the phospholipase A₂ described by Broekemeier *et al.* using immunoblots with *anti*-iPLA₂ antibodies [75]. As its name implies, this isoform is Ca²⁺-independent.

Cytosolic phospholipases A₂ have a higher molecular weight (39 – 110 kDa), and share an increased specificity for arachidonic acid at the *sn*-2 position of the phospholipid backbone allowing for the synthesis of eicosanoids. Generally, these can be divided into two groups, the Ca₂⁺-dependent (cPLA₂), and calcium-independent phospholipases (iPLA₂) [152]. In addition, different subgroups are defined within each group, depending on respective inhibitor sensitivity profiles, denoted by Greek alphabet symbols [147].

Regardless of the fact that subgroup classification does not refine isoforms originating from different organelles (*i.e.* mitochondria, endoplasmic reticulum, and Golgi apparatus), members of the cPLA₂γ, iPLA₂β, iPLA₂γ subgroups were localized to mitochondria in a variety of tissues [152]. Despite being classified as the cytosolic Ca²⁺-dependent cPLA phospholipase, cPLA₂γ, is rather thought to be functioning independently of calcium. This isoform is anchored to membranes of various organelles including mitochondria [153], perhaps through farnesylation or palmitoylation [154]. A calcium-independent splice variant of iPLA₂β has been identified to associate with membranes as well [155]. More importantly, the iPLA₂γ subgroup appears to be exclusively membrane bound with one of the isoforms localized to rat heart mitochondria [139]. In heart, the function of iPLA₂ was shown to be involved in preserving membrane function and dynamic integrity, bioenergetic status of the cell, and signaling [156–157]. Functional iPLA₂γ knock-out mice showed reduced growth rate, stamina, intolerance to cold, increased sensitivity to cardiac stress and the loss of myocardial cardiolipin content [158]. A membrane-repair role was ascribed to mitochondrial iPLA₂ also in kidney cells [152].

In experiments, bromoenol lactone (BEL), arachidonyltrifluoromethyl ketone (AACOCF₃), methyl arachidonyl fluorophosphonate (MAFP), mepacrine, dithiothreitol, just to note a few, were commonly used as inhibitors specific in particular for phospholipase A₂ activity [75]. *Tert*-butyl hydroperoxide (TBHP) was employed as the

stimulant of arachidonic acid release from membrane phospholipids in a PLA₂-dependent manner [159]. A specific inhibitor for phospholipase β iPLA₂ and γ iPLA₂-dependent activity is considered to be bromoenol lactone [143].

In summary, mitochondria have been reportedly shown to contain both, Ca²⁺-insensitive isoform of PLA₂ [74–75] and Ca²⁺-dependent PLA₂ isoform [160]. Mitochondrial phospholipases were reportedly described to be activated by superoxide or downstream ROS [161–162]. The first discovered Ca²⁺-dependent mtPLA₂ is insensitive to arachidonyltrifluoromethyl ketone (AACOCF₃), inhibitor specific for cPLA₂ [163], and was reported to be activated by O₂^{•-} with more pronounced effect upon peroxynitrite (ONOO⁻) inhibition of Complex III [160].

The presence of iPLA₂ phospholipase in rat lung mitochondria was shown in our laboratory on Western blots after the purification of the mitochondrial fraction by Percoll density gradient [164], see Fig. 10 (*page 25*).

anti-iPLA₂

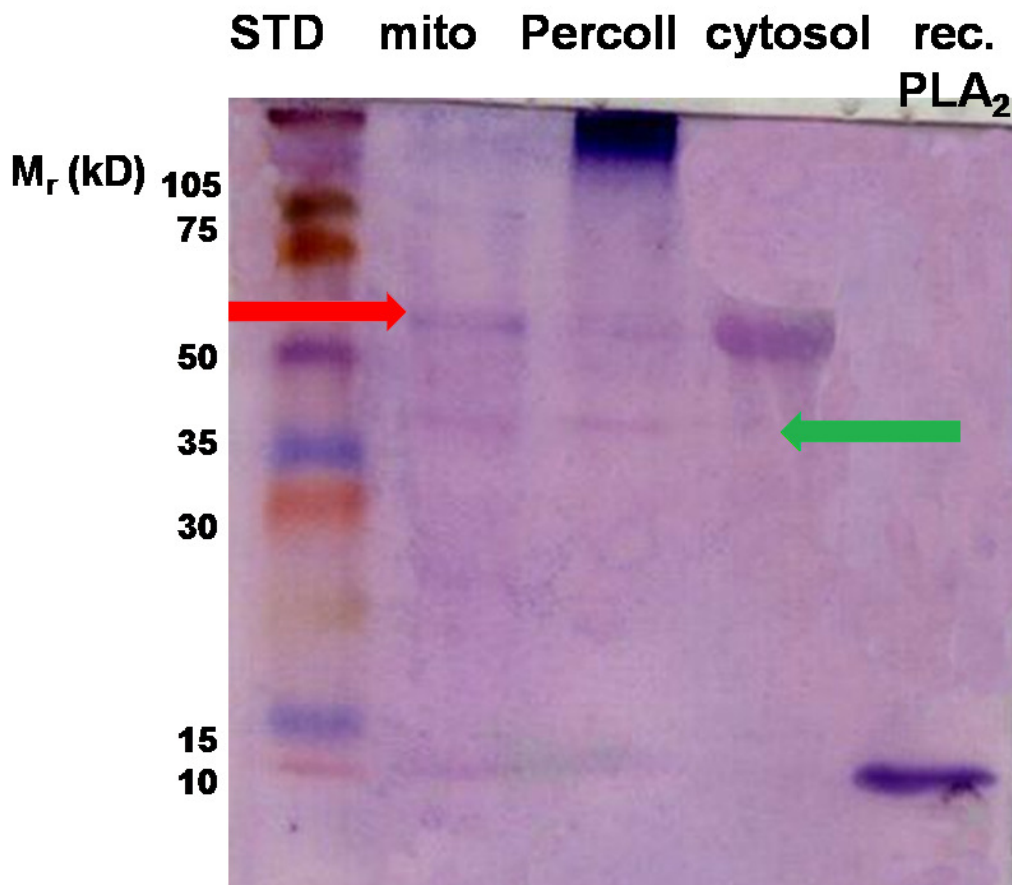


FIGURE 10 The presence of iPLA₂ in rat lung mitochondria, as demonstrated by immunoblot analysis. Lanes are shown for the following conditions from left to right: rainbow standards (STD), mitochondrial fraction (mito), mitochondria purified by Percoll density gradient (Percoll), cytosolic fraction (cytosol), and recombinant 14 kDa PLA₂ protein (Sigma). The effectiveness of the purification step by Percoll density gradient is substantiated by *green arrow*: the presence of mitochondrial iPLA₂; and *red arrow*: the absence of cytosolic iPLA₂. Equal amounts of mitochondrial and cytosolic proteins (25 µg) were separated by SDS-PAGE and transferred to PVDF membranes. Membranes were incubated with *anti-iPLA₂* antibodies (Abcam) at a dilution 1 to 500. Bound antibodies were visualized by alkaline phosphatase-conjugated *antiIgG* antibodies and BCIP/NBT. *Adopted from unpublished results of Mgr. Michal Růžička, Ph.D.*

2.5 Mitochondrial Uncoupling Protein 2

The ubiquitous mitochondrial uncoupling protein 2 is a homologue of the thermogenic, brown adipose tissue-specific uncoupling protein 1 (UCP1) [165]. Together with skeletal muscle-specific UCP3 [166] and brain-specific UCP4 and UCP5 [167–168] they form a distinct subfamily within the gene family of anion carriers [3]. Moreover, the plant uncoupling protein (PUMP) has been found in a variety of species [169–170]. All mitochondrial uncoupling proteins are transmembrane proteins of the inner mitochondrial membrane and catalyze fatty acid-dependent backflux of H^+ into the matrix, thus dissipating the proton motive force of the proton gradient across the membrane [171–172]. It has been predicted that even a slight increase in the H^+ backflux into the mitochondrial matrix might lead to significant suppression of ROS formation [173].

UCP2 mRNA has been ubiquitously found in all mammalian tissues including skeletal muscle, heart, lung, kidney, liver, brown and white adipose tissue, spleen, thymus, placenta, and in the cells of immune system – lymphocytes, monocytes and macrophages [174–176]. Nevertheless, UCP2 is present at one or two order of magnitude lower abundance than UCP1 [135, 177], suggesting that UCP2-mediated uncoupling is not significantly thermogenic.

The physiological role of UCP2 is not definitely understood. UCP2 might participate in body weight and energy balance regulation due to a weak uncoupling accumulated over time, in apoptosis initiation [178–179] and the involved signal transduction pathways, in regulation of glucose-stimulated insulin secretion (GSIS) [180] and Ca^{2+} homeostasis [181], or most significantly, in attenuation of mitochondrial production of reactive oxygen species [47, 182–185], see Fig. 11 (*page 27*).

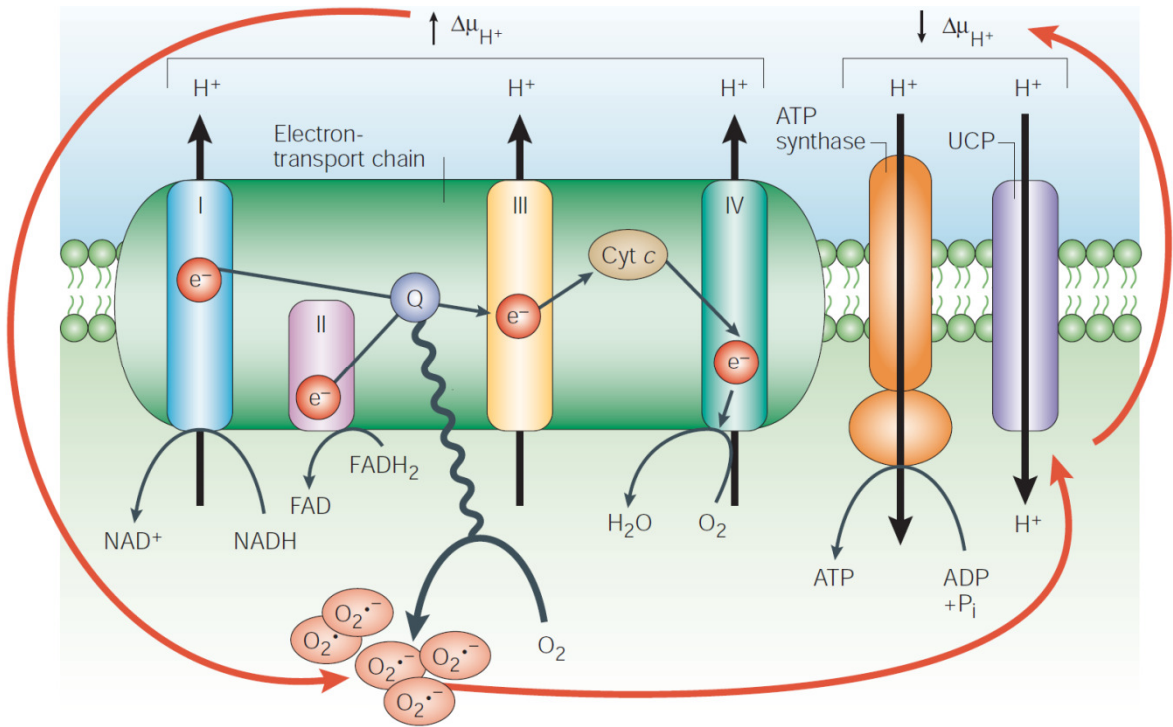


FIGURE 11 Feedback down-regulation of superoxide by uncoupling proteins.

Adopted from [165].

Mice lacking *ucp2* gene are not obese and have a normal response to cold exposure or high-fat diet [44]. However, the details of their phenotype are significantly different with the regard to ROS production [44] and beta cell insulin secretion [186–187], confirming the implication of UCP2 in ROS-related pathologies and diabetes mellitus II, respectively. The role of UCP2 in preventing oxidative stress can be also deduced from its increased expression in response to elevated mitochondrial oxidative damage [188]. Decrease in ROS or lipoperoxidation not only in mitochondria, but within the cell cytosol or even in the extracellular space may result also from a mild uncoupling [189–191]. For example, UCP2-mediated uncoupling in endothelial cells was able to attenuate extracellular ROS in coincubated low-density lipoproteins [189]. Moreover, UCP2 has also been implicated in preventing oxidative damage after experimental stroke and neurodegeneration [189] or having an antioxidant role in the liver [46, 48].

Not much information is available on molecular properties of UCP2 itself. It is usually assumed that UCP2 has identical properties to UCP1. Reconstitution studies have

shown some similarities, such as the essential requirement for fatty acids (FAs) to provide uncoupling [192], fatty acid cycling mechanism plausible for all UCPs, and inhibition by ATP, GDP and other purine nucleotides [45, 172, 182, 193]. Nevertheless, more aspects of UCP2 molecular phenotype has to be resolved yet. In the fatty acid cycling model, UCP2 is regarded as the transporter for FA anion substrates [135]. It has been shown in our laboratory, that such mechanism could hold true even with polyunsaturated fatty acids [134, 136] and fatty acid hydroperoxides [45].

One of the crucial unanswered question is, how the UCP2-mediated suppression of mitochondrial ROS production is regulated? A hypothetical scenario assumes that oxidative stress lies at the beginning of a feedback regulatory circuit encompassing lipid peroxidation and uncoupling protein activation which counteracts ROS production. Brand *et al.* suggested a direct activation of UCP2 by 4-hydroxynonenal (HNE), a reactive lipoperoxidation end-product, as a part of fast-response compensating mechanism to oxidative stress [133, 137, 194]. On the other hand, identical role could be ascribed to other products of lipid peroxidation, such as free polyunsaturated fatty acid hydroperoxides (PUFAOOH) cleaved by PLA₂ phospholipases [137–138]. These lipid peroxidation products have been implicated in functional stimulation of UCP2-dependent protonophoric activity [45], confirming the role of UCP2 in feedback down-regulation of mitochondrial ROS production [4, 45].

2.6 Physiological Hypoxia

The term “hypoxia” is not uniformly used, even if it stands for the same meaning, *i.e.* low oxygen. Biomedical investigations including studies of cultured cells are usually performed at the air atmosphere containing 20.9% oxygen, sometimes incorrectly called “normoxic”. However, the physiological oxygen pressure (pO₂) in organs and tissues is known to be lower than in the air environment, and corresponds to physiological normoxia [195]. Conversely, under some pathological conditions (ischemic disorders, diabetes, atherosclerosis, *etc.*) pO₂ is much lower than during physiological normoxia and consequently is defined as hypoxia. “Physiological hypoxia” refers to a condition of low but tolerable pO₂, during which cells are kept in a non-lethal state until pO₂ restores back

to normoxic conditions. It occurs for example during early development and pursues mainly a regulatory/signaling function. The pO_2 gradient starts with the first progressive drop in the lung (104 mm Hg in alveolar capillaries), followed by the second drop in the blood. The pO_2 of a given tissue/cell depends on the type of organ, its metabolic activity or demand, and the distance from the closest O_2 -supplying blood vessel, since the diffusion distance of O_2 is 100 – 200 μm [196]. For most tissues pO_2 values range from 4 to 40 mm Hg [195]. For instance, human or pig liver pO_2 correspond to 35 and 80 mm Hg for the perivenous and periportal zones, respectively [197].

The exposure of cells to low O_2 in the range of physiological hypoxia involves numerous instant metabolic and long-term transcriptional expression regulations. The main cellular pathways dealing with a hypoxic stress include the AMP-activated protein kinase (AMPK) pathway [198] and the hypoxia-inducible factor (HIF) pathway [199]. AMPK acts as a cellular energy sensor, since its activity increases with the increasing AMP:ATP ratio, and promotes catabolic processes such as glycolysis while inhibiting anabolic metabolism. Similarly, the HIF pathway responds to low O_2 by adjusting energy metabolism besides its impact on erythropoiesis, cell survival, apoptosis, cell adhesion, motility, and vascularization [199]. The critical step involves the stabilization and activation of HIF1 α , a master transcriptional regulator of hypoxia-dependent gene expression, counting over 70 genes. HIF1 α is activated at O_2 levels below 5% (40 mm Hg) with maximal activation near 0.5% (4 mm Hg) [200]. The transcriptional activity of HIF1 α is also potentiated by AMPK under hypoxic conditions in various cancer cells [201]. The crucial stabilization mechanism of HIF1 α protein is still a matter of scientific debate, since not only low O_2 levels activate HIF1 α but also growth factors, cytokines, and various mitochondrial activities can trigger HIF1 α induction [202]. Also pyruvate, lactate, succinate, and other intermediates of the Krebs cycle have been described to promote the stabilizing effect of HIF1 α , see below.

Hypoxia-inducible factor (HIF) is the main transcriptional factor of the O_2 sensing signal transduction pathway of higher eukaryotes, allowing cells to adapt and survive anoxia. HIF is involved in induction of genes involved in enhancing expression of glucose transporters and almost all glycolytic genes. In this way, cellular metabolism may be reprogrammed from oxidative phosphorylation to glycolysis [18, 199, 203–205]. The three

recognized classes of isoforms HIF1, HIF2, and HIF3 are distributed in almost every tissue of the body [206–209]. Two isoforms of the first class, HIF1 α and HIF1 β , are ubiquitously expressed in tissues [210–212].

The O₂-dependent degradation domain (ODDD) of the α subunit is the key regulatory element stabilizing HIF1 α when pO₂ level is dropped down to ~ 5% or lower [18], see Fig. 12. The most important O₂ sensors are dioxygenases that utilize oxygen to hydroxylate the ODDD regulatory domain. Hypoxia-induced stabilization of the HIF1 α subunit is followed by its migration to the nucleus and dimerization with HIF1 β [213–215]. HIFn α -HIF1 β (where n is 1,2 or 3) heterodimer binds to specific promoters of numerous downstream genes together with p300 and CREB coactivators [204, 216–218].

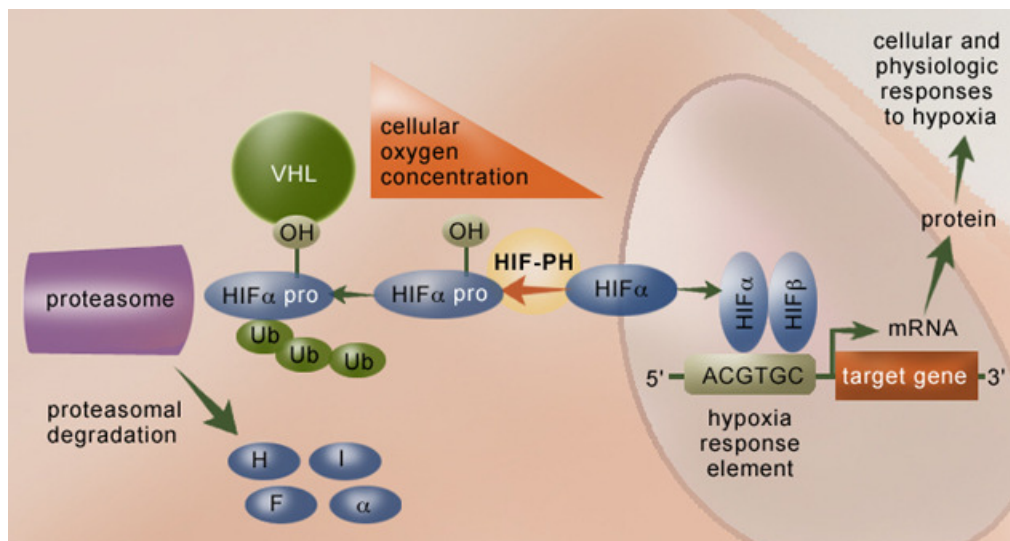


FIGURE 12 The mechanism of action of hypoxia-inducible factor.

[Adopted from [219].

Besides acting as a metabolic switch from aerobic respiration to the glycolytic mode of action, HIF also increases tissue oxygenation by stimulating angiogenesis and vasodilatation through up-regulation of vascular endothelial growth factor (VEGF), inducible NO synthase (iNOS) and erythropoietin. HIF upregulates insulin-like growth factor (IGF) during tumorigenesis, promotes proliferation, [220] and extracellular matrix metalloproteinase 2, thus stimulating tumor invasion [221].

Under normoxic conditions, HIF1 α is constantly degraded through oxygen-dependent hydroxylation of the O₂-dependent degradation domain (ODDD) conserved residues Pro 402 and Pro 564 in human HIF1 α . Hydroxylated HIF1 α subunits are degraded in a proteasome-dependent manner after selective polyubiquitination and sequestration by E3 ubiquitin ligase complex, see Fig. 12 (*page 30*). The complex is composed of von Hippel-Landau tumor-suppressor protein (VHL) [222–224], and elongins B and C. Hydroxylation of the ODDD is catalyzed by the prolyl hydroxylase domain (PHD) enzymes (isoforms 1 – 3). The reaction involves oxygen and α -ketoglutarate as substrates, Fe²⁺ and ascorbate as cofactors [225–228]. Inherited VHL deficiency causes carcinoma of the kidney by permanent activation of HIF1 α [229–230].

At anoxic conditions (1 – 5% O₂), PHD enzymes are deactivated because of their low affinity for O₂. Chandel *et al.* suggested and provided key evidence in series of elegant experiments of the last decade that the mechanism of deactivation can be attributed to the increased rate of mitochondrial O₂[•] production at the outward Q_o site of Complex III when oxygen level is low [18, 231–232]. Concomitant elevation of cytosolic O₂[•] and H₂O₂ (due to the action of CuZnSOD) levels result in enhanced oxidation of Fe²⁺, thus limiting its availability as a cofactor for PHD enzymes. The reduced activity of PHD enzymes leads to the stabilization of HIF1 α and the activation of HIF pathway [233].

Although hypoxic deactivation of PHD oxygenases is the pivotal regulatory mechanism of the HIF pathway, similar regulatory mechanism exists for asparaginyl hydroxylase enzyme. A factor inhibiting HIF (FIH) inactivates human HIF1 α by hydroxylating Asp 803 [234–237], thus sterically preventing its interaction with p300 and CREB-binding protein coactivators [217–218]. The HIF pathway is activated when the inhibition by FIH is relieved during hypoxia.

Krebs cycle intermediates (succinate, fumarate, and oxalacetate) and pyruvate are competitive inhibitors of PHD enzymes because of their structural resemblance to α -ketoglutarate. This is the reason why these metabolites also participate in HIF1 α stabilization [238–239]. Accumulation of intracellular fumarate and succinate predisposes renal cells to cancer with concomitant up-regulation of the HIF pathway [240–241].

HIF α -mediated transcription activation of downstream genes was reported to be stimulated also by SUMOylation [242], oncogenic activation *via* Ras/Raf/MAPK, phosphoinositide 3-kinase (PI3K), PTEN, or Akt pathways [243], insulin, and different growth factors and cytokines, *e.g.* insulin-like growth factor (IGF) and platelet-derived growth factor (PDGF) [220, 244–245], and last but not least, nitric oxide (\bullet NO) which inhibits PHD enzymes due to its analogy to molecular oxygen [246].

The function of HIF as an energetic switch between glycolytic and oxidative metabolism can be best documented on the following example. The funneling of pyruvate into the Krebs cycle and consequent utilization by oxidative phosphorylation is discontinued by HIF-activated lactate dehydrogenase A (LDHA). The resulting lactate is extruded from the cell by the plasma membrane monocarboxylate transporter 4 (MCT4) [253]. In this way, excessive pyruvate is removed and NAD⁺ regenerated for glyceraldehyde-3-phosphate dehydrogenase (GAPDH) to drive additional cycles of glycolysis stimulated by HIF.

To summarize, HIF1 upregulates proteins in pursuit to restore physiological normoxic cell homeostasis [204, 247–248]. In the nucleus, HIF α -HIF1 β heterodimer induces expression of proteins only after the recognition of hypoxia-responsive elements (HREs) in corresponding promoters of the target genes. Different subsets of genes are triggered by respective patterns of α and β subunit composition [207]. The main purpose is to stimulate glucose entry (by expression of GLUT1 and GLUT3 transporters), glycolysis (by up-regulating all glycolytic enzymes), and oxygen uptake (by supporting blood circulation, erythropoiesis, and angiogenesis) in order to reintroduce physiological levels of O₂ [249–251]. HIF-activated expression products are also implied in regulation of pH, apoptosis, cell-division cycle, DNA repair mechanisms, cell adhesion and motility [252].

3 MATERIALS AND METHODS

3.1 Isolation of Intact Mitochondria by Differential Centrifugation

3.1.1 Isolation of Rat Liver Mitochondria

Intact rat liver mitochondria (RLM) were isolated by differential centrifugation as previously described [1, 254]. Adult male Wistar rats were kept, handled and sacrificed in agreement with the regulations of the Institute of Physiology licensing committee and regulations of the European Union. All steps were carried out at $\sim 4^{\circ}\text{C}$. Liver was excised and cut into pieces in ice-cold sucrose isolation medium (250 mM sucrose, 10 mM MOPS, 1 mM EDTA, pH 7.2 adjusted at 25°C with Tris) and homogenized by hand in a glass Potter-Elvehjem homogenizer with a Teflon pestle (5 strokes). The homogenate was poured through a cheesecloth, brought to volume of ~ 150 ml with the sucrose isolation medium and centrifuged at $700 \times g$ for 10 min to remove cell debris. The resulting supernatant was centrifuged at $8,500 \times g$ for 10 min. The following step was repeated twice: pellets were resuspended into ~ 75 ml of sucrose isolation medium supplemented with 5 mg/ml fatty acid-free BSA and centrifuged at $8,500 \times g$ for 10 min. The pellets were resuspended into ~ 75 ml of the sucrose isolation medium without BSA and centrifuged at $8,500 \times g$ for 10 min. The pellets were resuspended into ~ 40 ml of the sucrose isolation medium without BSA and centrifuged at $8,500 \times g$ for 10 min. The pellets were resuspended in ~ 2 ml of the sucrose isolation medium without BSA. Mitochondrial protein content was estimated following the BCA method with BSA as a standard [255]. Mitochondrial stock suspension was kept on ice in an open test tube throughout the whole experiment.

3.1.2 Isolation of Mitochondria from Hepatocellular Carcinoma Cells

Functional mitochondria were isolated from HepG2 cells following the protocol of Bogenhagen and Clayton [256]. All steps were carried out at $\sim 4^{\circ}\text{C}$. The cells were trypsinized and counted. Cell suspension (~ 10 million cells) was washed with ice-cold PBS (15 ml) by centrifugation at $1000 \times g$ for 5 min. The pellet was resuspended in 2 ml of isolation buffer (210 mM mannitol, 70 mM sucrose, 20 mM HEPES, 1 mM EGTA, pH 7.2 adjusted at 25°C with KOH, moreover 1 mM PMSF and 0.1% FA-free BSA were included prior to use) and homogenized with 15 strokes in a Teflon-glass homogenizer (2 ml). Homogenate was transferred into a microcentrifuge tube and spun-down at $1000 \times g$ for 10 min. The resulting supernatant was centrifuged at $14,000 \times g$ for 15 min. The pellet was washed twice by centrifugation at $14,000 \times g$ for 10 min. The pellet was resuspended into isolation buffer without BSA and centrifuged at $14,000 \times g$ for 10 min. The final pellet, containing mitochondrial fraction, was resuspended into the corresponding assay medium (0.5 ml) defined in chapter 3.2 (*page 35*), see Table 3 (*page 36*). Mitochondrial protein content was estimated following the BCA method with BSA as a standard [255]. Mitochondrial stock suspension was kept on ice in an open test tube throughout the whole experiment.

3.1.3 Isolation of Rat Lung Mitochondria

Rat lung mitochondria (RLuM) were isolated by differential centrifugation in accordance with the original procedure [257]. Adult male Wistar rats were sacrificed and lungs excised. All further steps were carried out at $\sim 4^{\circ}\text{C}$. The tissue was briefly washed in 0.9% NaCl solution and cut into small pieces in ice-cold sucrose isolation medium with BSA (250 mM sucrose, 5 mM HEPES, 5 mM EGTA, pH 7.2 adjusted at 25°C with Tris, supplemented with 5 mg/ml fatty acid-free BSA just prior to use) and homogenized by hand in a glass Potter-Elvehjem homogenizer with a Teflon pestle. The homogenate was centrifuged at $700 \times g$ for 10 min to remove cell debris. Supernatant was poured through a cheesecloth and centrifuged at $10,000 \times g$ for 10 min. The resulting pellets were

resuspended into ~ 75 ml of sucrose isolation medium with BSA and centrifuged at $700 \times g$ for 10 min. Supernatant was centrifuged at $10,000 \times g$ for 10 min. The pellets were resuspended into ~ 40 ml of the sucrose isolation medium without BSA and centrifuged at $10,000 \times g$ for 10 min. The final pellet was resuspended in ~ 1 ml of the sucrose isolation medium without BSA. Mitochondrial protein content was estimated following the BCA method with BSA as a standard [255]. Mitochondrial stock suspension was kept on ice in an open test tube throughout the whole experiment.



3.1.4 Isolation of Mouse Lung Mitochondria

UCP2-WT (strain C57BL/6J) and UCP2-KO (strain B6.129S4-*Ucp2*^{tm1Lowl/J}) JAX GEMM Strain mice were purchased from the Jackson Laboratory (Bar Harbor, ME, U.S.A.) and bred in the animal house of the Institute of Physiology. Mice, either UCP2-WT or UCP2-KO at a time, were sacrificed, lungs excised and washed in ice-cold 0.9% NaCl solution. Mouse lung mitochondria (MLuM) were isolated by differential centrifugation, concisely following the protocol described in chapter 3.1.3 (*page 34*).

3.2 Assay Media and Chemicals

Throughout all the experiments, combination of 5 mM glutamate plus 1 mM malate, or 5 mM glutamate plus 1 mM malate and 5 mM succinate was typically used as substrates for respiration. State 4 (non-phosphorylating) and state 3 (phosphorylating) respiration was routinely distinguished by the addition of 0.5 mM ADP, 0.5 mM potassium phosphate (KP_i), and 100 μM $MgCl_2$ to induce state 3 respiration, which lasted for at least 10 minutes as verified by an Oxygraph, see chapter 3.4.1 (*page 38*). All aqueous solutions which were to be added into the assay media (Table 3, *page 36*) had a pH of 7.2, carefully adjusted at 25 °C. Water-insoluble compounds were dissolved in ethanol for UV spectroscopy or, alternatively, in DMSO. Any solvent influence on respiration or fluorescence signal was ruled out by verifying the effects of pure solvent. Fatty acid-free BSA was used exclusively throughout all experiments.

TABLE 3 Assay media composition. All media had pH 7.2 adjusted at 25 °C.

Experiment color code:		 ^a	 ^b
Substance	purpose	(mM)	(mM)
sucrose	osmolyte	125	–
KCl	retention of K ⁺ , osmolyte	65	110
HEPES	buffer	10	5
MgCl ₂	induction of state 3	0.1	0.5
KP _i	induction of state 3	0.5	0.5
ADP	induction of state 3	0.5	–
EGTA	chelation of Ca ²⁺	1	0.5
glutamate	substrate of Complex I	5	–
malate	substrate of Complex I	1	–
succinate	substrate of Complex II	5	10

^apH adjusted with Tris.

^bpH adjusted with KOH.

MitoQ₁₀ and decyltriphenylphosphonium bromide were obtained under a license agreement from Antipodean Pharmaceuticals Inc. (Menlo Park, CA, U.S.A.). Fluorescent probes, Amplex Red and BCECF, AM were obtained from Invitrogen (Carlsbad, CA, U.S.A.). Rotenone, 5-(*N*-ethyl-*N*-isopropyl)amiloride (EIPA), 2-thenoyltrifluoroacetone (TTFA), antimycin A, myxothiazol, stigmatellin, oligomycin, potassium cyanide, carbonyl cyanide 4-(trifluoromethoxy)phenylhydrazone, *tert*-butyl hydroperoxide, magnesium chloride, ADP (Na⁺ salt), GDP (Tris salt), GTP (Tris salt), lactate, succinate, glutamate, malate and horseradish peroxidase were all purchased from Sigma. Bromoenol lactone (racemic mixture) was purchased from Calbiochem. Hydrogenpotassium phosphate was obtained from Penta (Prague, Czech Republic). Ethanol for UV spectroscopy, hydrogen peroxide, and sodium hydroxide were from Lach - Ner (Neratovice, Czech Republic). Cell culture media and chemicals were supplied from the Institute of Molecular Genetics (Prague, Czech Republic).

3.3 Assay for Mitochondrial H₂O₂ Generation *In Vitro*

Mitochondrial hydrogen peroxide (H₂O₂) production was monitored *in vitro* at 30 °C as the increase of fluorescence by Amplex Red (*N*-acetyl-3,7-dihydroxyphenoxazine) oxidation product, resorufin. In this enzymatic determination Amplex Red is used as a substrate for horseradish peroxidase (HRP). The amount of H₂O₂ consumed by HRP for Amplex Red oxidation is directly proportional to the fluorescence signal of accumulated resorufin [1, 258–259]. Therefore, 5 μM Amplex Red and 0.5 μM HRP was added into the assay medium (2 ml, Table 3, *page 36*) prior to the addition of mitochondria (0.1 mg/ml), see chapter 3.2 (*page 35*).

Amplex Red fluorescence was followed for at least 20 minutes by the use of Fluorolog-3 (model 322) fluorometer (SPEX, Horiba Jobin Yvon, Longjumeau, France) with excitation wavelength fixed at 570 nm (slit width 8 nm) and emission at 585 nm (slit width 1.45 nm). Assay medium (2 ml) was constantly stirred inside the thermostated cuvette. Fluorescence signal was calibrated by successive additions of 125 nM H₂O₂ at the end of each run. Rates were calculated by least squares linear regression. In order to exclude the possibility that mitochondria had used up all the substrate, parallel detection of O₂ consumption rate has been performed at least once for each set of experimental conditions applied, see chapter 3.4.1 (*page 38*).

Note that the Amplex Red assay detects overall mitochondrial O₂^{•-} production, *i.e.* superoxide released into the mitochondrial matrix (by Complex I and III) and directly into the surrounding assay medium (by Complex III). This stems from the fact that matrix and intermembrane space O₂^{•-} is readily dismuted to H₂O₂ by MnSOD and CuZnSOD mitochondrial enzymes, respectively (Eq. 2, *page 8*). The intrinsic property of H₂O₂ to diffuse through membranes facilitates its sensitive detection.

3.4 Assay for Polarographic Detection of Oxygen Consumption

3.4.1 High-Resolution Respiration Measurements

Respiration was measured as oxygen consumption by cells (1 million cells/ml) or isolated mitochondria (0.1 mg/ml unless indicated otherwise), which was monitored by Oxygraph-2k high-resolution respirometer (Oroboros, Innsbruck, Austria), with constant stirring at 37 °C or 30 °C, respectively. The assay medium (2 ml) for cells was their cultivation medium. Assay media used for measurements with isolated mitochondria are recapitulated in chapter 3.2 (*page 35*), see Table 3 (*page 36*). Respiratory rates were obtained as first order time derivatives of the air calibrated and background corrected oxygen signal [260]. During the run after each addition of agent, certain time is needed for the signal to reequilibrate because of the minuscule amount of oxygen dissolved in the injected aliquot. Apparent half-maximum activation constants AC_{50} 's for reagents have been calculated from corresponding Hill plots.

3.4.2 Respiration Measurements of Cells at Physiological Oxygen Levels

Continuous cellular oxygen consumption was detected by Oxygraph-2k respirometer (Oroboros, Innsbruck, Austria) in the same fashion as described in chapter 3.4.1 (*page 38*). But for determining O_2 consumption under physiological normoxic conditions several precautions had been made. The assay medium (cell cultivation medium) was left to preequilibrate in the atmosphere of 5% O_2 well ahead of the measurement. Special emphasis was put on the background correction with sufficient times repeated nitrogen addition to correct for the signal at the lowest O_2 levels. Before each run oxygen in the respirometer chamber was expelled by N_2 to attain the level of 5% O_2 . Instant transfer of cells, that had been cultivated at 5% O_2 , into the respirometer

chamber was necessary to avoid their risk of being exposed to the air atmosphere. Endogenous respiration was followed routinely by subsequent additions of oligomycin, FCCP, rotenone, and stigmatellin. Whenever it happened that O₂ had been completely depleted, the air-tight chamber stoppers were briefly opened to restore the 5% O₂ level.

3.5 Assay for Complex I Proton Pumping

Proton pumping was monitored at 30 °C as matrix alkalinization indicated by BCECF, AM probe in preloaded rat liver mitochondria after its conversion to fluorescent BCECF product *via* the action of mitochondrial esterases [261]. The increase of BCECF fluorescence corresponded to greater mitochondrial matrix alkalinization after the addition of respiratory substrates (5 mM glutamate plus 1 mM malate). Freshly isolated rat liver mitochondria (1 mg/ml) were incubated with 1 μM BCECF, AM optimally for 20 minutes at room temperature with constant stirring, washed twice by spinning down the mitochondrial pellet at 8,500 × g for 5 min at 4 °C, and resuspended into assay medium specified in chapter 3.2 (*page 35*), see Table 3 (*page 36*), while reaching final mitochondrial protein concentration of 1 mg/ml. Aliquots of 1 mM lactic acid (Lac) were added at the end of each run for calibration (as illustrated in Fig. 15, *page 45*). A special care was taken to adjust pH 7.2 of all aqueous solutions (with the exception of lactate) added during the experiments.

BCECF fluorescence was measured with emission set at 530 nm (slit width 20 nm) and excitation at 500 nm (slit width 3 nm) on a RF5301 PC fluorometer (Shimadzu, Kyoto, Japan) equipped with Polaroid polarizers at cross-orientation, eliminating light scattering, and in-built stirrer. Alternatively, Fluorolog 322 fluorometer (SPEX, Horiba Jobin Yvon, Longjumeau, France) was used instead operating with the same settings.

3.6 Cell Cultures

Human hepatoblastoma HepG2 cells (cell line ECACC 85011430) were cultivated at 37 °C in humidified air with 5% CO₂ under sterile conditions in DMEM medium

(Invitrogen, Carlsbad, CA, U.S.A., contains no glucose) containing 3 mM glutamine, 5% (v/v) fetal calf serum (Biochrome, Berlin, Germany), 1 mM sodium pyruvate, 45 mM NaHCO₃, 10 mM HEPES, 100 IU/ml penicillin, and 100 µg/ml streptomycin, according to standard procedures [262] assisted by the use of laminar flow cabinet HERAsafe KS 12 (Heraeus, Langenselbold, Germany). Either 25 mM glucose (GLC25 cells), 5 mM glucose (GLC5 cells), or 10 mM galactose plus 2 mM glutamine (OXPHOS cells) was used as the carbon source, with dialyzed glucose-free fetal calf serum (PAA Laboratories, Pasching, Austria). Prior to the respiration and mitochondrial H₂O₂ generation assays, HepG2 cells were detached by incubation with 0.25% trypsin for ~ 5 min at 37 °C and counted under a microscope.

For mimicking physiological normoxic conditions, nitrogen was pumped into the thermostat equipped with oxygen electrode (Jouan IG750, Saint-Herblain, France) in order to reach 5% O₂ (corresponding to 40 mm Hg) besides the 5% CO₂ level.

3.7 Statistical Analysis

Individual means were compared using Student's *t*-test with $P \leq 0.05$ considered to represent significantly different values from the control. These are designated in deviation bar graphs by asterisks right above the error bar of the the corresponding columns.

4 RESULTS

4.1 The Inhibition of Mitochondrial Complex I Proton Pumping

4.1.1 EIPA Inhibits Complex I Proton Pumping in Isolated Rat Liver Mitochondria Respiring in State 4

My colleagues have shown that chemical uncoupler attenuates $O_2^{\bullet-}$ formation within Complex I [1], *i.e.* ~ 30% reduction of rotenone-induced H_2O_2 production by FCCP detected by Amplex Red in experiments with isolated rat liver mitochondria respiring in state 4 on glutamate and malate. I have contributed to this work by identifying the properties of EIPA regarding its inhibition of Complex I-mediated H^+ -pumping in the mitochondrial model. Proton pumping has been evaluated in BCECF, AM-loaded isolated rat liver mitochondria as a pH-sensitive fluorescence of BCECF. Hence, mitochondrial matrix alkalization reflects the increase in H^+ -pumping activity.

Matrix alkalization was apparent after the addition of Complex I respiratory substrates, 5 mM glutamate and 1 mM malate (Fig. 13, *page 43*). A pronounced matrix acidification was observed after the addition of Complex III inhibitor, stigmatellin (Fig. 13, *page 43*), which restored pH to even lower values than the initial level. As expected, similar acidification was also obtained after the addition of Complex I inhibitor, rotenone (Fig. 17, *page 47*), or FCCP (Fig. 14, *page 44*).

My colleagues had also shown that attenuation of rotenone-induced $O_2^{\bullet-}$ production by uncoupling could be prevented by EIPA [1]. It stems from the observed fact that EIPA is a real inhibitor of H^+ -pumping. Here, matrix alkalization, reflecting the increase in H^+ -pumping, was prevented by EIPA added before glutamate and malate (Fig. 15, *page 45*), but not before glutamate, malate plus succinate (not shown). The half-maximum

effect for EIPA inhibition before the addition of glutamate and malate occurred at 27 μM EIPA (Fig. 20, *page 51*). When put together, these results indicate the existence of a feedback pressure exerted by the proton motive force (or $\Delta\Psi_m$) as a necessary prerequisite for $\text{O}_2^{\bullet-}$ production within Complex I, given by the observed fact that $\text{O}_2^{\bullet-}$ production is diminished by the presence of an uncoupler eliminating Δp [1].

In order to show the specificity of EIPA inhibition for Complex I H^+ -pumping, Complex I-supported electron flow was bypassed by the addition of rotenone and succinate (Fig. 15, *page 45*), allowing Complex III and Complex IV-mediated H^+ -pumping to take place. A strong matrix alkalization was reintroduced by the addition of succinate (Fig. 15, *page 45*). Addition of FCCP resulted in a pronounced acidification drop, restoring the original level of fluorescence intensity (Fig. 15, *page 45*).

Glutamate and malate-driven matrix alkalization could be interrupted by saturating concentrations of EIPA (Fig. 16, *page 46*) with the rough estimate of IC_{50} to be $\sim 140 \mu\text{M}$ EIPA. Again, succinate added after rotenone caused FCCP-inhibitable matrix

alkalinization (Fig. 16, *page 46*). Even EIPA added after rotenone was able to stimulate matrix acidification, reflecting a potential residuum of H^+ -pumping activity (Fig. 17, *page 47*). No acidification occurred in the absence of succinate upon the addition of stigmatellin or FCCP (Fig. 17, *page 47*), since electron traffic through the respiratory chain was blocked by rotenone, effectively preventing H^+ -pumping by Complex III and IV to take place.

Amiloride derivatives are well established inhibitors of Na^+/H^+ antiporters [108]. In order to exclude the possibility that EIPA affects mitochondrial Na^+/H^+ antiporter instead of Complex I, monensin was tested in the presence and absence of Na^+ ions. Monensin acts as a monovalent ionophore simulating Na^+/H^+ antiporter activity. Nonetheless, acidification brought on by EIPA is retained when 1 μM monensin is applied, in the presence (Fig. 18a, *page 48*) or absence of Na^+ ions (Fig. 18b, *page 48*). This

demonstrates that the reason standing behind the observed EIPA-mediated acidification excludes the involvement of mitochondrial Na^+/H^+ antiporter.

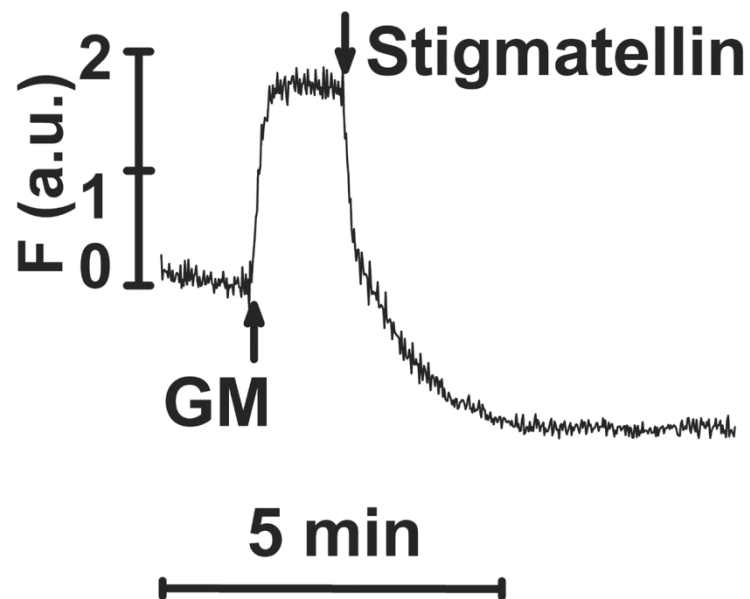


FIGURE 13 Glutamate and malate-driven H^+ -pumping is blocked by stigmatellin in isolated rat liver mitochondria respiring in state 4. Matrix alkalization is shown for the following additions: 5 mM glutamate plus 1 mM malate (GM, pH 7.2 adjusted with Tris), and 0.5 μM stigmatellin.

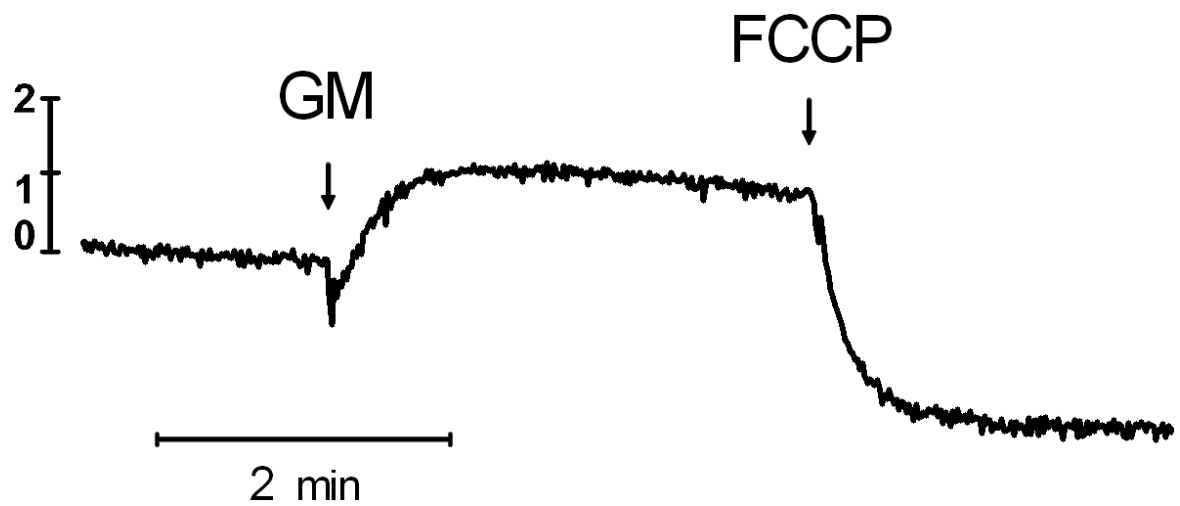


FIGURE 14 Glutamate and malate-driven H^+ -pumping is blocked by FCCP in isolated rat liver mitochondria respiring in state 4. Matrix alkalization is shown for the following additions: 5 mM glutamate plus 1 mM malate (GM, pH 7.2 adjusted with Tris), and 0.5 μ M stigmatellin.

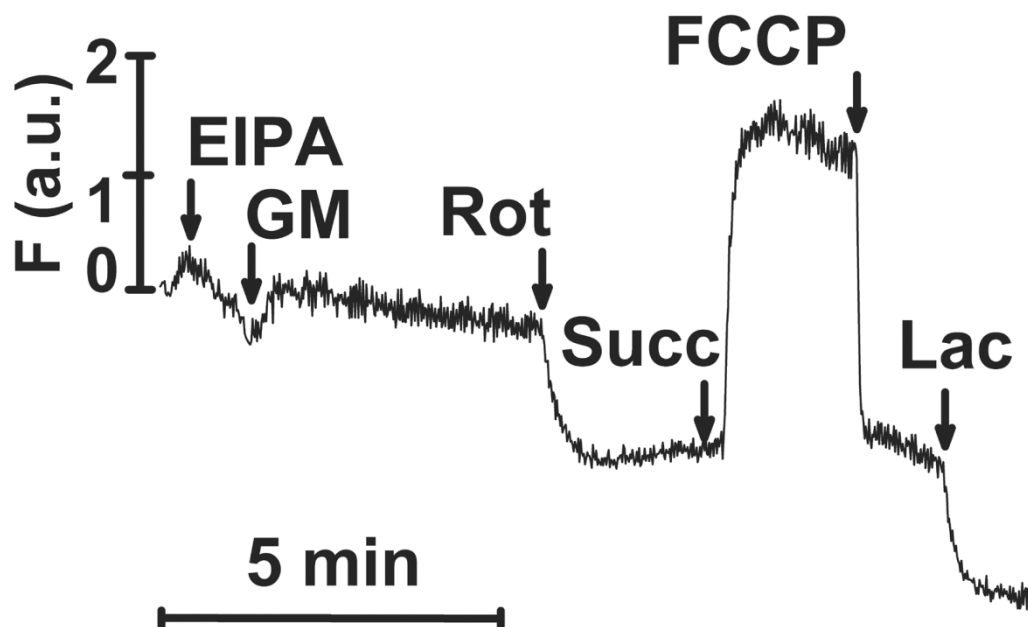


FIGURE 15 Glutamate and malate-driven H^+ -pumping is prevented by EIPA added before the substrates in isolated rat liver mitochondria respiring in state 4. Matrix alkalization is shown for the following additions: 100 μ M EIPA, 5 mM glutamate plus 1 mM malate (GM, pH 7.2 adjusted with Tris), 10 μ M rotenone (Rot), 5 mM succinate (Succ, pH 7.2 adjusted with Tris), 1 μ M FCCP, and 1 mM lactate (Lac).

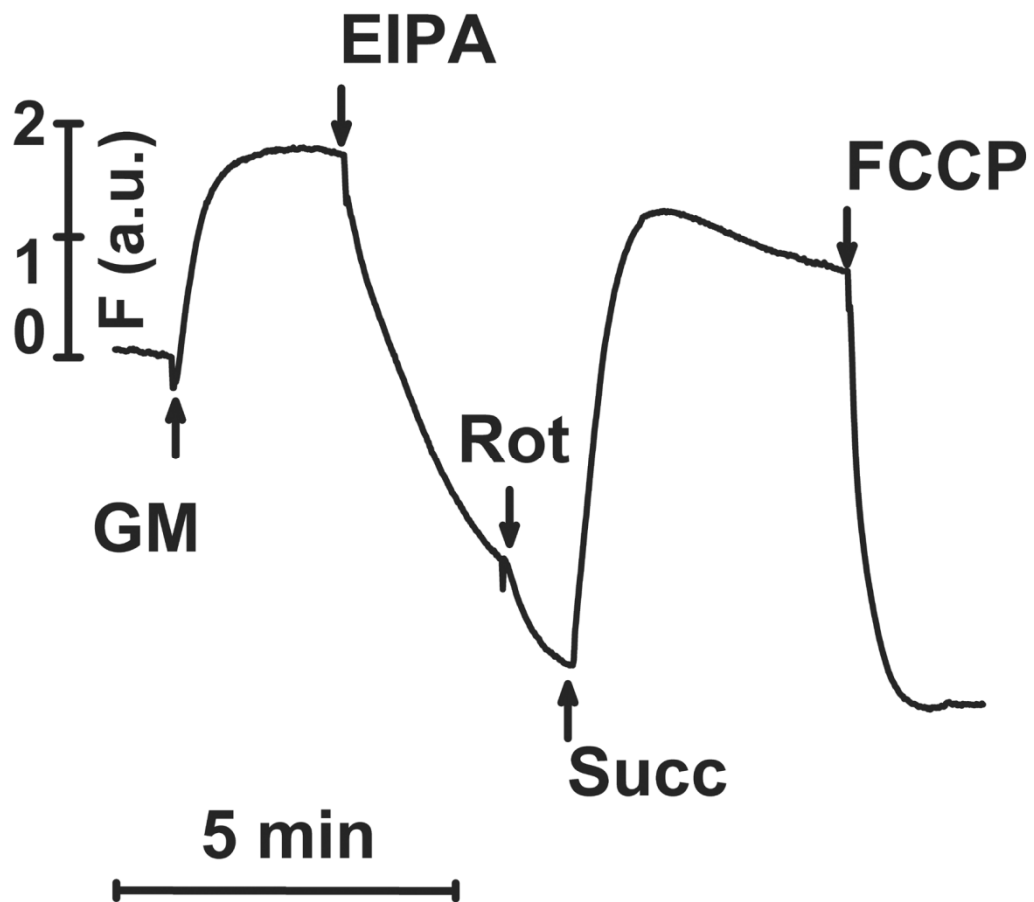


FIGURE 16 Glutamate and malate-driven H^+ -pumping is abolished by EIPA added after the substrates in isolated rat liver mitochondria respiring in state 4. Matrix alkalinization is shown for the following additions: 5 mM glutamate plus 1 mM malate (GM, pH 7.2 adjusted with Tris), 250 μ M EIPA, 10 μ M rotenone (Rot), 5 mM succinate (Succ, pH 7.2 adjusted with Tris), and 1 μ M FCCP.

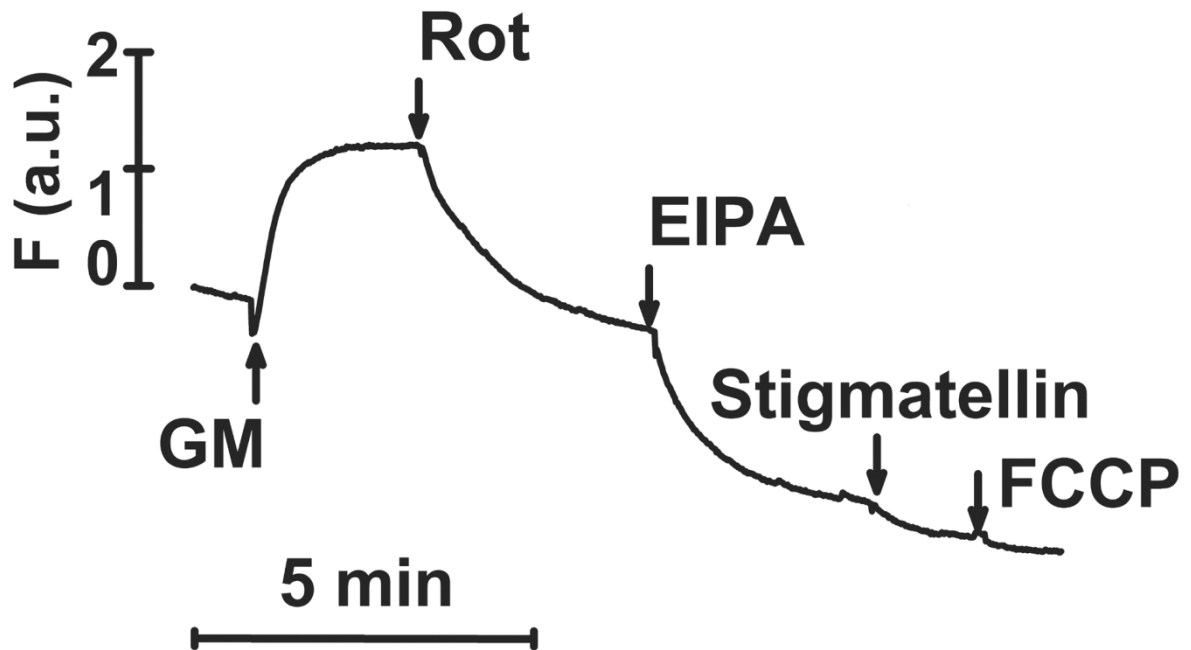


FIGURE 17 Inhibition of glutamate and malate-driven H^+ -pumping by rotenone is further suppressed by EIPA in isolated rat liver mitochondria respiring in state 4. Matrix alkalization is shown for the following additions: 5 mM glutamate plus 1 mM malate (GM, pH 7.2 adjusted with Tris), 10 μ M rotenone (Rot), 100 μ M EIPA, 0.5 μ M stigmatellin, and 1 μ M FCCP.

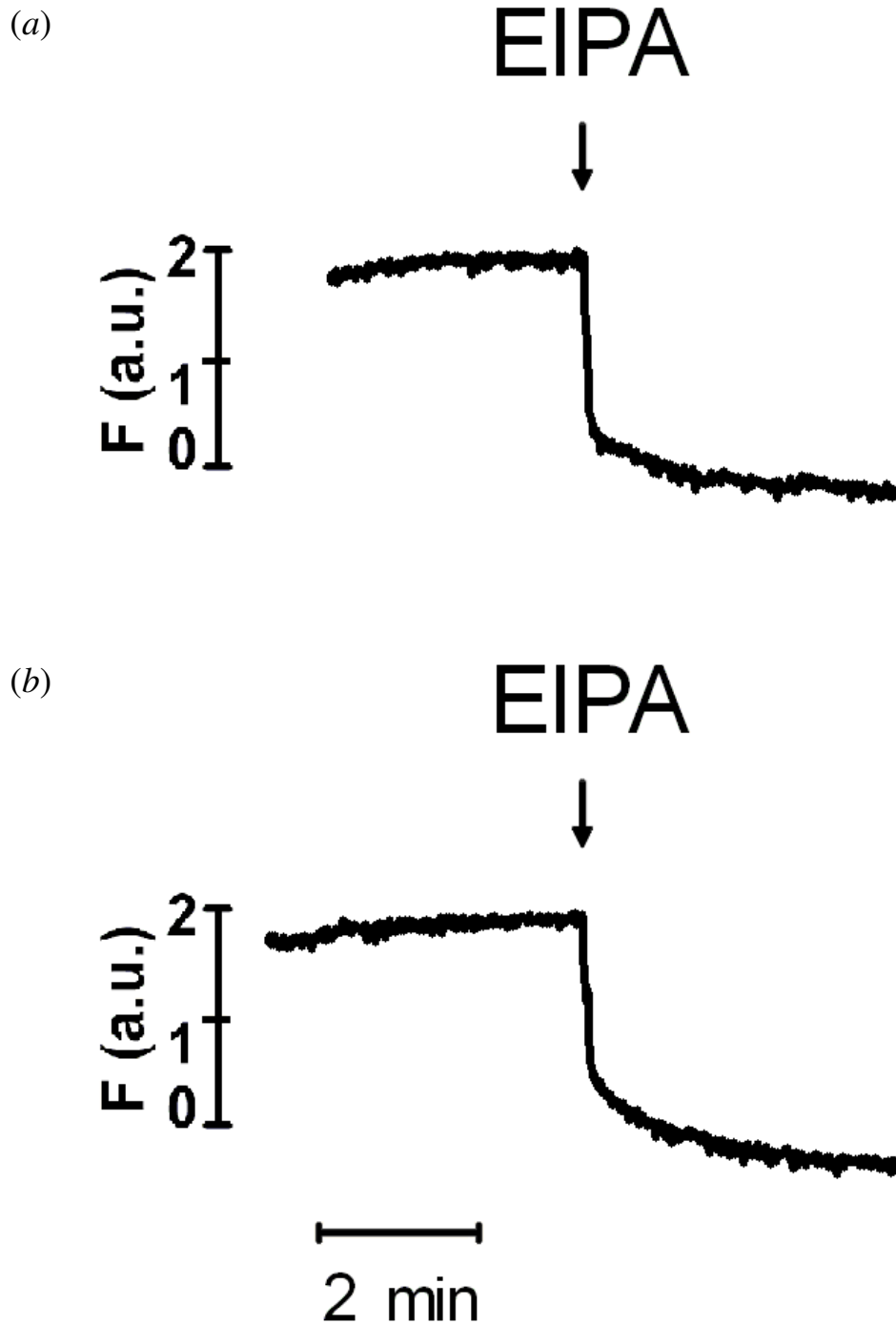


FIGURE 18 EIPA causes matrix acidification in the presence of glutamate, malate, and monensin in isolated rat liver mitochondria respiring in state 4. Matrix acidification is shown for 500 μ M EIPA. Assay medium was supplemented (prior to EIPA) with 1 μ M monensin in both traces and (a) 1 mM NaOH; (b) no further supplementation.

4.1.2 EIPA Inhibits Complex I Proton Pumping in Isolated Rat Liver Mitochondria Respiring in State 3

It has been shown by Dlasková *et al.* that FCCP was able to decrease rotenone-induced H_2O_2 production by $\sim 30\%$ in isolated rat liver mitochondria respiring in state 3 on glutamate and malate [1]. Hence, analogical conditions were used in the H^+ -pumping assay. State 3 was induced by 0.5 mM ADP, 0.5 mM potassium phosphate, and 100 μM MgCl_2 added after glutamate and malate (Fig. 19). This led to further matrix alkalization reflecting faster H^+ -pumping in phosphorylating mitochondria with released respiratory control. Predictably, phosphorylation-linked H^+ -pumping was subject to inhibition by oligomycin (Fig. 19). Addition of EIPA again stimulated matrix acidification accompanying the inhibition of H^+ -pumping (Fig. 19) with half-maximum inhibitory concentration of 50 μM EIPA (Fig. 20, page 51).

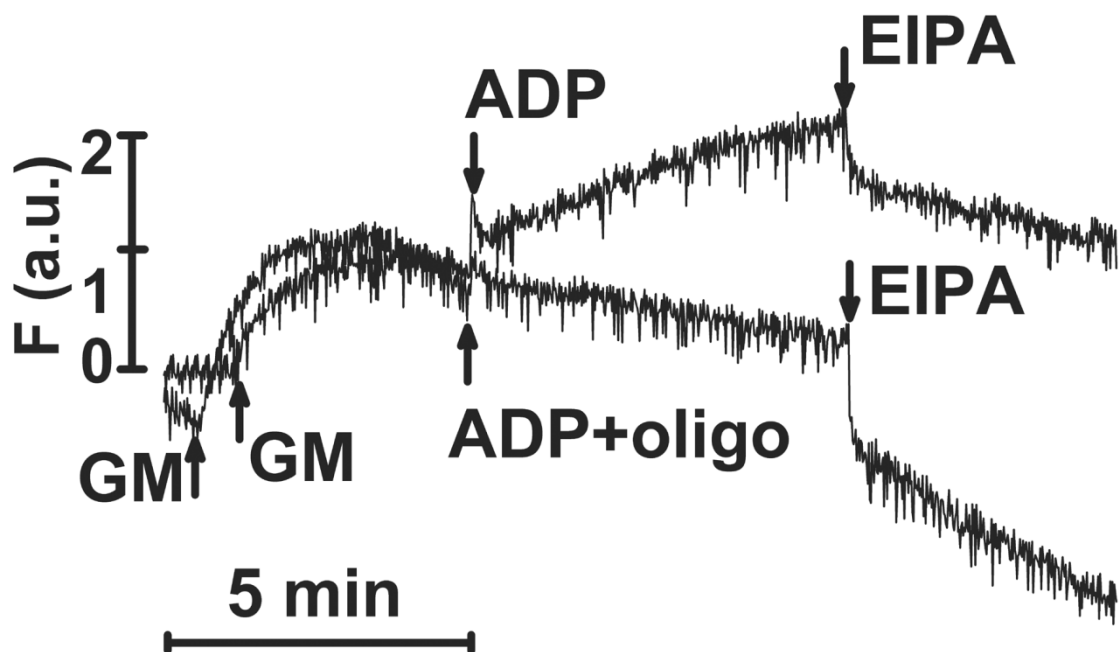


FIGURE 19 Glutamate and malate-driven H^+ -pumping is abolished by EIPA in isolated rat liver mitochondria respiring in state 3. Matrix alkalization is shown for two traces, distinguished by the presence of oligomycin, with the following additions: 5 mM glutamate plus 1 mM malate (GM, pH 7.2 adjusted with Tris), 100 μM EIPA, and 0.5 mM ADP which was added simultaneously with 0.5 mM KPi , 100 μM MgCl_2 plus or minus 2 $\mu\text{g/ml}$ oligomycin (oligo).

4.1.3 EIPA Exerts No Significant Effects on Respiration of Isolated Rat Liver Mitochondria

EIPA failed to inhibit mitochondrial state 4 respiration on glutamate and malate until EIPA levels went as high as 250 – 500 μM (Fig. 20, *page 51*). Within this concentration range, H^+ -pumping by Complex I was completely inhibited (Fig. 20, *page 51*). To conclude, experiments with EIPA indicate that electron flow is still conducted by the respiratory chain despite the inhibition of Complex I H^+ -pumping brought on by EIPA.

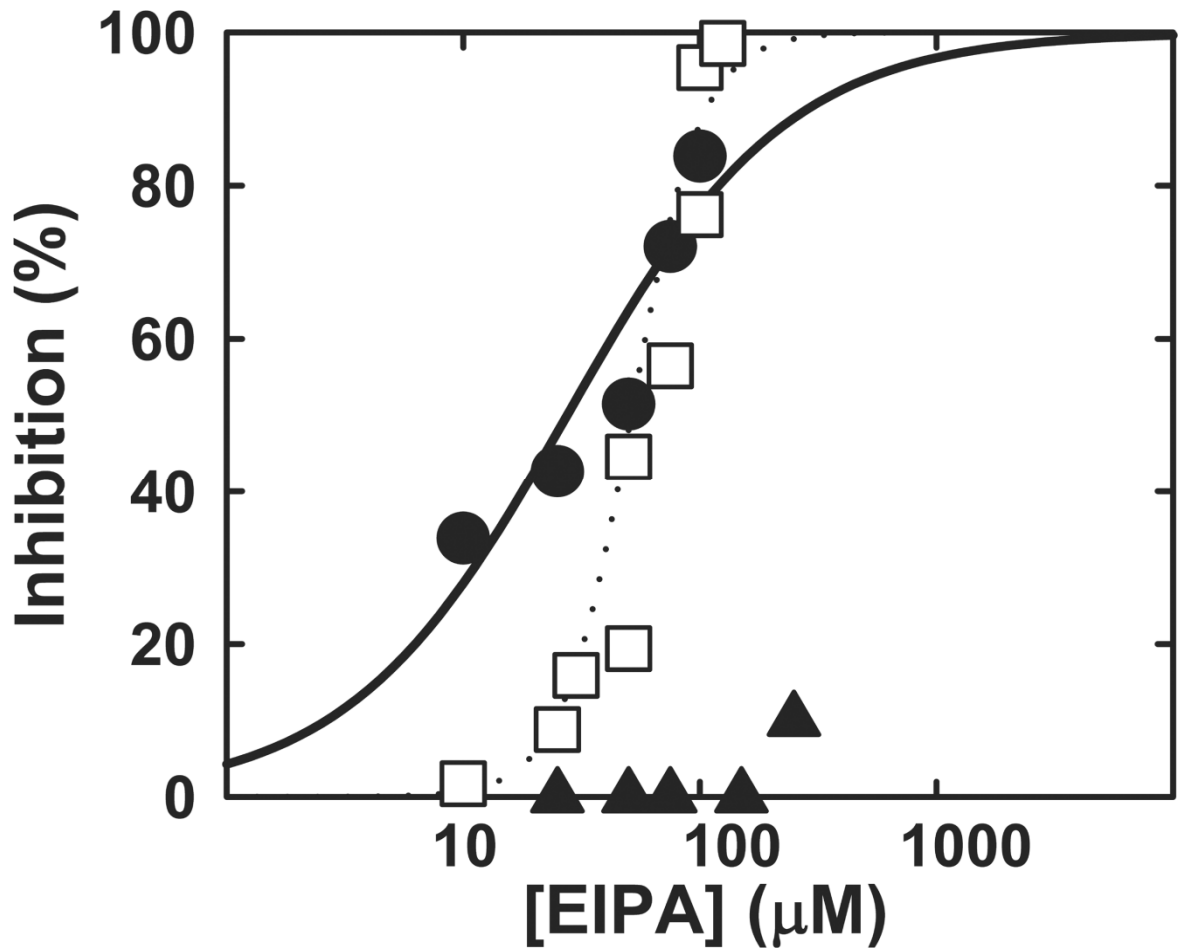


FIGURE 20 EIPA Dose-response curves for respiratory and H⁺-pumping inhibition of isolated rat liver mitochondria. Inhibitory action of EIPA was quantified for ● *closed circles*: H⁺-pumping in state 4 as the decrease in matrix alkalization stimulated by glutamate and malate after the addition of EIPA, IC₅₀ = 27 µM; □ *open squares*: H⁺-pumping in state 3 as the acidification induced by EIPA after the addition of glutamate and malate, IC₅₀ = 50 µM; ▲ *closed triangles*: respiratory rate in state 4. Data were fit using a Hill equation.

4.2 The Mechanism of Action of Mitochondrial Matrix-targeted Ubiquinone MitoQ₁₀

4.2.1 MitoQ₁₀ Accelerates Respiration of HepG2 Cells

The influences of MitoQ₁₀ on respiration of HepG2 cells were investigated by using high-resolution respirometry under two different cellular metabolic conditions (Table 4, pages 53–54). When cultivated in high glucose (25 mM), cells (GLC25) are forced to use glycolysis as the main metabolic pathway for energy production. At saturating concentration added to GLC25 cells, MitoQ₁₀ sequentially increased state 3 respiration (Fig. 21, page 55, Table 4, pages 53–54), *i.e.* basal respiration before the addition of oligomycin, on average up to 1.5-fold over the basal value. The accelerated level corresponds to ~ 60% of uncoupled respiration, *i.e.* maximum sustainable rotenone-sensitive respiration stimulated by uncoupler (FCCP) added after oligomycin (Fig. 22, page 56, Table 4, pages 53–54). The half-maximum activation took place on average at 0.8 nM MitoQ₁₀ (Fig. 25, page 59, Table 4, pages 53–54). Analogous acceleration with comparable AC₅₀ was obtained for HepG2 cells grown in medium containing galactose and glutamine (Fig. 26, page 60, Table 4, pages 53–54). These cells rely predominantly on oxidative phosphorylation (OXPHOS cells) as the primary energy source. To compare the MitoQ₁₀ effect with a relevant negative control, DecylTPP, which lacks the ubiquinone moiety, was employed. It came as no surprise that almost no activation took place when DecylTPP was tested in GLC25 or OXPHOS cells (Fig. 25, page 59, Table 4, pages 53–54). According to Dlasková *et al.*, rotenone stimulates O₂^{•-} production by inhibiting Complex I electron transport [1, 114]. At saturating doses of rotenone (20 μM), respiration of GLC25 and OXPHOS cells was suppressed down to residual 15% and 11%, respectively (Fig. 23, page 57, Table 4, pages 53–54). Consequent pulses of MitoQ₁₀ reestablished 67% and 45% levels of state 3 respiration in GLC25 and OXPHOS cells, respectively (Fig. 23, page 57, Table 4, pages 53–54). The half-maximum effect took place at similar concentrations when no rotenone was present for both GLC25 (Fig. 25, page 59) and OXPHOS (Fig. 26, page 60) cells, see also Table 4 (pages 53–54).

DecylTPP elicited an insignificant effect (Fig. 24, page 58, Table 4, pages 53–54).

TABLE 4 Effects of MitoQ₁₀ in GLC25 and OXPPOS HepG2 cells^a.

Parameter	HepG2 cells cultivated in 25 mM glucose		HepG2 cells cultivated in galactose and glutamine	
	GLC25 cells		OXPPOS cells	
<i>MitoQ₁₀ activation of cell respiration</i>				
State 3 activation by MitoQ₁₀ (% of state 3)	146 ± 15%	<i>n</i> = 7	150 ± 40%	<i>n</i> = 9
Activation by MitoQ₁₀ after rotenone (% of state 3)	67 ± 30%	<i>n</i> = 7	45 ± 21%	<i>n</i> = 3
MitoQ₁₀ activation after rotenone (% of rotenone- treated cells)	450 ± 250%	<i>n</i> = 5	550 ± 100%	<i>n</i> = 3
MitoQ₁₀ activation after rotenone and TTFA (% of state 3)	51 ± 27%	<i>n</i> = 3	28 ± 11%	<i>n</i> = 3
<i>Dose-response AC₅₀ values for activation of cell respiration</i>				
State 3 activation by MitoQ₁₀	0.8 ± 0.3 nM	<i>n</i> = 5	0.9 ± 0.3 nM	<i>n</i> = 9
Activation by MitoQ₁₀ after rotenone	1.0 ± 0.5 nM	<i>n</i> = 3	1.3 ± 0.4 nM	<i>n</i> = 3
Activation by MitoQ₁₀ after rotenone and TTFA	2.0 ± 0.5 nM	<i>n</i> = 3	3.5 ± 2.0 nM	<i>n</i> = 3
<i>Lack of respiratory activation by DecylTPP</i>				
State-3 activation by DecylTPP (% of state 3)	105 ± 10%	<i>n</i> = 7	110 ± 8%	<i>n</i> = 5
Activation by DecylTPP after rotenone (% of state 3)	19 ± 2%	<i>n</i> = 5	17 ± 5%	<i>n</i> = 5
Activation by DecylTPP after rotenone (% of rotenone-treated cells)	104 ± 20%	<i>n</i> = 5	109 ± 8%	<i>n</i> = 5
Activation by DecylTPP after rotenone and TTFA (% of state 3)	30 ± 8%	<i>n</i> = 3	10 ± 7%	<i>n</i> = 3

Main respiratory parameters

State 3 respiration per 10⁶ cells (pmol.O₂.s⁻¹)	51 ± 17	n = 50	97 ± 24	n = 40
State 3/state 4 respiration	4 ± 0.5	n = 8	5.1 ± 1.6	n = 8
Uncoupled state/state 3	1.7 ± 0.2	n = 8	1.8 ± 0.2	n = 5
Remaining respiration at 20 µM rotenone (% of state 3)	15 ± 5%	n = 6	11 ± 1%	n = 5
State 3/state 4 respiration after a 24-h incubation with MitoQ₁₀	3.2 ± 0.3	n = 4	4 ± 0.1	n = 2
State 3/state 4 respiration after a 24-h incubation with DecylTPP	1.9 ± 0.1	n = 2	2.05 ± 0.1	n = 2

^aState 4 respiration was established by 1 µg.ml⁻¹ oligomycin.

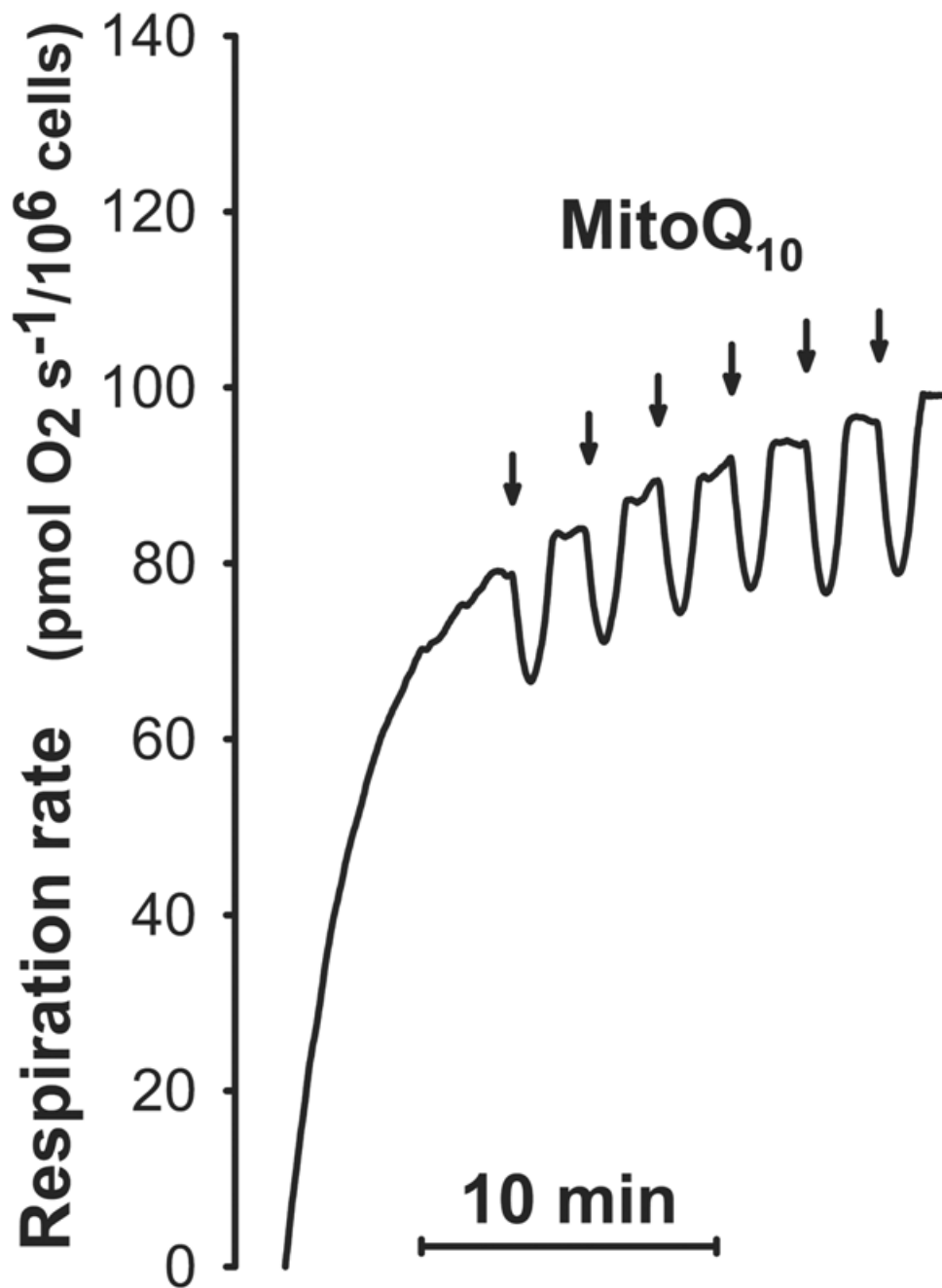


FIGURE 21 MitoQ₁₀ stimulates state 3 respiration of GLC25 HepG2 cells. Cells were treated, as indicated at each arrow, with 0.2 nM MitoQ₁₀.

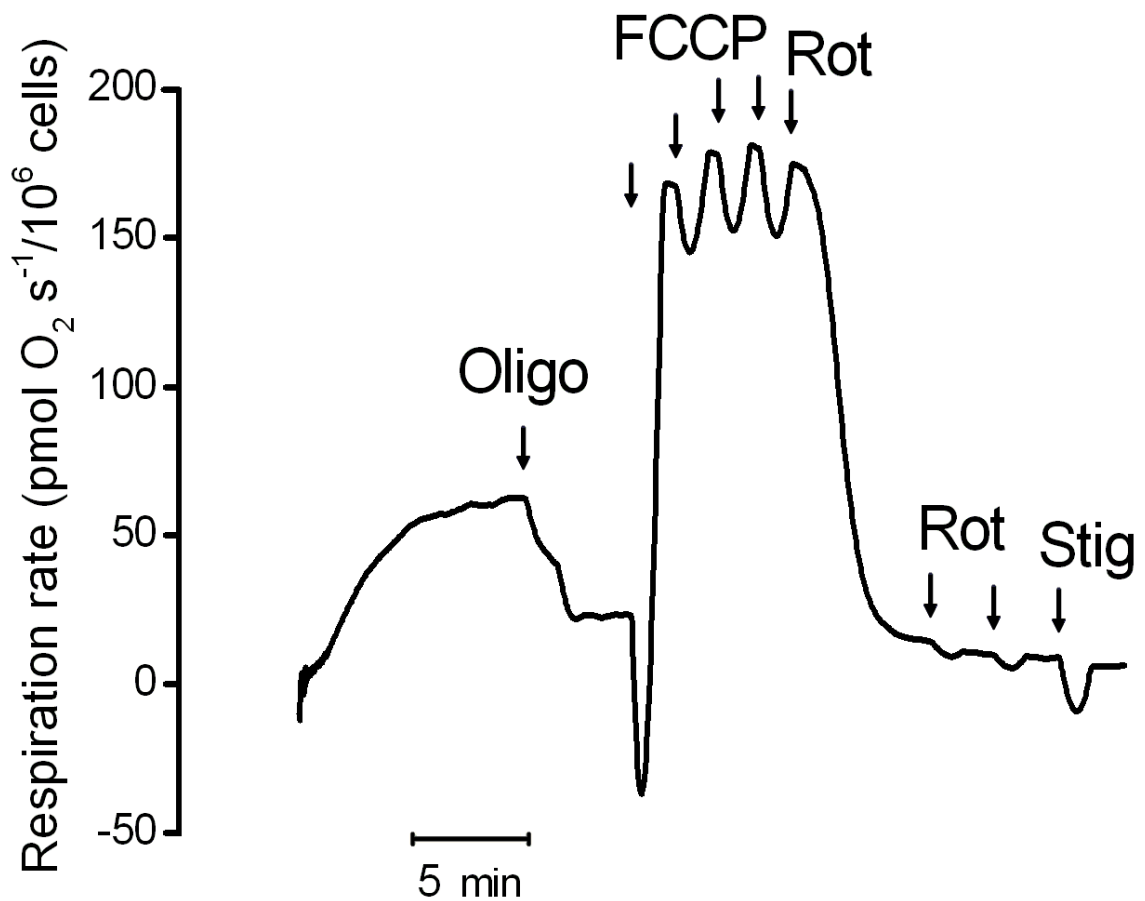


FIGURE 22 Increased state 4 respiration of GLC25 HepG2 cells. After the addition of 0.1 $\mu\text{g/ml}$ oligomycin to establish state 4, the respiration was uncoupled by 4 μM FCCP with maximum respiration achieved by the titration with 1 μM FCCP aliquots (added three times), followed by three subsequent additions of 100 nM Rot and fully inhibited by 1 μM stigmatellin.

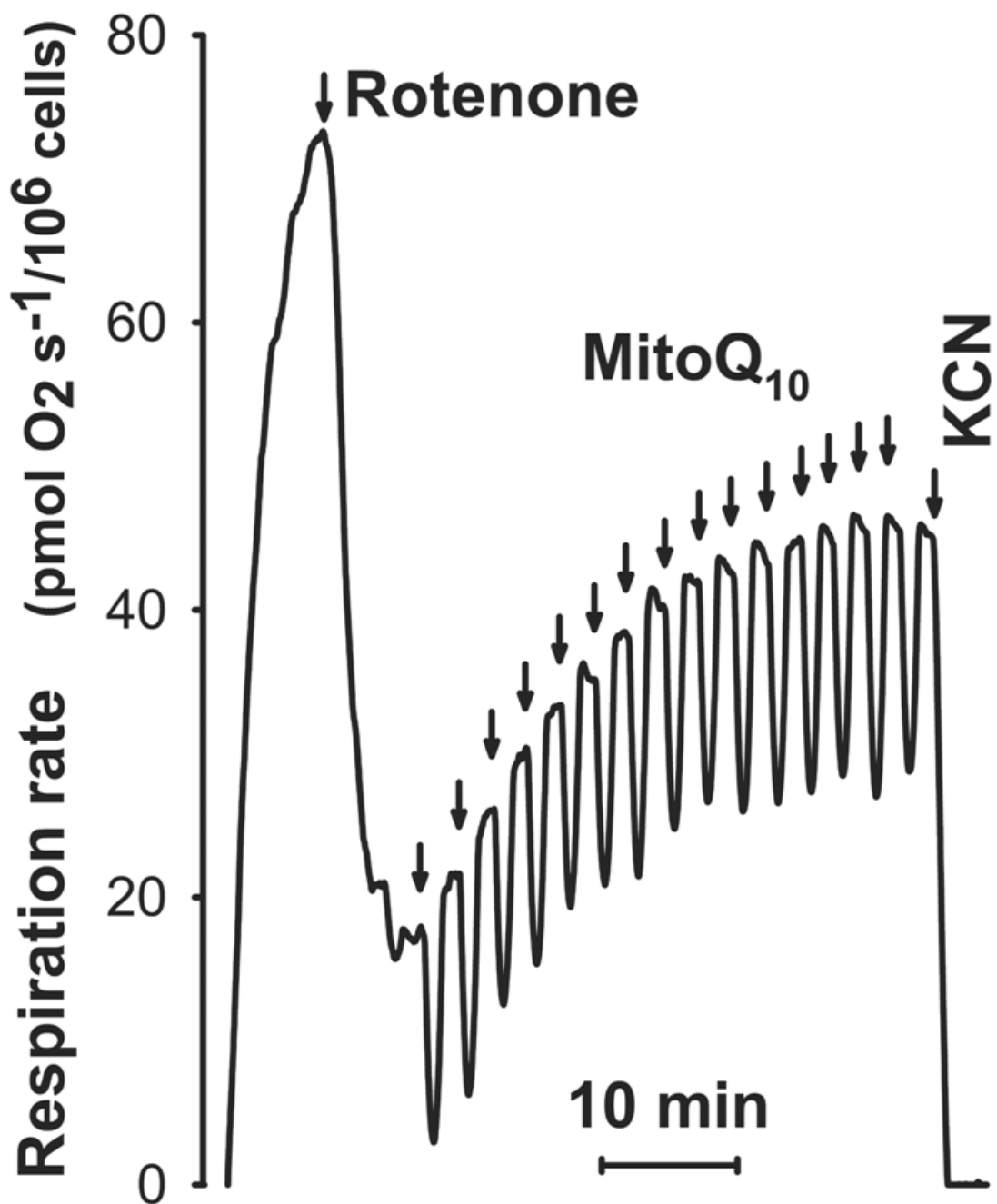


FIGURE 23 MitoQ₁₀ activation of state 3 respiration in the presence of rotenone. GLC25 cells were treated, as indicated at each arrow, with 1 μM rotenone plus 0.2 nM MitoQ₁₀ and 1 mM KCN.

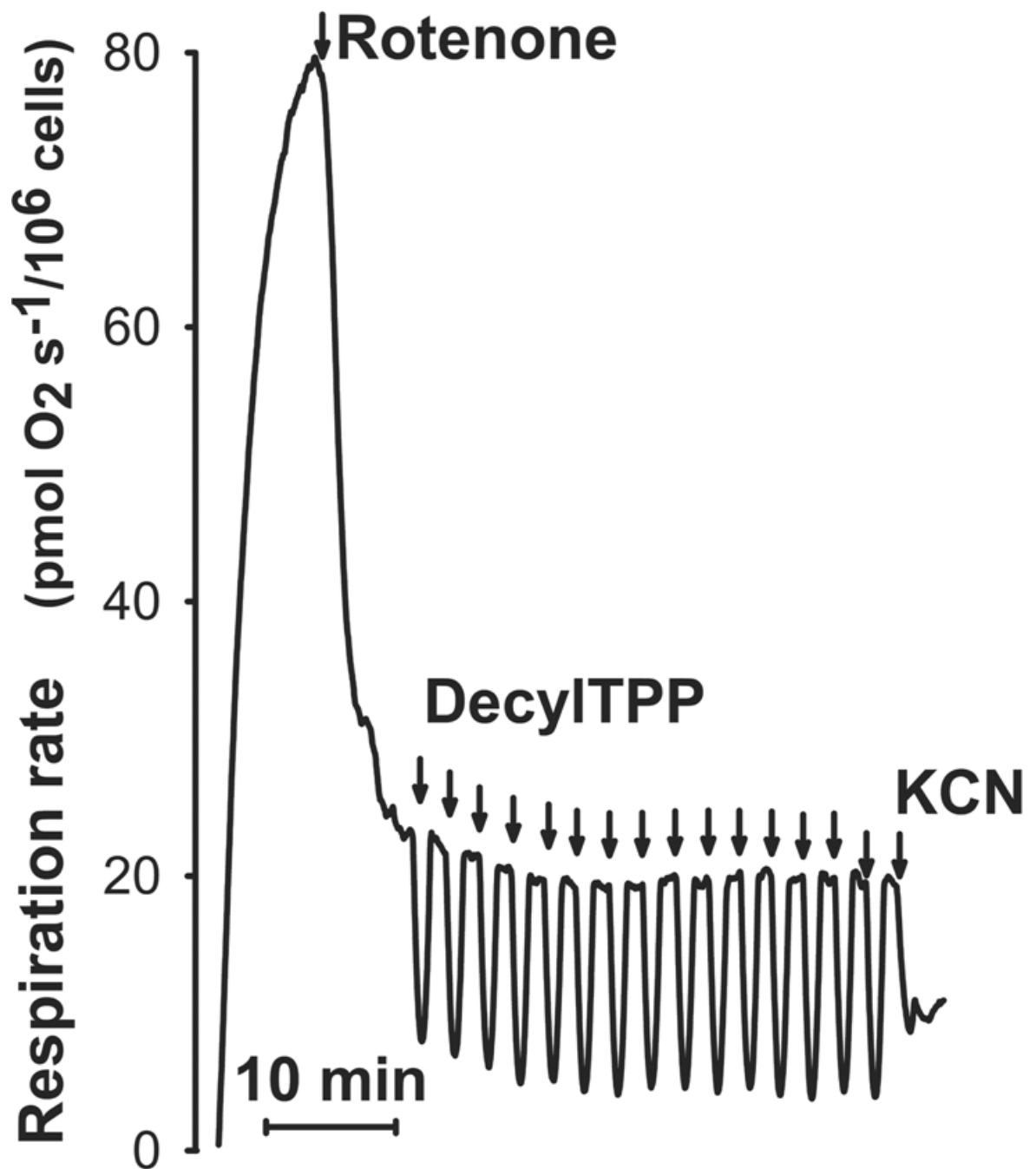


FIGURE 24 DecylTPP fails to stimulate state 3 respiration of GLC25 HepG2 cells. Cells were treated, as indicated at each arrow, with 1 μ M rotenone plus 0.2 nM DecylTPP and 1 mM KCN.

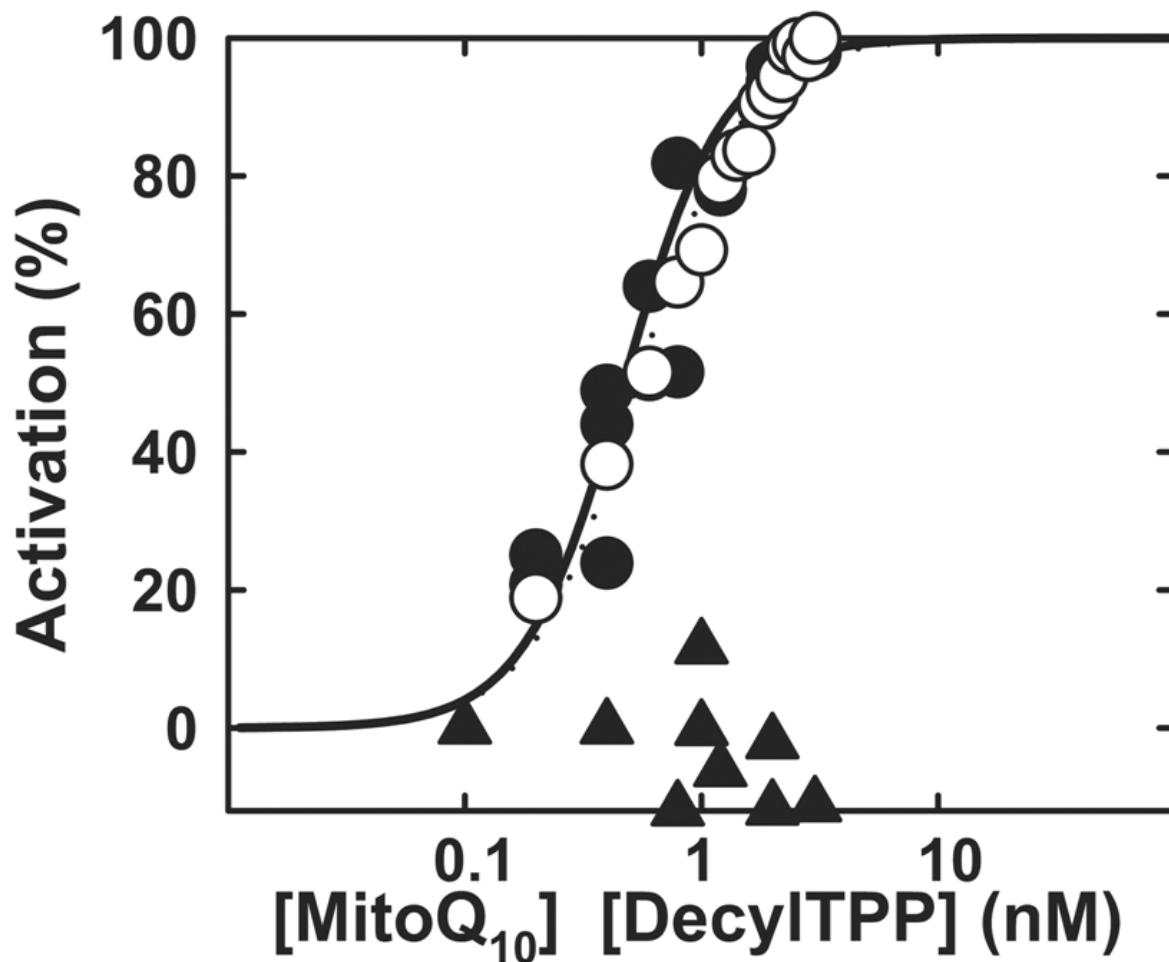


FIGURE 25 MitoQ₁₀ dose responses for respiratory acceleration in GLC25 HepG2 cells. Cells were treated with MitoQ₁₀ in the ● *closed circles*: absence of rotenone, AC₅₀ = 0.6 nM; ○ *open circles*: presence of 1 μM rotenone, AC₅₀ = 0.6 nM; or ▲ *closed triangles*: with DecylTPP alone. Titration data, exemplified in Figs. 21, 23–24 (pages 55, 57–58), were fit using a Hill equation.

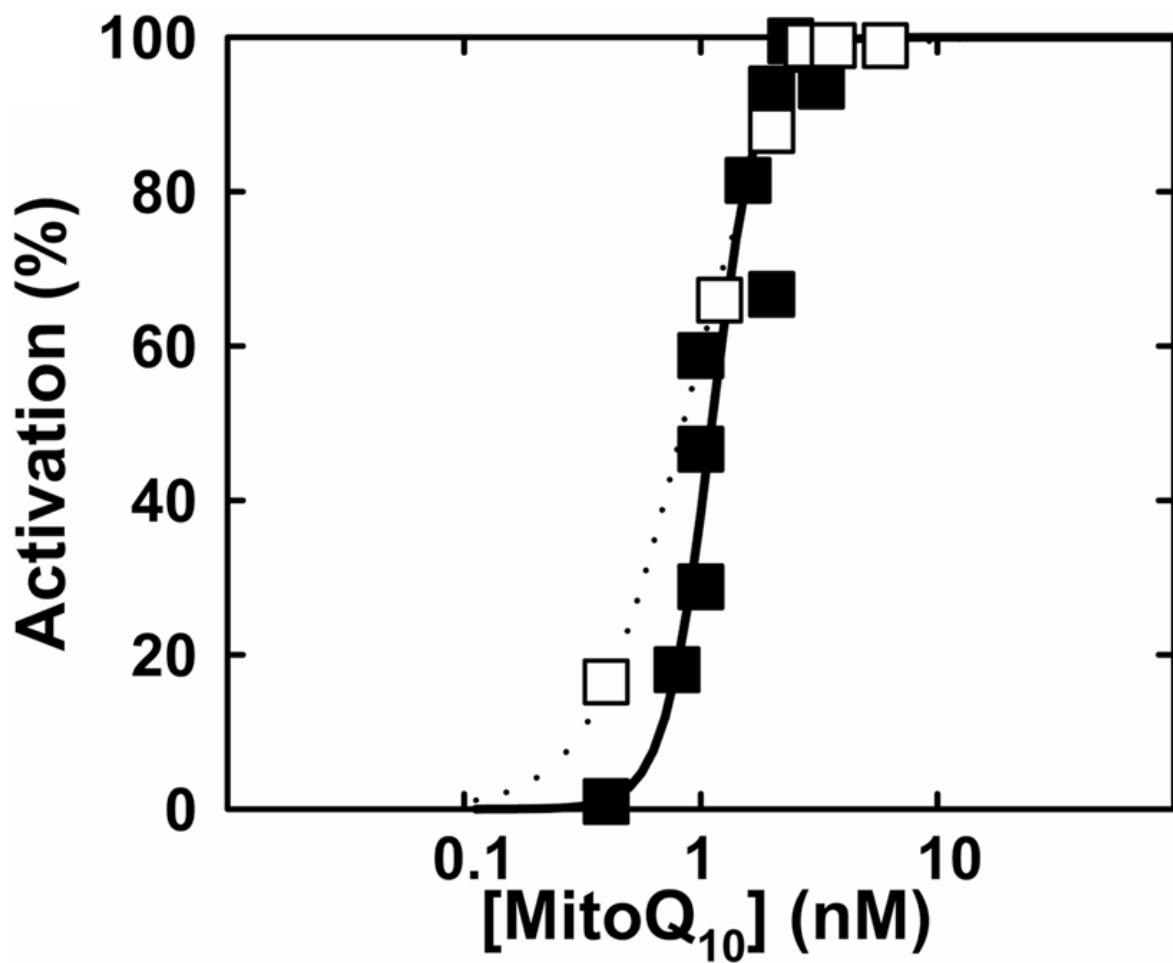


FIGURE 26 MitoQ₁₀ dose responses for respiratory acceleration in OXPHOS HepG2 cells. Cells were treated with MitoQ₁₀ in the *closed squares*: absence of rotenone, AC₅₀ = 1.1 nM; *open squares*: presence of 1 μM rotenone, AC₅₀ = 0.9 nM. Titration data were fit using a Hill equation.

4.2.2 Respiration Increase Induced by MitoQ₁₀ Requires Complexes II and III

MitoQ₁₀-induced HepG2 cell respiration increase was abolished by Complex III inhibitors antimycin A (Fig. 27, *page 62*), myxothiazol, and stigmatellin (not shown) independently of rotenone, thus localizing the MitoQ₁₀ effect upstream of Complex III. Similarly, 2-thenoyltrifluoroacetone (TTFA), a Complex II inhibitor [263], in conjunction with rotenone entirely prevented substrate funneling into the electron transport of HepG2 GLC25 and OXPHOS cells, virtually slowing down their respiration to zero. Surprisingly, MitoQ₁₀ slightly restored the rotenone and TTFA-inhibited respiration (Fig. 28, *page 63*, Table 4, *pages 53–54*). This could be prevented by antimycin A, myxothiazol, or stigmatellin (not shown), suggesting the possibility that MitoQ₁₀ mimicks the role of substrate for either of, Complex III or Complex IV (cytochrome *c* oxidase). Another explanation would involve direct competition between MitoQ₁₀ and TTFA on Complex II, allowing respiration to become slightly reaccelerated.

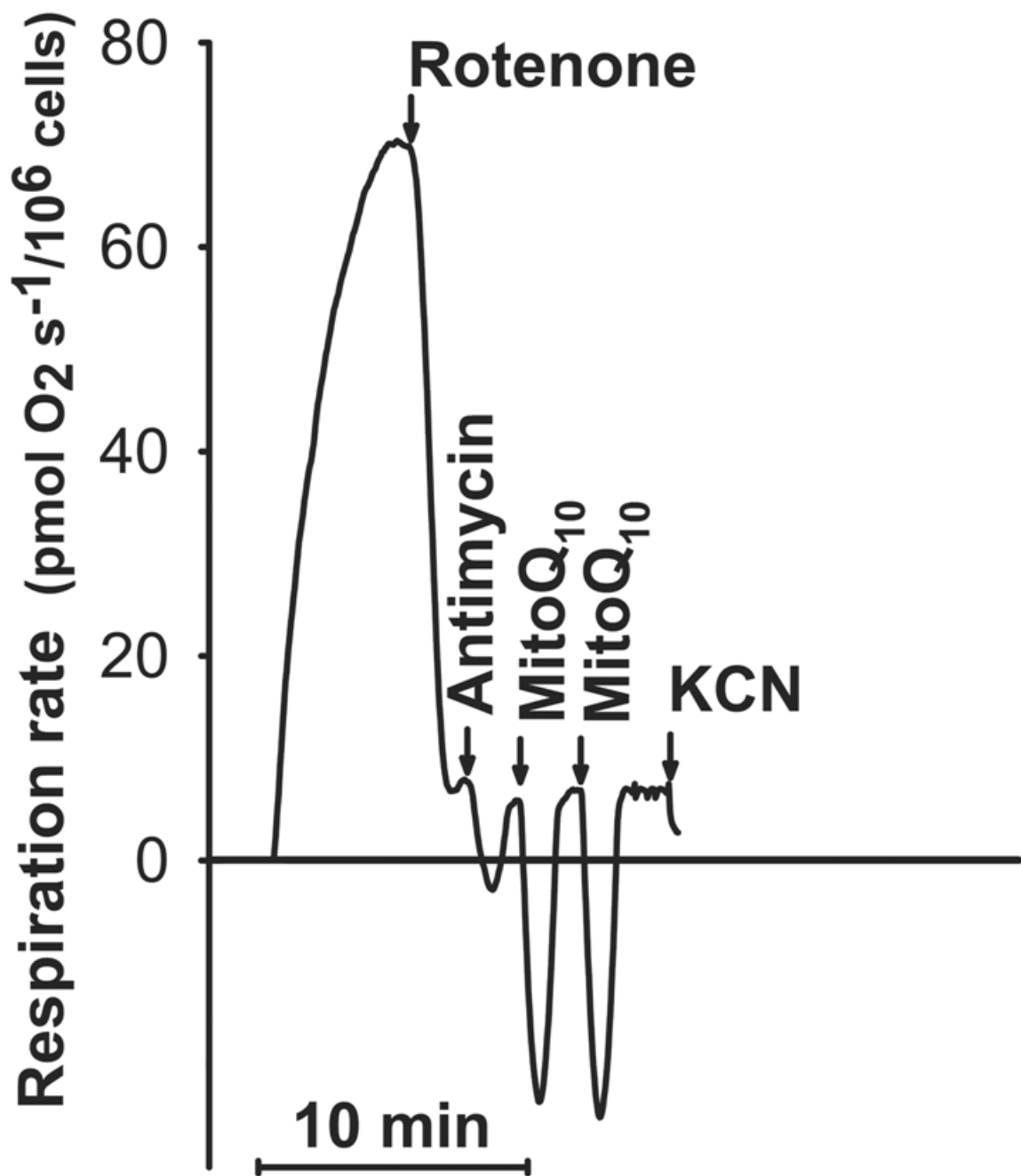


FIGURE 27 MitoQ₁₀ fails to restore rotenone-inhibited respiration in the presence of antimycin A in OXPHOS HepG2 cells. Respiration rates are shown for the following additions: 10 μM rotenone, 1.25 μM antimycin A, 1 nM MitoQ₁₀ (added twice), and 1 mM KCN.

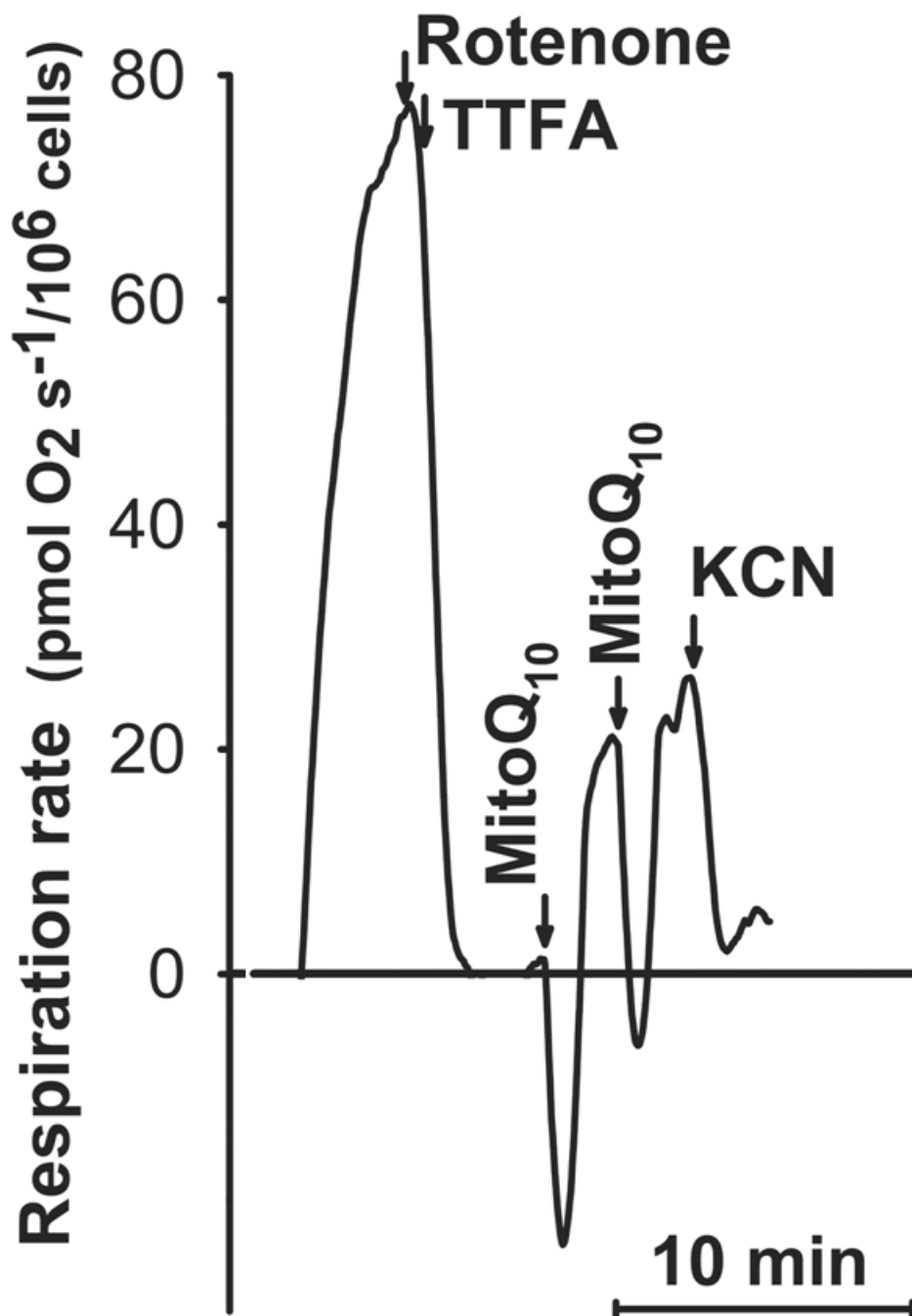


FIGURE 28 MitoQ₁₀ restores completely inhibited respiration in the presence of rotenone and TTFA in OXPPOS HepG2 cells. Respiration rates are shown for the following additions: 10 μ M rotenone, 40 μ M TTFA, 1 nM MitoQ₁₀ (added twice), and 1 mM KCN.

4.2.3 MitoQ₁₀ Effects on Total H₂O₂ Formation in Isolated Rat Liver Mitochondria

Plecitá-Hlavatá *et al.* claim that MitoQ₁₀ exerts its pro-oxidant action in intact cells, but by contrast it serves as an antioxidant due to excess superoxide generation by Complex I when electron flow is inhibited, *e.g.* by rotenone [2]. To compare these results, which were obtained by using MitoSOX Red fluorescence confocal microscopy O₂^{•-} monitoring, with the behavior of isolated mitochondria, Amplex Red H₂O₂ detection assay was used on mitochondria supplemented with a mix of respiratory substrates. The combination of both, Complex I-linked substrates (glutamate plus malate) and Complex II-linked substrates (succinate) applied to rat liver mitochondria, contributes to a better approximation of *in vivo* conditions. Mitochondria were allowed to undergo either state 4 respiration or state 3 respiration, the latter was induced by 0.5 mM ADP, 0.5 mM potassium phosphate together with 100 μM MgCl₂, and lasted more than 10 minutes (this was verified by an Oxygraph).

H₂O₂ production was slightly elevated by rotenone in state 3 of mitochondrial respiration (Fig. 29, page 65), which is the only observation in accordance with the results of Plecitá *et al.* reported for cells [2]. In contrast, H₂O₂ production was slightly reduced by rotenone in state 4 respiration (Fig. 29, page 65), indicating an inhibitory effect of rotenone on the reverse electron transport. Moreover, MitoQ₁₀ showed only a slight pro-oxidant effect in state 4 respiration whereas doubled H₂O₂ production in state 3 as compared to the controls (Fig. 29, page 65). In the presence of rotenone, MitoQ₁₀ raised state 4 and state 3 H₂O₂ formation 1.75-fold and 2.5-fold, respectively (Fig. 29, page 65). A significant MitoQ₁₀ pro-oxidant effect was observed also with rotenone, EIPA, and FCCP (Fig. 29, page 65). The modest increase of H₂O₂ production brought on by MitoQ₁₀ in state 4 respiration with TTFA, in either presence or absence of rotenone, was exceeded in state 3 (Fig. 30, page 66). DecylTPP took no effect (Figs. 29–30, pages 65–66), while TTFA diminished the basal level of H₂O₂ formation stipulated by rotenone. High levels of H₂O₂ formation ($\geq 250\%$ of the level established by rotenone) occurred upon the application of antimycin A, stigmatellin, and myxothiazol, Complex III inhibitors, in

combination with rotenone and MitoQ₁₀, plus or minus TTFA (Fig. 31, page 67).

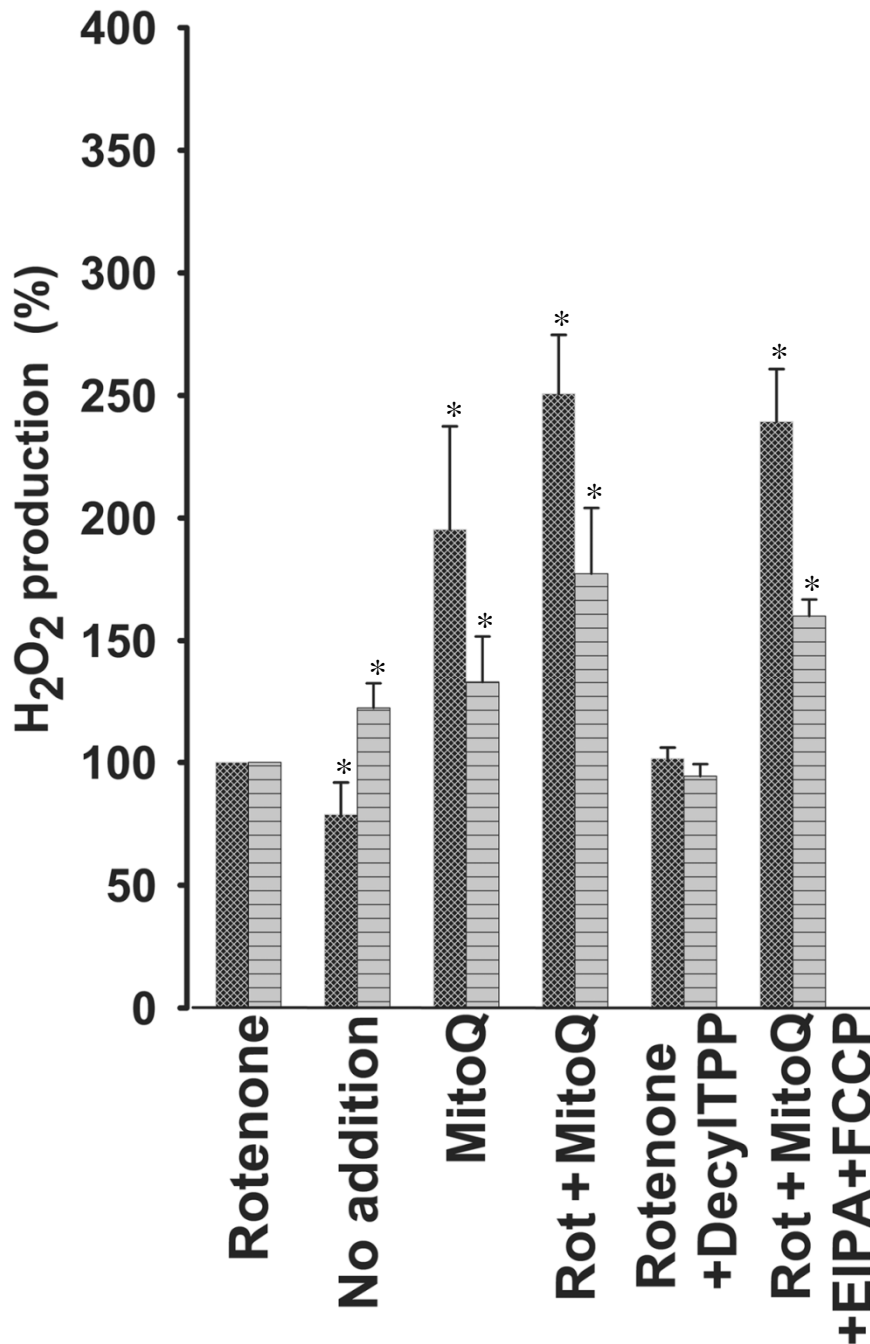




FIGURE 29 MitoQ₁₀-induced generation of H₂O₂ by isolated rat liver mitochondria. Mitochondria were allowed to respire on 5 mM glutamate, 1 mM malate, and 5 mM succinate.  *hatched bars*: H₂O₂ production at state 3 respiration set by 0.5 mM ADP, 0.5 mM K_P_i, and 100 μM MgCl₂ (n = 3);  *horizontally-crossed bars*: H₂O₂ production at state 4 respiration. Reagent concentrations were: 1 nM MitoQ₁₀, 1 nM DecylTPP, 1 μM EIPA, 1 μM FCCP. Rates were normalized to 20 μM rotenone (taken as 100%).

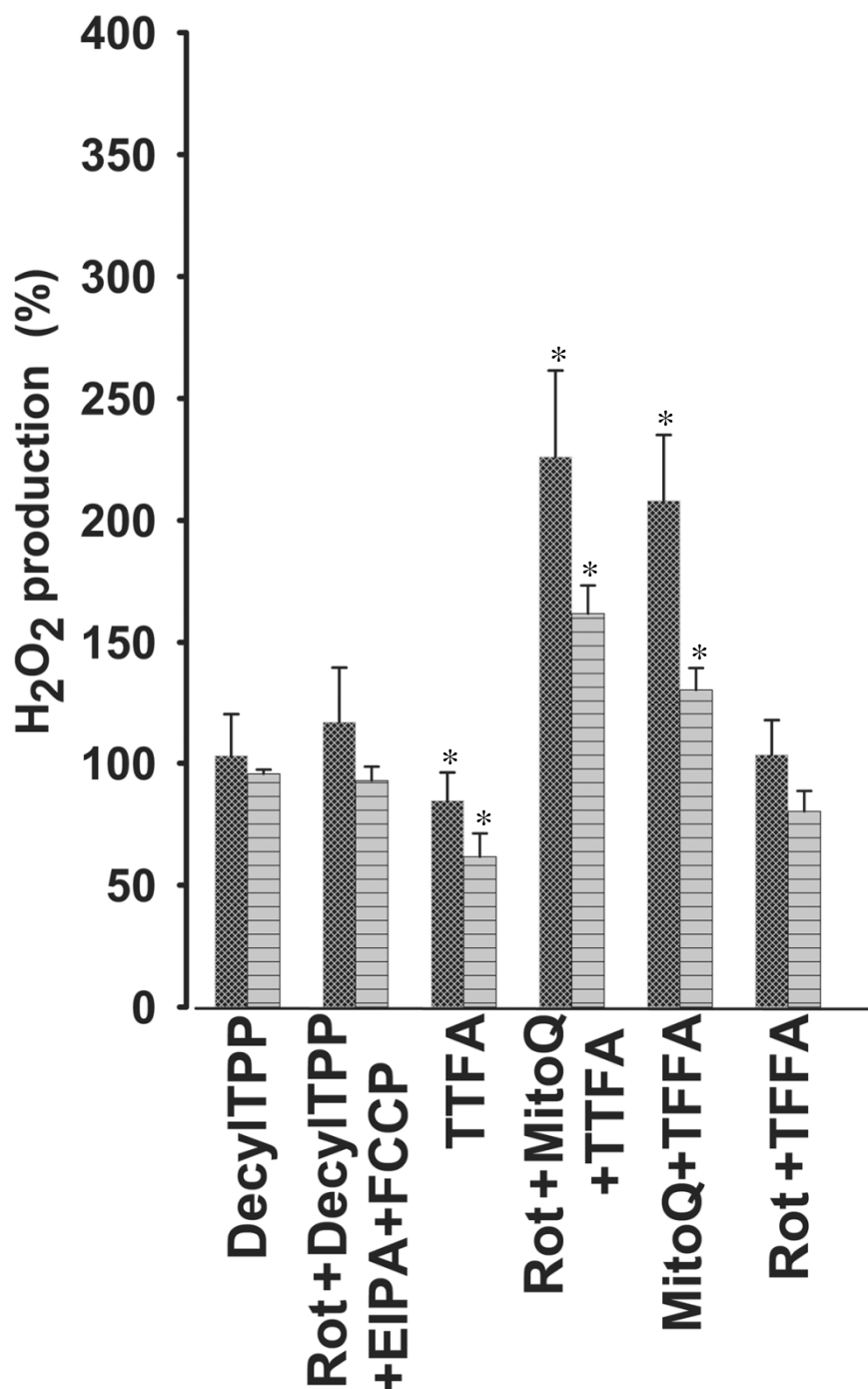




FIGURE 30 MitoQ₁₀-induced generation of H₂O₂ by isolated rat liver mitochondria in the presence of TTFA. Isolated mitochondria were allowed to respire on 5 mM glutamate, 1 mM malate, and 5 mM succinate.  *hatched bars*: H₂O₂ production at state 3 respiration set by 0.5 mM ADP, 0.5 mM KP₁, and 100 μM MgCl₂ (n = 3);  *horizontally crossed bars*: H₂O₂ production at state 4. Reagent doses were: 1 nM MitoQ₁₀, 1 nM DecylITPP, 1 μM EIPA, 1 μM FCCP, and 10 μM TTFA. Rates were normalized to 20 μM rotenone (taken as 100%).

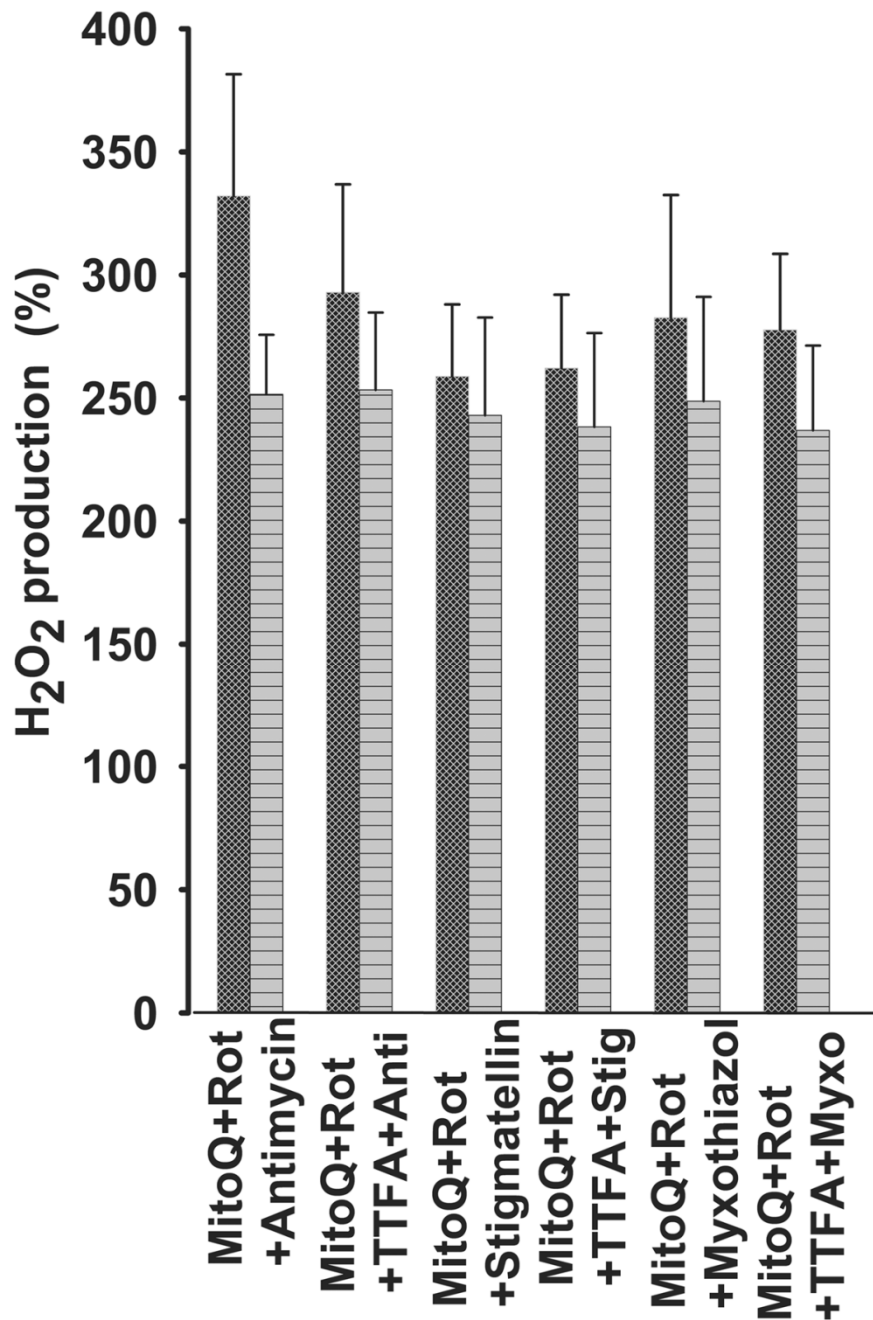

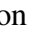


FIGURE 31 MitoQ₁₀-induced generation of H₂O₂ by isolated rat liver mitochondria in the presence of Complex III inhibitors. Isolated mitochondria were allowed to respire on 5 mM glutamate, 1 mM malate, and 5 mM succinate.  *hatched bars*: H₂O₂ production at state 3 respiration set by 0.5 mM ADP, 0.5 mM KP_i, and 100 μM MgCl₂ (*n* = 3);  *horizontally crossed bars*: H₂O₂ production at state 4 respiration. Reagent concentrations were: 1 nM MitoQ₁₀, 10 μM TTFa, 2.5 μM antimycin A, 0.5 μM stigmatellin, and 1 μM myxothiazol. Rates were normalized to 20 μM rotenone (taken as 100%).

4.2.4 MitoQ₁₀ Effects on Respiration of Mitochondria Isolated from HepG2 Cells

Respiration experiments with isolated rat liver mitochondria had shown respiratory acceleration stimulated not only by MitoQ₁₀ but also by DecylTPP. This finding evoked the need of conducting further experiments with mitochondria isolated from HepG2 GLC25 cells. State 3 respiration driven by 5 mM glutamate, 1 mM malate and 5 mM succinate was induced, as previously, by the addition of 0.5 mM ADP, 0.5 mM potassium phosphate, and 100 μ M MgCl₂. The outcome (Fig. 32, page 69) was again a 1.37-fold (\pm 0.05, n = 3) increase in MitoQ₁₀-induced state 3 respiration with half-maximum effect occurring at 1 nM MitoQ₁₀, and a 1.4-fold (\pm 0.10) increase in rotenone-inhibited MitoQ₁₀-induced state 3 respiration acceleration with an AC₅₀ of 0.7 nM. High numbers were again obtained with DecylTPP, 1.36-fold (\pm 0.1) and 1.5-fold respiratory activation in the absence and presence of rotenone, respectively (state 3, glutamate, malate plus succinate substrate conditions, not shown). Different behavior of DecylTPP from the observed in experiments with cells *in situ* can be best explained by more pronounced partitioning of DecylTPP into the membranes of isolated mitochondria [264].

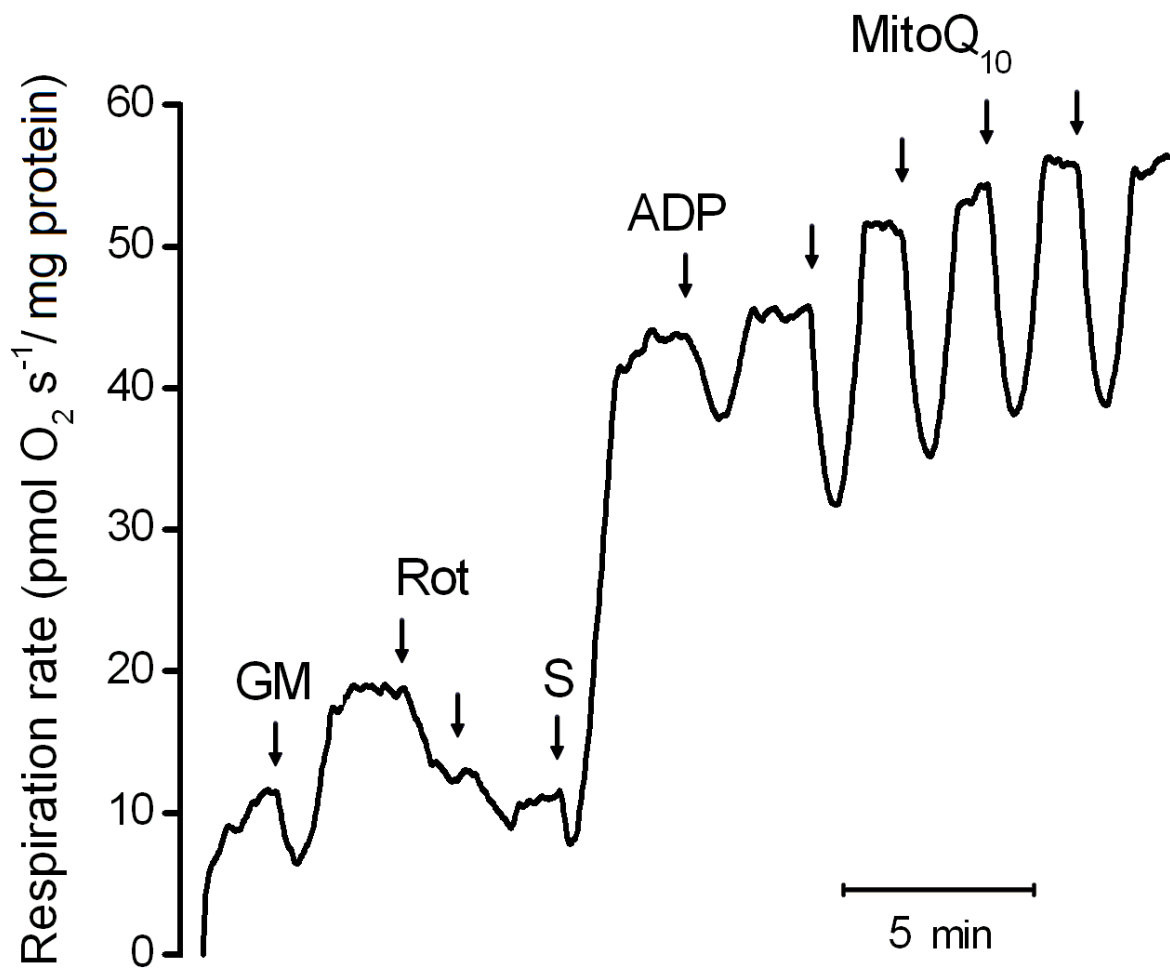


FIGURE 32 MitoQ₁₀ stimulates state 3 respiration of mitochondria isolated from GLC25 HepG2 cells in the presence of rotenone. Mitochondria (0.75 mg/ml) were treated with 5 mM glutamate plus 1 mM malate (GM), 0.5 μM rotenone (Rot) added twice, 5 mM succinate (S), 0.5 mM ADP added together with 0.5 mM potassium phosphate plus 100 μM MgCl₂, and 0.2 nM MitoQ₁₀ as indicated at each arrow.

4.3 ● Mitochondrial Phospholipase iPLA₂-Dependent Regulation of Uncoupling Protein 2

4.3.1 TBHP Induces Increase in Respiration of Isolated Rat Lung Mitochondria

Alán *et al.* determined the highest content of mouse UCP2 mRNA levels in lung among all other tissues analyzed by real-time RT-PCR [174], justifying lung as an eligible choice of tissue used in this project with the prospect of engaging UCP2-deficient mice in experiments described in chapter 4.3.3 (*page 77*). Abundant levels of UCP2 mRNA transcripts were found in rat lung as well, although surpassed by the content of UCP2 mRNA in spleen and heart tissues [174]. Hence, high-resolution respirometry was used to monitor respiration of isolated rat lung mitochondria respiring in state 4 with succinate as a substrate. Rotenone and oligomycin were included in the assay medium to ensure that respiration relies solely on forward electron transport originating from Complex II-linked substrates and no phosphorylation by Complex V was in effect, respectively.

Pro-oxidant *tert*-butyl hydroperoxide (TBHP) treatment was used to simulate lipid peroxidation. Possibly, traces of free Fe²⁺ and other transient metals in isolated mitochondria lead to a Fenton reaction under which species' ability to initiate lipid peroxidation arises. The resulting lipoperoxidized mitochondria would serve as the model for fatty acid release from membrane phospholipids. It was shown before that phospholipases A₂ are activated upon TBHP treatment [159]. Here, *tert*-butyl hydroperoxide (5 μM) stimulated basal respiration of rat lung mitochondria at saturating doses, see Fig. 33 (*page 71*). The observed respiratory acceleration might be explained on the basis of more pronounced uncoupling. Hence, FCCP (5 nM), a chemical uncoupler, was added to assess a partially uncoupled state of respiration (Fig. 33, *page 71*). Both, stimulated and the control trace leveled off at an equal rate of uncoupled respiration, but the former had been already elevated by TBHP.

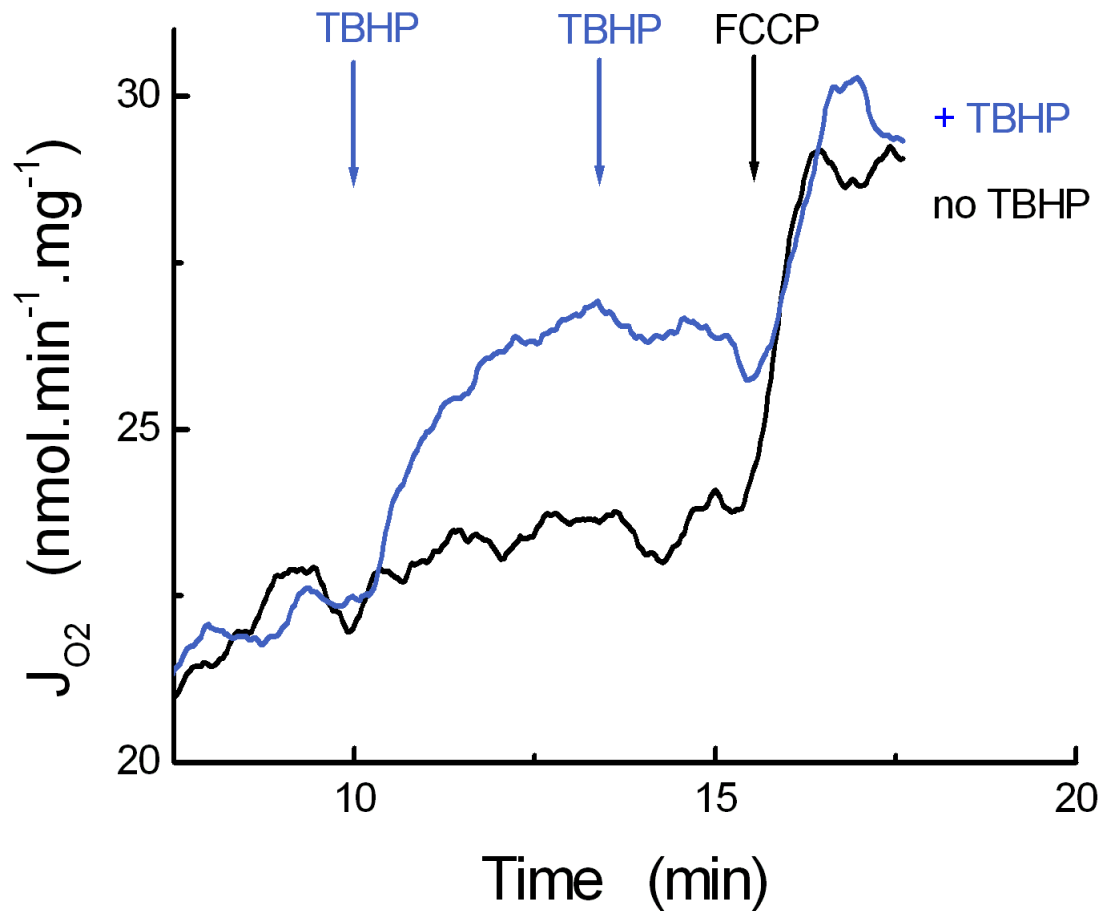


FIGURE 33 *tert*-Butyl hydroperoxide induces increase in respiration of isolated rat lung mitochondria. Mitochondria (0.2 mg/ml) were allowed to respire in the assay medium containing 10 mM succinate, 1 μM rotenone, and 1 $\mu\text{g}/\text{ml}$ oligomycin. Rates are shown for the following additions: 5 nM FCCP to both traces, and *black trace*: no further additions; *blue trace*: 5 μM TBHP (added twice).

4.3.2 Mitochondrial iPLA₂ Promotes UCP2-dependent Uncoupling

The respiration increase induced by TBHP was fully inhibited by BSA (Fig. 34, *page 73*), added before TBHP, indicating the participation of free fatty acids in the observed uncoupling. Note that free acids are required as substrates for UCP-dependent uncoupling. Furthermore, the TBHP-induced respiration increase was blocked by bromoenol lactone (BEL), see Figs. 35–36 (*pages 74–75*), a specific inhibitor of phospholipase iPLA₂ isoforms β and γ [143]. This is in line with the theoretical presumption that indeed free PUFAs and/or PUFAOOH were cleaved off the peroxidized phospholipids, thus supporting activation of mitochondrial iPLA₂ along with the proposed uncoupling activity (Fig. 33, *page 71*). This result could not have been reproduced by neither methyl arachidonyl fluorophosphonate (MAFP), nor arachidonyltrifluoromethyl ketone (AACOCF₃), specific inhibitors of α and β isoforms of mitochondrial iPLA₂ (not shown), pointing to the involvement of iPLA₂ γ isoform. The respiration increase brought on by TBHP was further amenable to partial inhibition by GTP (Fig. 37, *page 76*), an inhibitor of UCP2 [265].

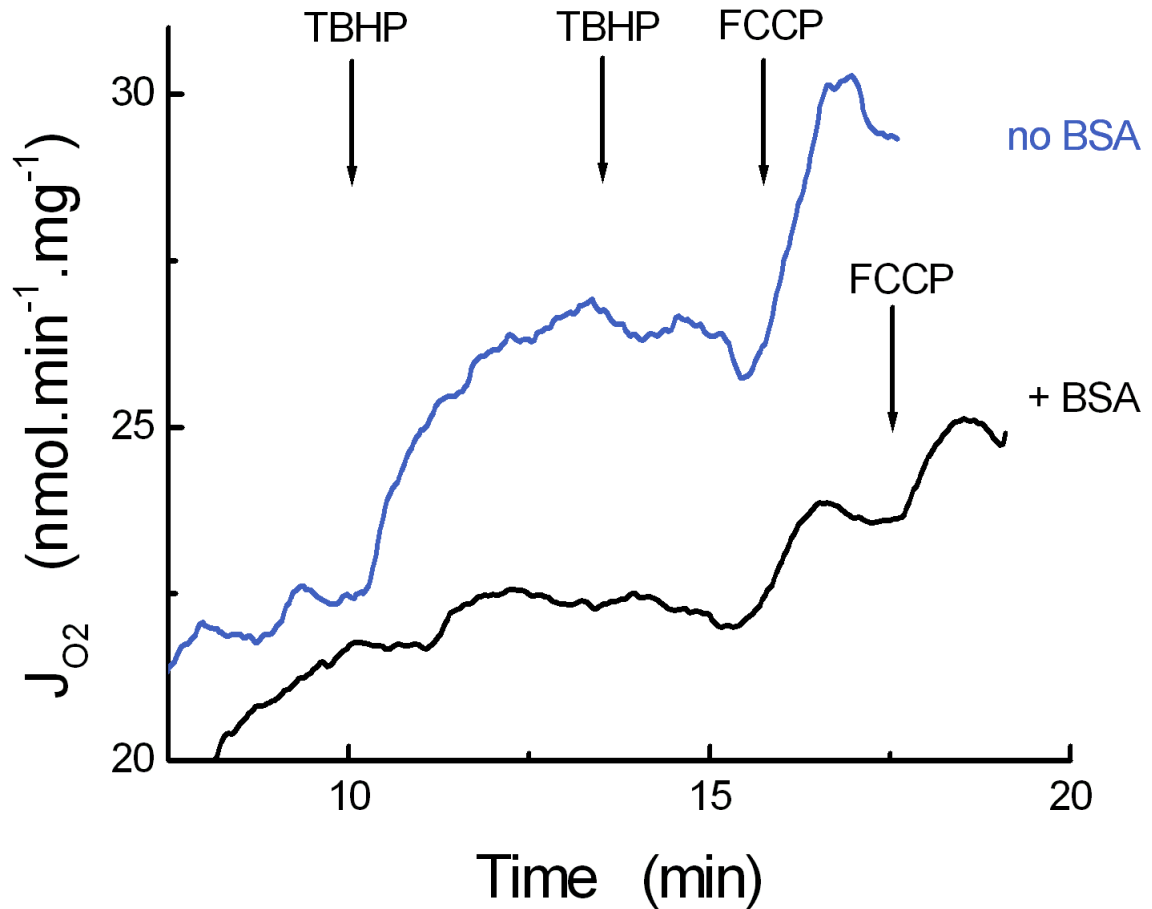


FIGURE 34 The TBHP-dependent increase in respiration of isolated rat lung mitochondria is inhibited by BSA. Mitochondria (0.2 mg/ml) were allowed to respire in the assay medium containing 10 mM succinate, 1 μM rotenone, and 1 $\mu\text{g}/\text{ml}$ oligomycin. Rates are shown for the following additions: 5 μM TBHP (added twice) and 5 nM FCCP to both traces. The assay medium was further supplemented (prior to TBHP) with *black trace*: 0.2 mg/ml BSA; *blue trace*: no further supplementation.

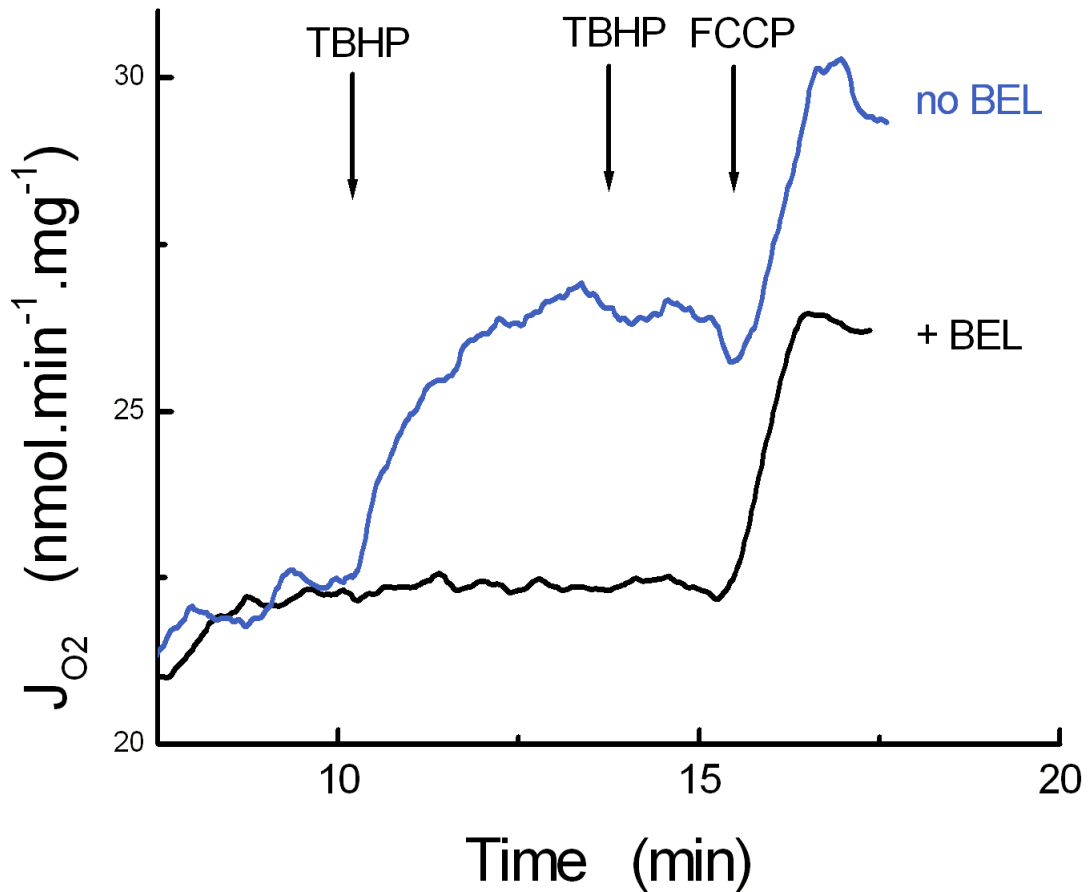


FIGURE 35 The TBHP-dependent increase in respiration of isolated rat lung mitochondria is inhibited by bromoenol lactone. Mitochondria (0.2 mg/ml) were allowed to respire in the assay medium containing 10 mM succinate, 1 μ M rotenone, and 1 μ g/ml oligomycin. Rates are shown for the following additions: 5 μ M TBHP (added twice) and 5 nM FCCP to both traces. The assay medium was further supplemented (prior to TBHP) with *black trace*: 10 μ M BEL; *blue trace*: no further supplementation.

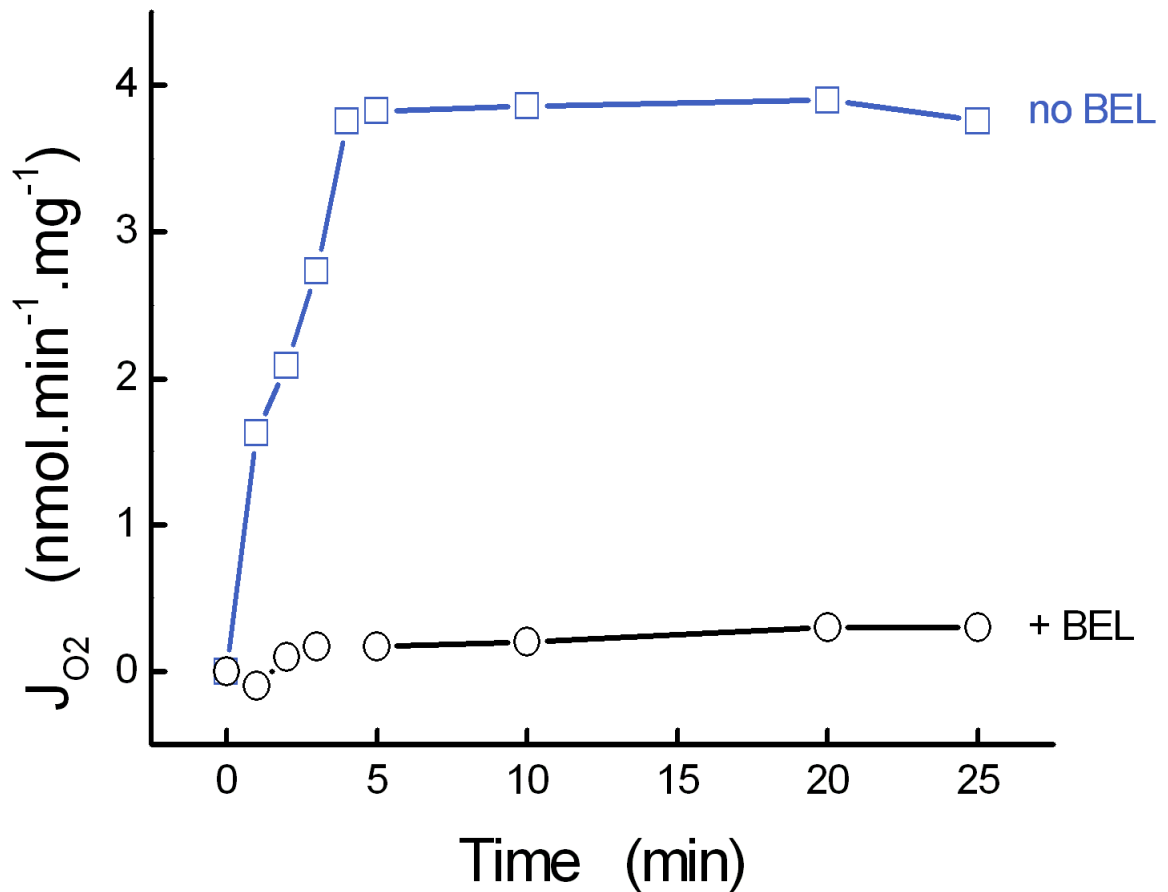


FIGURE 36 TBHP dose response for increase in respiration of isolated rat lung mitochondria with and without BEL. Mitochondria (0.2 mg/ml) were allowed to respire in the assay medium containing 10 mM succinate, 1 μ M rotenone, and 1 μ g/ml oligomycin. Rates are shown for varying amounts of added TBHP, as exemplified in Fig. 35 (page 74). The assay medium was further supplemented (prior to TBHP) with *black trace*: 10 μ M BEL; *blue trace*: no further supplementation.

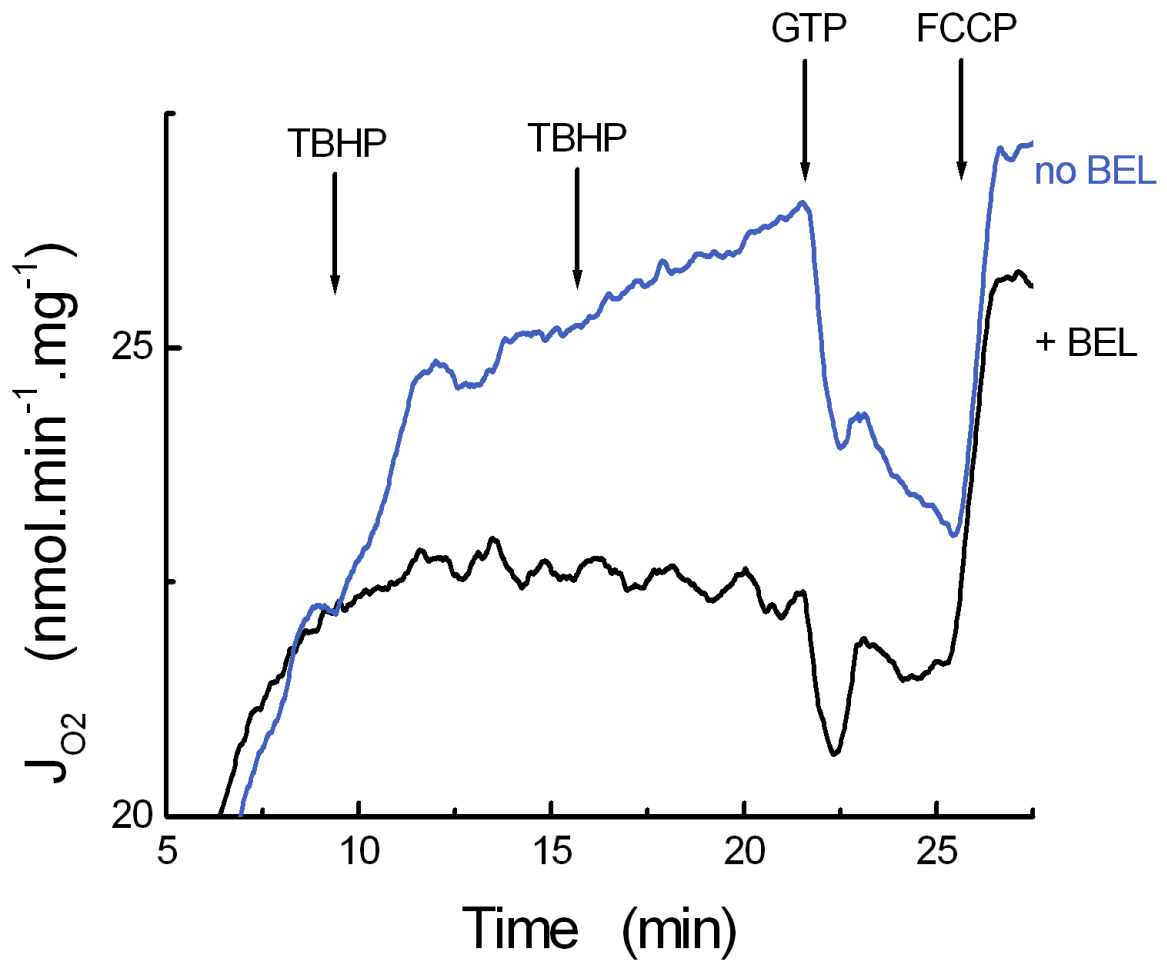


FIGURE 37 The TBHP-dependent increase in respiration of isolated rat lung mitochondria is inhibited by GTP. Mitochondria (0.2 mg/ml) were allowed to respire in the assay medium containing 10 mM succinate, 1 μ M rotenone, and 1 μ g/ml oligomycin. Rates are shown for the following additions: 10 μ M TBHP (added twice), 0.5 mM GTP, and 5 nM FCCP to both traces. The assay medium was further supplemented (prior to TBHP) with *black trace*: 10 μ M BEL; *blue trace*: no further supplementation.

4.3.3 The Effect of TBHP and GDP on Lung Mitochondria Isolated from UCP2-WT and UCP2-KO Mice – the Effect is Absent in KO

The most important support for the UCP2-dependent increase in respiration evoked by TBHP comes from the experiments with UCP2 knock-out mice. When compared to mitochondria isolated from the wild-type mice, much lower TBHP effect and no effect of GDP is gained with mitochondria isolated from UCP2-KO mice (Fig. 38).

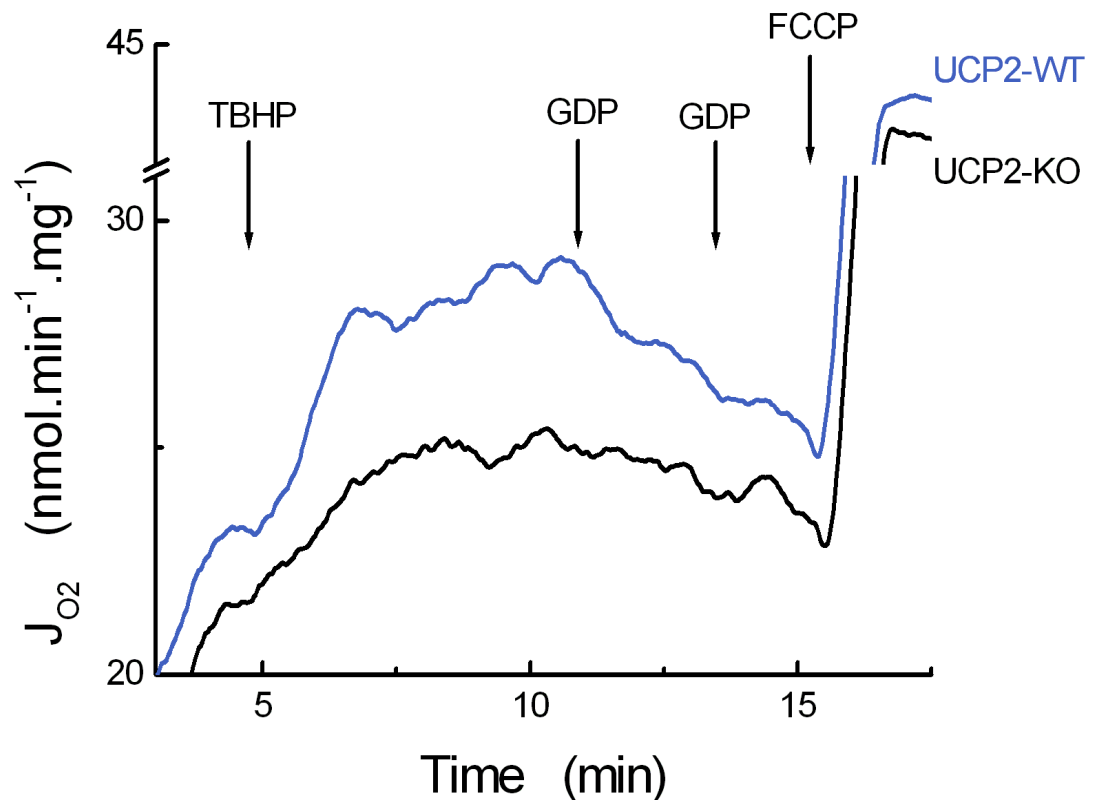


FIGURE 38 The effect of TBHP and GDP on lung mitochondria isolated from UCP2-WT and UCP2-KO mice. Mitochondria (0.1 mg/ml) were allowed to respire in the assay medium containing 10 mM succinate, 1 μM rotenone, and 1 $\mu\text{g}/\text{ml}$ oligomycin. Rates are shown for the following additions: 25 μM TBHP, 0.5 mM GDP (added twice), and 20 nM FCCP to both traces. Mitochondria were

isolated from *black trace*: UCP2-KO mice; *blue trace*: UCP2-WT mice. Y-axis was manipulated to include the off-scale part of both traces.

4.3.4 H₂O₂ Production Monitored with Amplex Red during TBHP-induced Oxidative Stress and its Acceleration by BEL

Parallel detection of H₂O₂ and possibly of other ROS by Amplex Red revealed that BSA and BEL accelerated ROS production upon TBHP treatment in mitochondria isolated from rat lung tissue under the given experimental conditions (Fig. 39, *page 79*). It reflects the fact that at sole TBHP treatment, the UCP2-mediated uncoupling initiated by free FAOOHs (its cycling substrates) partially suppresses the mitochondrial superoxide production which is reflected by our assay as H₂O₂ formation. With the removal of these free FAOOHs by BSA or with blockage of their cleavage off the phospholipids by BEL the attenuation of the H₂O₂ formation is not observed.

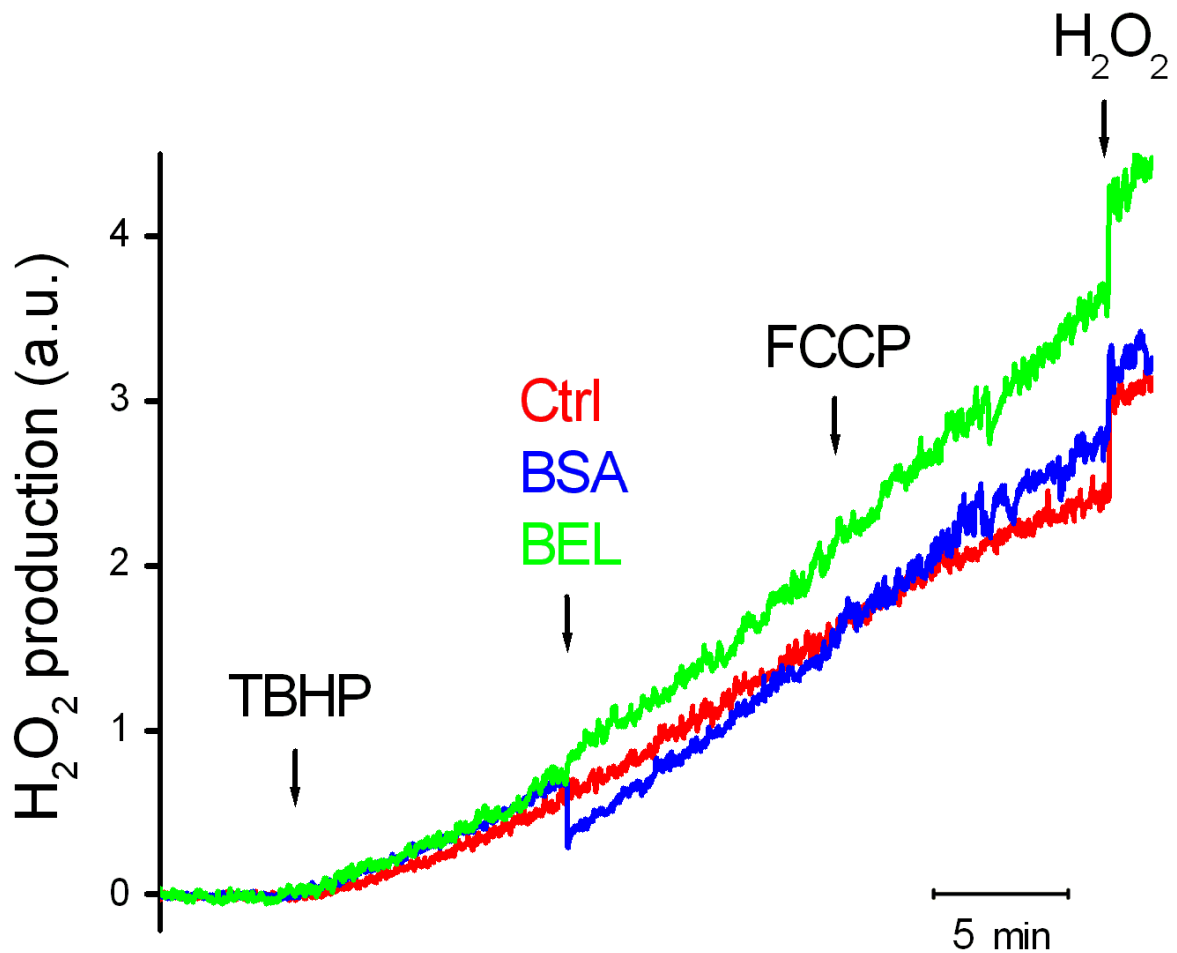


FIGURE 39 TBHP-induced generation of H₂O₂ and appearance of ROS by isolated rat lung mitochondria is accelerated by BSA and bromoenol lactone. Mitochondria (0.2 mg/ml) were allowed to respire in the assay medium containing 10 mM succinate, 1 μM rotenone, and 1 μg/ml oligomycin. Rates are shown for the following additions: 10 μM TBHP, 50 nM FCCCP, and 0.1 μM H₂O₂ to all traces, and *red trace*: no additions (Ctrl); *blue trace*: 0.2 mg/ml BSA; *green trace*: 10 μM BEL.

4.4 The Elevation of State 4 Respiration upon Adaptation to Physiological Normoxia

4.4.1 Glycolytic Cells Reduce Respiration at 5% Oxygen in Parallel with Eliciting Less Efficient Oxidative Phosphorylation than OXPHOS Cells

Hepatocellular Carcinoma Cells (HepG2) were incubated at 5% O₂ for three days under three different metabolic states. Control cells were incubated at atmospheric O₂ in parallel for the same period of time under the same conditions. Metabolic status of the cell was modulated by varying cell culture medium components with OXPHOS cells (cultivated in galactose plus glutamine) utilizing mainly oxidative phosphorylation, and GLC5 or GLC25 cells (cultivated in 5 mM or 25 mM glucose, respectively) relying predominantly on anaerobic pathways of energy production, as previously established [1, 114]. After three days, respiratory properties of cells incubated either at atmospheric (21%) oxygen or at 5% O₂ were assessed either at atmospheric or 5% O₂ levels. These conditions, tagged as normal, adapted, instant adapted, and recovered cells, are summarized in Table 5 (*page 81*). Normal condition refers to the atmospheric cultivation of cells and respiration measurement initiated at atmospheric O₂. Adapted condition refers to a three-day cultivation of cells at 5% O₂ and respiration measurement initiated at 5% O₂. Instant adapted condition means atmospheric cultivation and the cells measured at initial 5% O₂. Recovered condition means three-day cultivation at 5% O₂ and the cells measured at initial atmospheric O₂. Endogenous respiration of glucose-cultivated cells, GLC5 and GLC25, dropped by 55% and 61%, respectively, after a 3-day adaptation to 5% O₂ (Figs. 40–41, *pages 82–83*). In contrast, OXPHOS cells elicited only 16% decline in endogenous respiration (Figs. 40–41, *pages 82–83*). Therefore, cells with lower oxidative phosphorylation content are more prone to decline of respiration. No statistically significant differences in the respiratory rates were observed upon instant adaptation independently of the cell metabolic type (Figs. 40–41, *pages 82–83*). Furthermore, elevated state 3/state 4 respiratory control ratio (*i.e.* the ratio of respiratory rates before and

after the addition of 0.1 $\mu\text{g/ml}$ oligomycin) calculated for OXPHOS cells indicates that these cells contain higher proportion of phosphorylating mitochondria than glycolytic cells (Fig. 42, *page 84*). This is in agreement with the presumption that OXPHOS cells utilize efficient oxidative phosphorylation tightly coupled to mitochondrial respiration. On the other hand, uncoupled state/state 4 respiratory control ratio (*i.e.* the ratio of respiratory rates after and before the titration of FCCP to saturation, occurring between 2 and 6 μM) takes into account maximally obtainable respiration of fully uncoupled state imposed by saturating amounts of FCCP. High-amplitudes of uncoupled state were observed for all metabolic conditions independently of the O_2 level during adaptation, with the exception of GLC5 cells adapted to 5% O_2 (Fig. 43, *page 85*).

TABLE 5 Oxygen conditions during HepG2 cell cultivation and the following respiration measurement.

Condition of the cells	O_2 level during a 3-day cultivation	O_2 level during respiration measurement ^a
normal	atmospheric	atmospheric
adapted	5%	5%
instant adapted	atmospheric	5%
recovered	5%	atmospheric

^aValue at which the respiration was initiated.

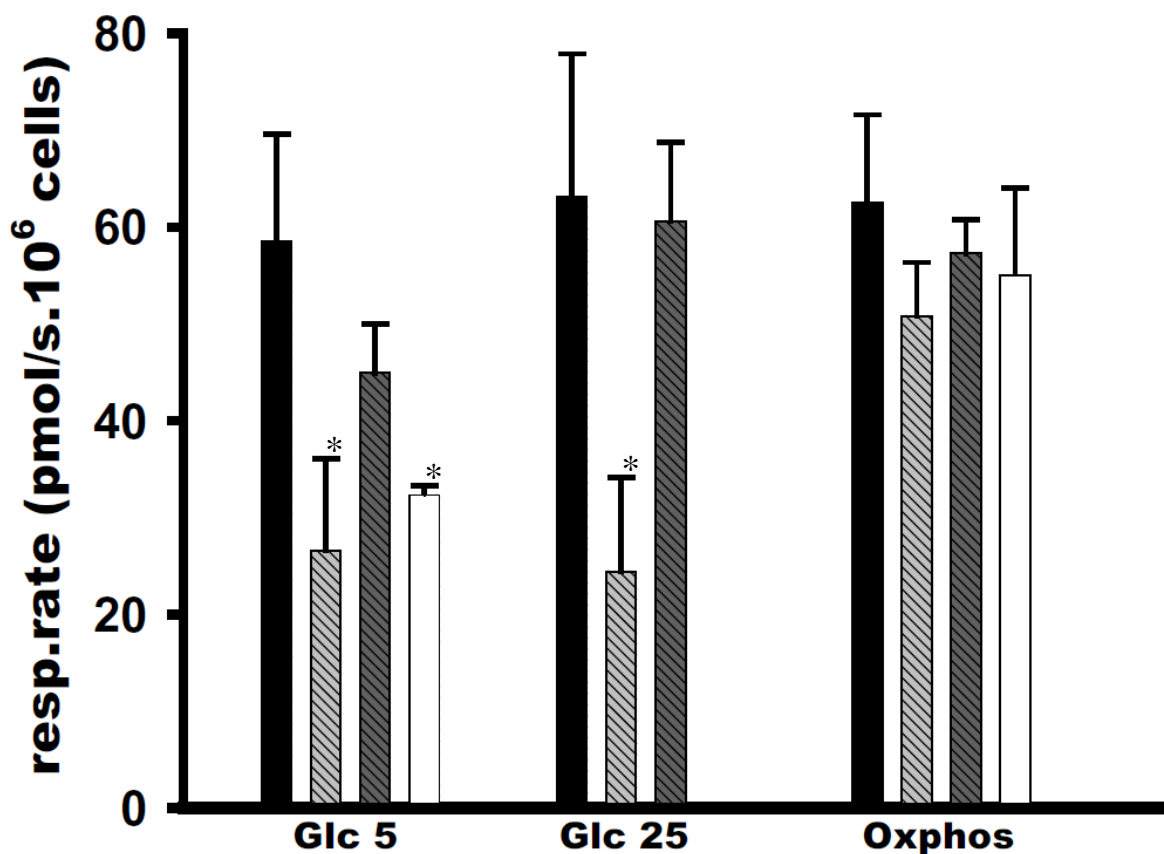


FIGURE 40 Respiratory rates of HepG2 cells in atmospheric and 5% oxygen. Cellular respiration rates, *i.e.* without any agents added, are shown for the following conditions (defined in Table 5, page 81): **black bars:** normal; **dashed light grey bars:** adapted; **dashed dark grey bars:** instant adapted; and **white bars:** recovered. Data are compiled from 7 different experimental cultivations for each condition with n ranging between 1 and 7 for each cultivation.

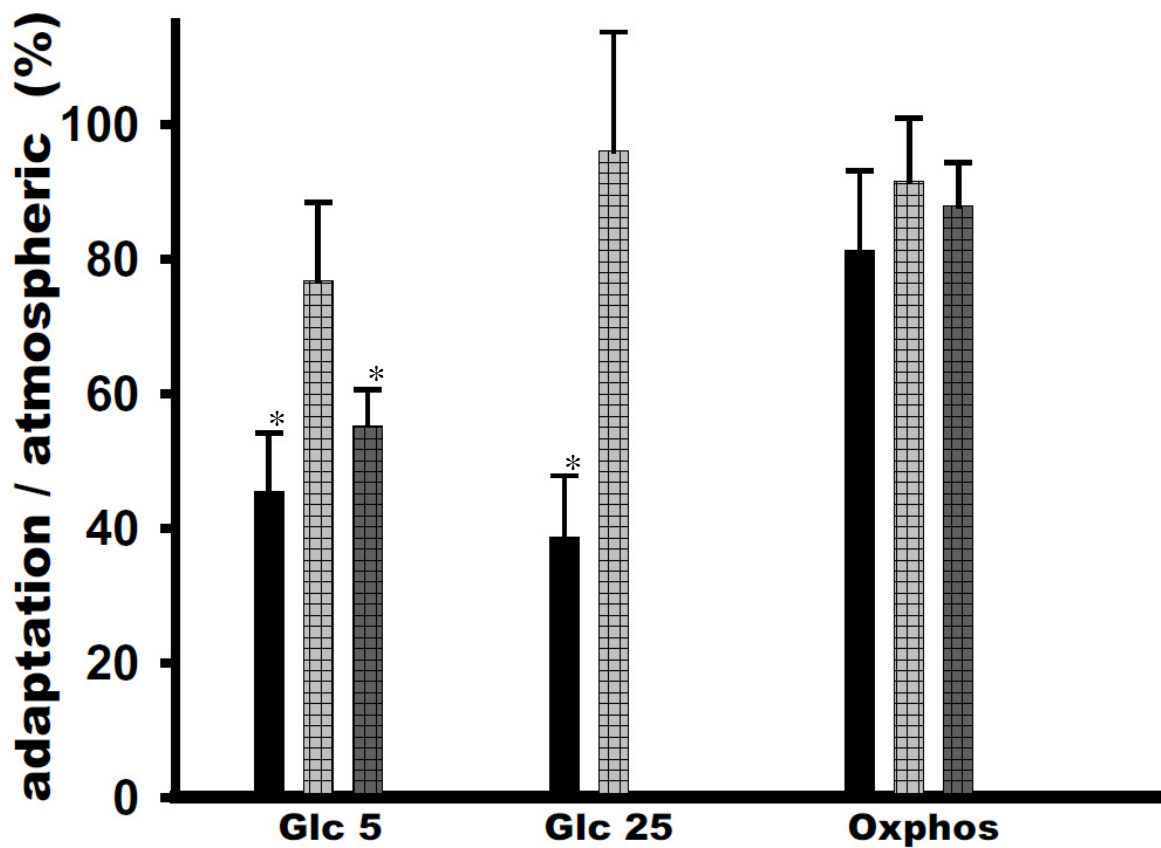


FIGURE 41 Extent of adaptation of HepG2 cells to 5% oxygen. Respiration rates from Fig. 40 (page 82) were normalized to the rate for the condition, in which cells were not subjected to low O₂ atmosphere (taken as 100%), for the following conditions (defined in Table 5, page 81): **black bars**: adapted; **dashed light grey bars**: instant adapted; **dashed dark grey bars**: recovered. Data are compiled from 7 different experimental cultivations for each condition with n ranging between 1 and 7 for each cultivation.

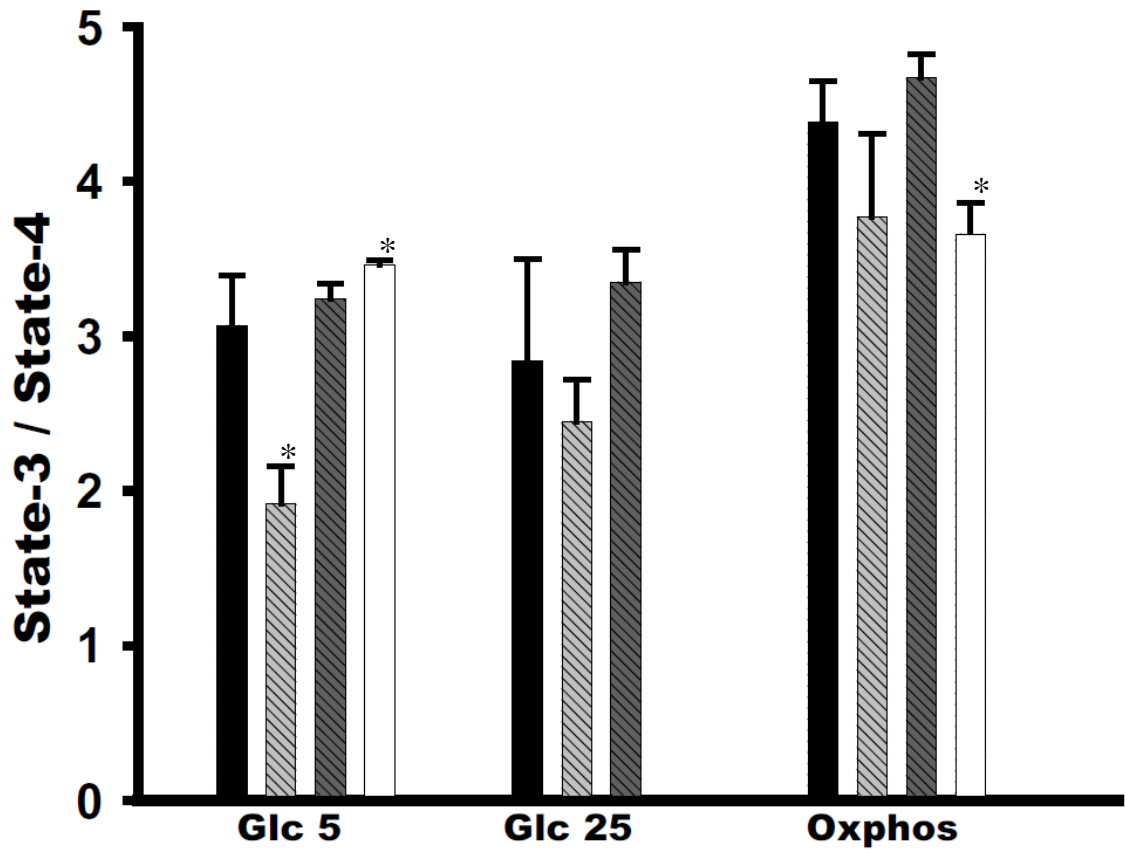


FIGURE 42 State 3/state 4 respiratory control ratios of HepG2 cells in atmospheric and 5% oxygen. State 3/state 4 respiratory control ratios are shown for the following conditions (defined in Table 5, page 81): **black bars**: normal; **dashed light grey bars**: adapted; **dashed dark grey bars**: instant adapted; and **white bars**: recovered. State 3 represents endogenous respiration and state 4 was established by the addition of 0.1 $\mu\text{g/ml}$ oligomycin. Data are compiled from 7 different experimental cultivations for each condition with n ranging between 1 and 7 for each cultivation.

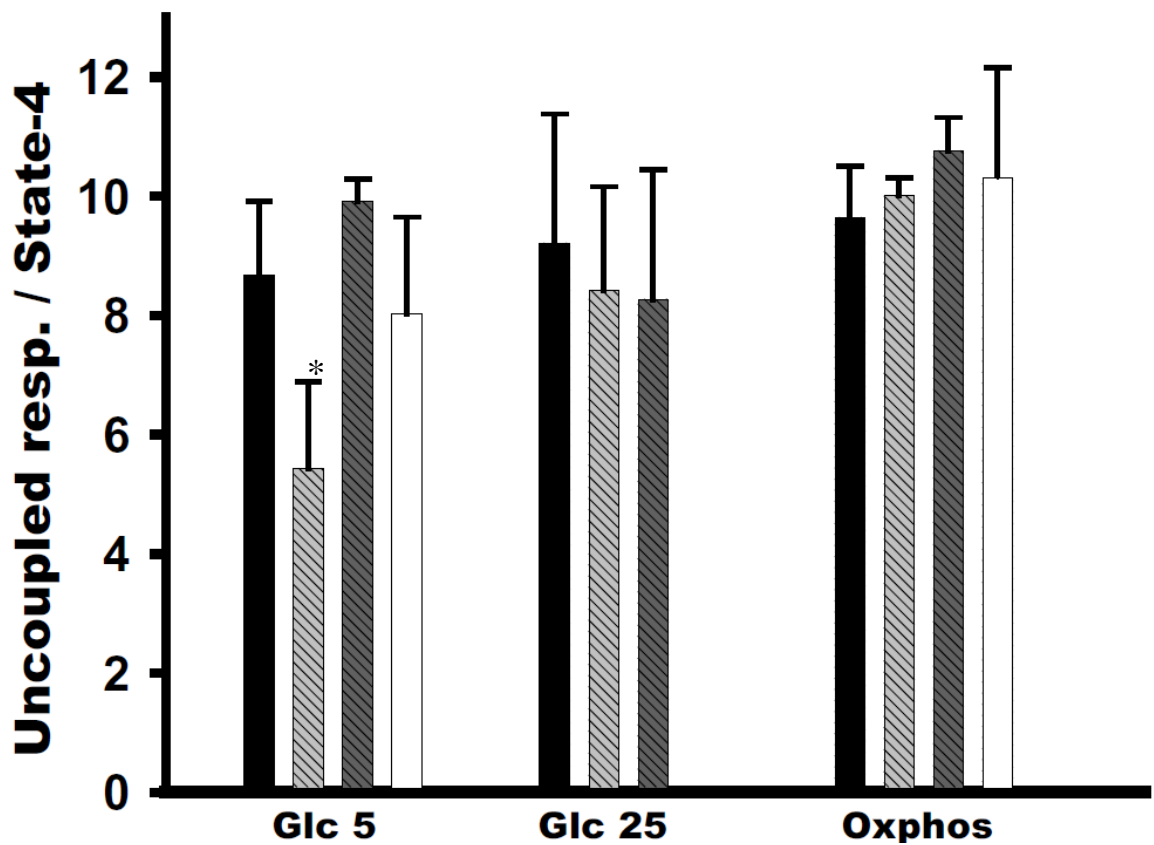


FIGURE 43 Uncoupled respiration/state 4 respiratory control ratios of HepG2 cells in atmospheric and 5% oxygen. Uncoupled respiration/state 4 control ratios are shown for the following conditions (defined in Table 5, page 81): **black bars:** normal; **dashed light grey bars:** adapted; **dashed dark grey bars:** instant adapted; and **white bars:** recovered. Uncoupling was induced by saturating amounts of FCCP (between 2 and 6 μ M) and state 4 was established by the addition of 0.1 μ g/ml oligomycin. Data are compiled from 7 different experimental cultivations for each condition with n ranging between 1 and 7 for each cultivation.

4.4.2 Glycolytic Normoglycemic Cells Adapt to 5% Oxygen by Elevated State 4 Respiration

On average, a 37%, 14%, and 15% decrease of state 3/state 4 respiratory control ratio was observed for GLC5, GLC25, and OXPHOS cells after a 3-day adaptation to 5% O₂, respectively (Fig. 42, *page 84*). Likewise, a 37% decrease (on average) of uncoupled state/state 4 respiratory control ratio was observed for GLC5 cells after a 3 day-adaptation to 5% O₂ (Fig. 43, *page 85*). The cause behind these phenomena was a relatively increased state 4 respiration of cells adapted to 5% O₂. This observation can be derived from Figs. 42–43 (*pages 84–85*).

However, no statistically significant decrease of respiratory control ratios occurred neither after the recovery of GLC5 cells from a 3-day incubation at 5% O₂, either after instant transfer of GLC5 cells to 5% O₂ during the actual respiration measurement (Figs. 42–43, *pages 84–85*).

4.4.3 Dependence of Cellular Respiration Rate on Oxygen Concentration

Instant adaptation (for definition see Table 5, *page 81*) of HepG2 cells cultivated for 3 days at atmospheric O₂ was also stimulated by their continuous oxygen depletion inside the respirometer chamber, as exemplified for OXPHOS cells in Fig. 44 (*page 87*). No significant difference in the rate of respiration was observed within the plateau reached after the initial addition of cells. Constant rate of O₂ consumption sustained until O₂ concentration reached 2%, followed by a rapid drop to zero. This result well coincides with measurements of cells instant-adapted by their direct transfer to 5% O₂, as no statistically significant difference in respiratory rates occurred there as well when compared to the control (Fig. 40, *page 82*). Similar dependence was gained for glycolytic GLC5 and GLC25 cells (not shown).

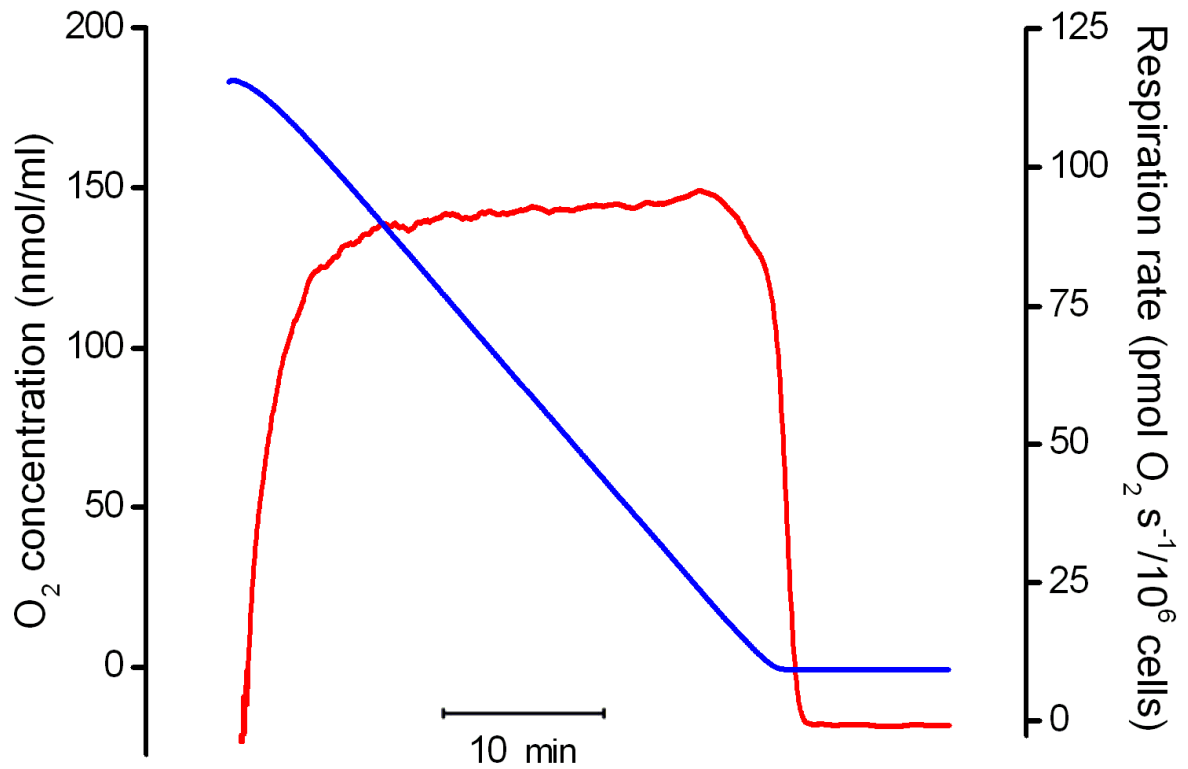


FIGURE 44 Rate of Respiration monitored during oxygen depletion by normoxic OXPHOS HepG2 cells. Traces are shown for OXPHOS cells (cultivated at atmospheric O₂) undergoing endogenous respiration without any agents added until depleting all the oxygen, *blue*: O₂ concentration (left axis); *red*: respiratory rate (right axis). Note that 5% O₂ corresponds to ~ 45 nmol/ml (45 μM) oxygen.

5 DISCUSSION

5.1 Mechanism of Attenuation of Mitochondrial Complex I Superoxide Production by Uncoupling

It was established in our group that superoxide production within mitochondrial Complex I could be regulated by feedback pressure of the proton motive force (Δp) or its membrane potential part ($\Delta\Psi_m$) [1, 114]. In order to support this working hypothesis and to study the relationship between Complex I-derived $O_2^{\bullet-}$ production and Δp , one can either take advantage of chemical uncouplers (such as FCCP), which dissipate overall Δp , or more direct strategy would be to prevent its build-up. This can be elegantly achieved by inhibiting proton pumping mediated by Complex I, allowing the interrelationships among respiration (*i.e.* rate of electron flow), $O_2^{\bullet-}$ production, and H^+ -pumping to be scrutinized in more detail. I have revealed for the first time that 5-(*N*-ethyl-*N*-isopropyl)amiloride (EIPA) is a true inhibitor of H^+ -pumping specific for mitochondrial Complex I (Figs. 13–19, *pages 43–49*).

Employing EIPA as Complex I H^+ -pumping inhibitor has important consequences on ascribing the role of conformational changes transducing redox energy of the electron transport to H^+ -pumping. Based on the resolved crystal structure of Complex I membrane domain, Baranova *et al.* predicts that these loose conformational changes are acting over a long-range distance [94]. Na^+/H^+ antiporter-like subunits NuoL, NuoM, and NuoN, or their human ND5, ND4, and ND2 homologues, lie at the distal end of the membrane domain. At the other side, the origin of conformational changes lies within the peripheral domain of Complex I and it has been predicted to involve semiquinone intermediates [80].

Our hypothetical model (Fig. 45, *pages 89–90*) brings into scope the attributes associated with Complex I, *i.e.* rate of superoxide $O_2^{\bullet-}$ production, electron transport, H^+ -pumping, and the intensity of conformational changes coupling these events, NADH

pressure from the electron entrance side, and proton motive force backpressure (Δp).

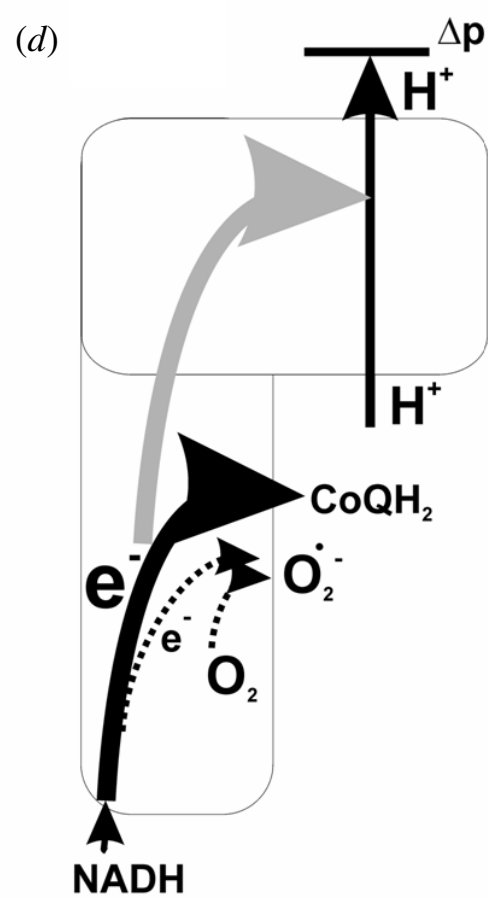
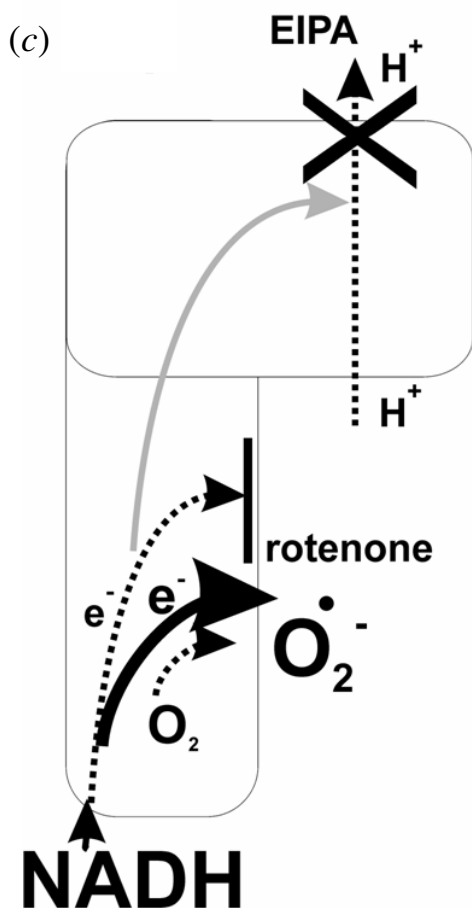
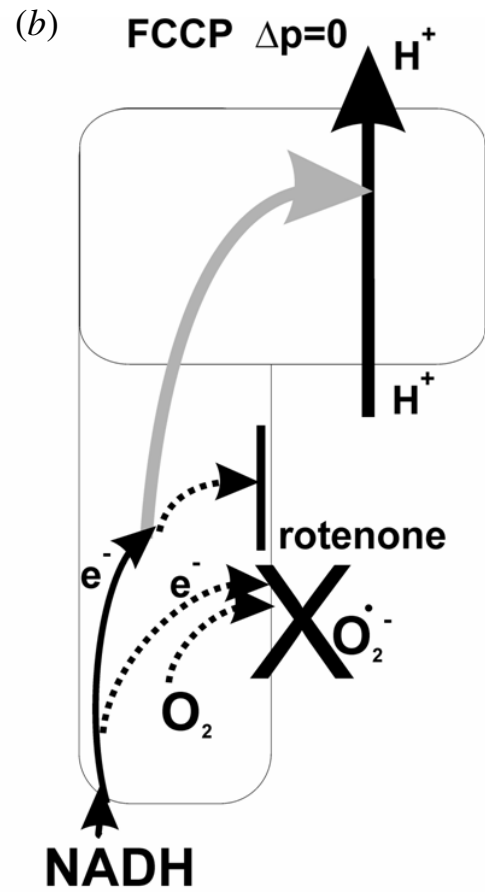
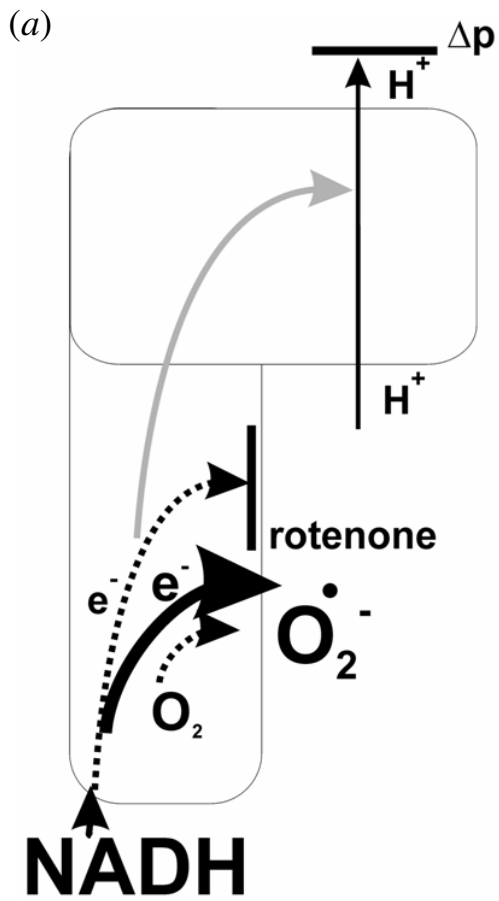


FIGURE 45 Hypothetical interrelationship among the rates of electron flow, H⁺-pumping, and intensities of the associated conformational changes within Complex I. Predicted mode of Complex I action is shown for the following states: (a) rotenone block; (b) rotenone plus FCCP; (c) rotenone plus EIPA; and (d) no additions. Accumulation of NADH (NADH), faster electron transport (e⁻), higher rate of superoxide production (O₂^{•-}), and faster H⁺-pumping (H⁺), are indicated by larger font size of the symbols in parentheses, and *vice versa*. Larger arrow and arrow line thickness corresponds to black arrows: faster rates of redox reactions or H⁺-pumping; gray arrows: higher intensity of conformational changes acting between the peripheral and membrane arm of Complex I; and *vice versa*. Dotted arrow lines represent very low or negligible fluxes. Note that the Complex I diagrams are oriented with the matrix-exposed peripheral arm facing down.

In intact Complex I (Fig. 45d, pages 89–90), NADH pressure is very low because of unobstructed electron flow which is thus very fast. Unimpeded electron flow is the cause also for low probability of electron diversion to oxygen, hence diminishing O₂^{•-} production, but also for very high intensity of conformational changes causing fast H⁺-pumping. From the other side of the membrane high Δp exerts feedback inhibition pressure directed against the excessive H⁺-pumping. Based on the hypothetical localization of O₂^{•-} formation to FMN [59, 100–101] and/or to either of the three predicted semiquinone radicals [40, 102], we may predict that conformational changes develop somewhere on the way between these sites and the N2 subunit of Complex I [267].

When Complex I inhibitor is present, such as rotenone, the situation becomes more complex due to the stimulated blockade of electron flow within the peripheral arm of Complex I (Fig. 45a, pages 89–90). Accumulation of electrons leads to a high O₂^{•-} generation imposed by bifurcation of the electron flow to molecular oxygen induced by rotenone and high NADH pressure. But high O₂^{•-} formation is favored also because of another, more indirect reason, taking into account conformational changes. Again, high Δp backpressure reduces the intensity of H⁺-pumping and the concomitant conformational changes, hence contributing to the hindered electron throughput within Complex I.

High Δp can be dissipated by the addition of FCCP (to rotenone-inhibited mitochondria, Fig. 45b, pages 89–90), which shortcircuits H^+ -pumping. Uncoupler essentially reduces Δp to zero, relieving the regulatory block of very fast H^+ -pumping and the accompanying high-intensity conformational changes. The re-established fast electron flow not only drives conformational changes but also reduces $O_2^{\bullet-}$ production to low levels, so that the diversion of electron flow to O_2 is no more preferred, even if electron flow retardation by rotenone prevails. In turn, NADH-associated pressure is relieved with the reaccelerated electron/proton traffic as well. It has been found by Dlasková *et al.* that EIPA prevents FCCP-mediated attenuation of rotenone-induced $O_2^{\bullet-}$ production [1], confirming that the FCCP-induced release of pressure exerted by proton motive force slows down $O_2^{\bullet-}$ formation through rapid reacceleration of H^+ -pumping.

Circumstances are reversed again when rotenone and EIPA are used in combination, as depicted in Fig. 45c (pages 89–90). Assuming that EIPA blocks Complex I H^+ -pumping independently of Δp , the intensity of conformational changes would be lowered by the block instigated by EIPA. Consequently, slow electron flux would lead to increase in the rate of $O_2^{\bullet-}$ generation by Complex I and the pressure coming from NADH. This is a parallel situation to the one described in Fig. 45a (pages 89–90) for sole rotenone. Taken together, EIPA substitutes for the block imposed by the proton motive force if no uncoupler is present. However, the loose character of conformational changes would still allow some residual electron transfer throughout the peripheral arm of Complex I to occur despite the inhibition of H^+ -pumps by EIPA.

Our hypothesis stating that high-intensity conformational changes would enable increased redox energy transmission to H^+ -pumping, thus relieving “electron congestion” at superoxide-evolving sites (Fig. 45b, pages 89–90), is fully in agreement with Peter Mitchell's chemiosmotic theory [266] which postulates respiratory control on the proton pumps of the respiratory chain by the backpressure of proton motive force. H^+ -pumping rate increases with Δp pressure release during uncoupling or Complex V-mediated phosphorylation. One may speculate that the Δp feedback pressure is an essential prerequisite for $O_2^{\bullet-}$ generation by Complex I due to the low intensity of conformational changes (Fig. 45a, pages 89–90).

By providing EIPA as a reliable H⁺-inhibitor, I have extended the work of Dlasková *et al.* [114] to demonstrate that in addition to the electron flow retardation induced by rotenone, O₂^{•-} production takes place, also when H⁺-pumping is limited by the presence of high Δ*p* (or high Δ*Ψ*_m). We may also hypothesize that similar feedback mechanism exists for the H⁺-pumping pathway in the retrospective of generally accepted theory of respiratory control [4, 50–52]. In this view, feedback pressure by Δ*p* (or Δ*Ψ*_m) would limit H⁺-pumping together with the accompanying conformational changes, which would retard the redox traffic at the peripheral arm of Complex I leading to prolonged half-lives of ubisemiquinone species, hence giving rise to elevated O₂^{•-} production. These effects would be more pronounced in state 4 respiration due to higher Δ*p* backpressure, explaining the low but constant rate of ROS production in the presence of respiratory control exerted *via* H⁺-pumping [4, 23, 80].

Our interpretation could be disputed by the fact that the mitochondrial Na⁺/H⁺ antiporter but not Complex I is inhibited by EIPA [268]. In this case one would expect much higher mitochondrial matrix alkalinization to occur but this was not observed even in media containing Na⁺ (Fig. 18, *page 48*). Further support for our hypothesis comes from the experiment in which Na⁺/H⁺ antiport was mimicked by the addition of monensin showing that this perturbation does not influence the acidification induced by EIPA (Fig. 18, *page 48*). The observation that EIPA-stimulated Complex I inhibition takes place also in the presence of the simulated Na⁺/H⁺ antiport excludes the possibility that EIPA would inhibit mitochondrial Na⁺/H⁺ antiporter. Hence we can reason out that the Na⁺/H⁺ antiport activity is negligible when compared to proton pumping and conclude that the Na⁺/H⁺ carrier does not interfere with our results neither with their interpretation. If this was not true, the inhibition of mitochondrial Na⁺/H⁺ antiporter by EIPA would also lead to a slight increase of proton motive force Δ*p*, by the amount which is consumed to drive the Na⁺/H⁺ antiport when no EIPA is present. Even a slight Δ*p* increase would raise O₂^{•-} production. This fact would contradict the beneficial use of hydrophobic amiloride drugs that are administered to prevent ischemic injury [269].

The attenuation of Complex I-derived O₂^{•-} production by uncoupling is important with respect to hazards that oxidative stress could pose on ambient cellular components. Assuming that the entire O₂^{•-} production is released by Complex I to mitochondrial matrix

[43, 54], the mechanism described by us (Fig. 45, *pages 89–90*) can be considered plausible in context with the self-potentiating vicious cycle model [4, 20–22]. Among all the matrix constituents, mitochondrial DNA (mtDNA) is the most susceptible element to oxidative stress [112–113, 269–270]. When mtDNA mutations happen to occur in the coding regions of Complex I H⁺-pumping subunits (*e.g.* ND5, ND2, or ND4), the consequent retardation of H⁺-pumping would presumably cause increased O₂^{•-} production by Complex I and more pronounced oxidative stress [1, 114]. Elevated oxidative stress would represent higher risk to inflict further oxidative damage to mtDNA, but also to lipids, and proteins. By this mechanism the continuous self-accelerating vicious cycle augments oxidative damage until an ultimate threshold for apoptosis and/or pathological condition is met [4, 17].

To summarize, the contribution of Complex I-mediated O₂^{•-} production to oxidative stress as well as the capability to regulate oxidative stress by uncoupling is a vital attribute of mitochondria as a DNA-containing organelle. We may speculate whether uncoupling proteins play the major part in down-regulating reactive oxygen species *in vivo* [4, 43, 165, 271]. However, we show for the first time that uncoupling is not efficient enough to attenuate Complex I-derived O₂^{•-} production under circumstances when H⁺-pumping is disabled, *i.e.* by EIPA in the experimental set-up or by mutated ND2, ND4, or ND5 Complex I subunits in diseases. Our work clearly shows that strategies counting solely on uncoupling cannot be exercised to counteract maladies associated with defective mitochondrial genome-encoded H⁺-pumping subunit.

5.2 Targeting of MitoQ₁₀-related Therapeutics to Oxidative Stress

Results of my colleagues have evidenced antioxidant action of MitoQ₁₀ in HepG2 cells when oxidative stress was simulated by inhibition of Complex I with rotenone, as well as the characteristic of MitoQ₁₀ to interact with ubiquinone binding sites of Complex I and Complex II [2]. I have contributed to unraveling the mechanism of MitoQ₁₀ pro-oxidant and anti-oxidant effects by observing respiratory acceleration either in the

absence of rotenone (pro-oxidant effect) or in its presence (an antioxidant effect).

Excessive production of Complex I-generated $O_2^{\bullet-}$ can be alleviated by mild uncoupling, achieved either by artificial uncoupler or through the action of uncoupling proteins [272]. The main advantage of MitoQ₁₀ over uncoupler-based antioxidants is that it remains effective even when H^+ -pumping by Complex I is hindered, as is the case of aging and diseases arising from accumulation of oxidative damage to segments of mtDNA encoding Complex I H^+ -pumping subunits ND2, ND4, and ND5 [1, 114]. This fact makes mitochondria-targeted antioxidants, such as MitoQ₁₀ or SkQ1 [273], worthy candidates when considering effective therapeutic intervention.

In my results, I have systematically elucidated the mechanism of antioxidant action of MitoQ₁₀, *i.e.* when the electron flow is blocked within Complex I (by rotenone). MitoQ₁₀ causes an overall bypass of the electron blockade since the rotenone-retarded respiration was reaccelerated by nanomolar concentrations of MitoQ₁₀ (Fig. 23, *page 57*, Table 4, *pages 53–54*). The reaccelerated electron flow allows for the attenuation of rotenone-induced $O_2^{\bullet-}$ production generated by Complex I [1]. To estimate the degree of oxidative stress, MitoSOX Red method was developed by my colleague Ing. Andrea Dlasková, Ph.D., allowing for the detection of *in situ* mitochondrial $O_2^{\bullet-}$ production released to the mitochondrial matrix, *i.e.* the fraction of $O_2^{\bullet-}$ which is not neutralized by MnSOD [114].

According to our hypothesis (Fig. 46a, *pages 95–96*), antioxidant role of MitoQ₁₀ can take place only when its reduced form MitoQ₁₀H₂ is regenerated by the participation of Complex II. MitoQ₁₀ accepts electrons from Complex I prior the downstream Q-site blocked by rotenone (Fig. 46a, *pages 95–96*). Electron flow is further conveyed *via* a fraction of Complex II molecules operating in the reverse mode (equivalent to reverse electron transport), so that succinate is produced from fumarate. The biased electron flow is then merged with the usual succinate-driven forward electron transfer pathway delivering the electrons into the Q-pool.

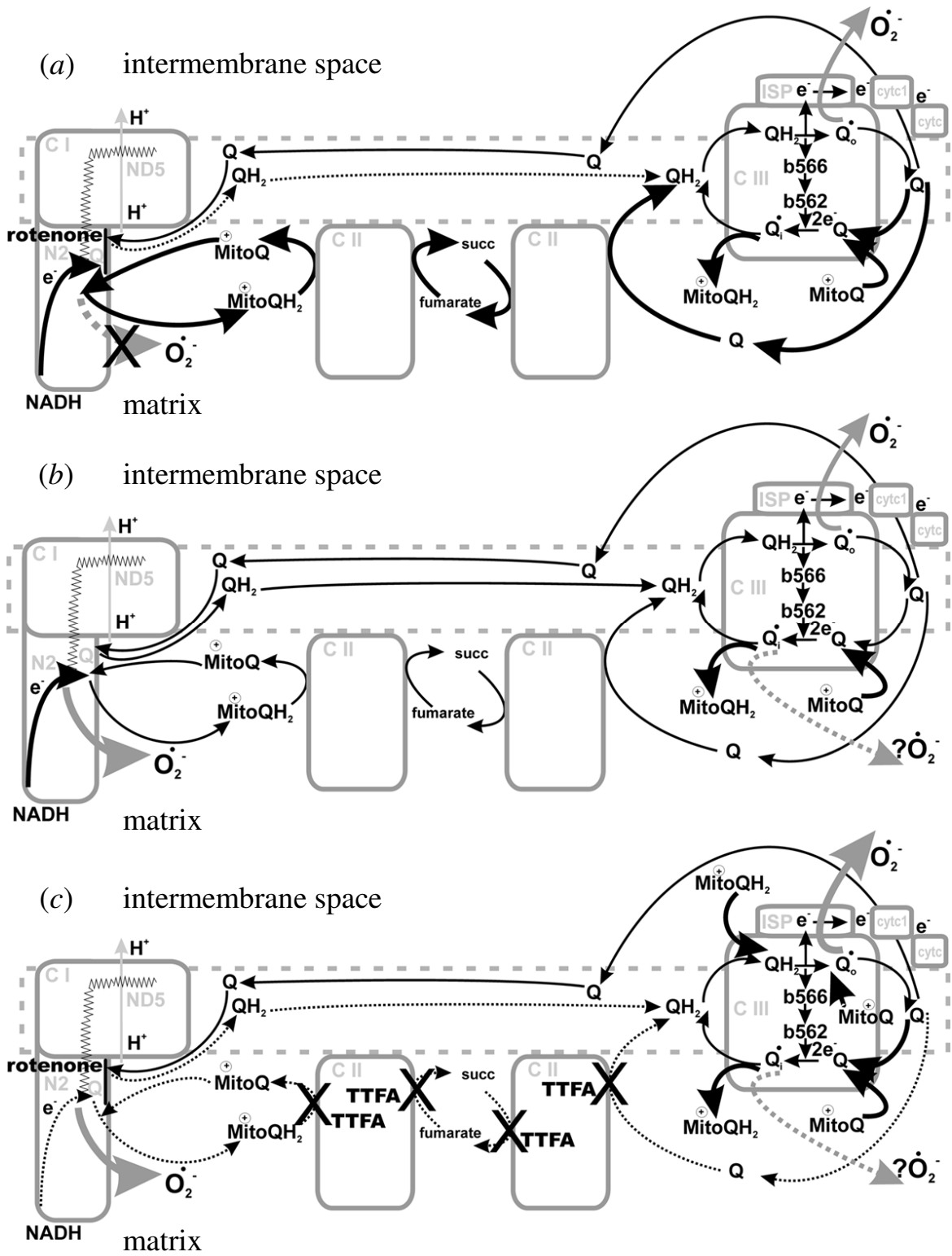


FIGURE 46 MitoQ shuttle. The scheme shows interconnected activities of the MitoQ₁₀ (MitoQ, MitoQH₂) and coenzyme Q (Q, QH₂) cycles with accompanying electron flow through the respiratory chain under the following conditions: **(a)** Complex I electron flow blocked by rotenone; **(b)** no further additions; **(c)** Complex I and Complex II electron flow blocked by rotenone and TTFA, respectively. Larger arrow and arrow line thickness corresponds to higher flux intensity, and *vice versa*. Dotted arrow lines represent reduced or repressed fluxes. Complex I (C I) is shown to comprise the Fe-S cluster N2 (N2), H⁺-pumping subunit ND5 (ND5), and the putative conformational changes (zig-zag line). Two molecules of Complex II (C II) are displayed, one acting in the reverse mode (shown on the left). Complex III (C III) contains cytochromes *b*₅₆₆ (b566), *b*₅₆₂ (b562), iron-sulfur protein (ISP), cytochrome *c*₁ (cytc1), mobile cytochrome *c* (cytc), and the Q_o and Q_i binding sites for coenzyme Q.

My results support this hypothesis (Fig. 46, pages 95–96) because the acceleration of respiration is absent after the addition of TTFA, an inhibitor of Complex II (Fig. 28, page 63, Table 4, pages 53–54). The result of succinate and fumarate cycling is continuously increasing concentration of ubiquinol (QH₂) at the expense of the oxidized Q-pool, mainly due to the presence of rotenone and the competition between the native CoQ and MitoQ₁₀ for the ubiquinone-binding site. The possibility that the electron flow is relayed directly to the Q_o site on Complex III by MitoQ₁₀ is excluded because of the positive charge of MitoQ₁₀ that restricts its localization to negatively-charged matrix side of the inner mitochondrial membrane at sufficient $\Delta\Psi_m$.

Amplex Red monitoring of H₂O₂ generation by isolated rat liver mitochondria under simulated *in situ* conditions did not reveal any antioxidant properties of MitoQ₁₀ (Fig. 29, page 65). The reasons why Plecítá-Hlavatá *et al.* found different profile for O₂^{•-} generation in cells, depicted in Fig. 8 (page 20), may stem from the different methods used [2]. In cells, MitoSOX Red assay detects direct O₂^{•-} generation arising from Complex I and III inward ubisemiquinone sites, *i.e.* oriented towards matrix [2], whereas Amplex Red is sensitive to hydrogen peroxide, downstream dismutation product of O₂^{•-}, no matter where it originates (at inward oriented sites, or at Complex III outward-oriented ubisemiquinone site Q_o). Hence, these has to be viewed as completely different quantities.

As a result, Amplex Red assays total ROS production. This explains the reason why Plecítá-Hlavatá *et al.* observed antioxidant properties of MitoQ₁₀ only when poised by electron flow blockade or H⁺-pumping retardation within Complex I [2], see Fig. 8 (page 20). The blockage of electron flow brought on by rotenone shifts equilibrium of the Q-cycle towards the oxidized form of coenzyme Q resulting in elevated O₂^{•-} formation at the external Q_o site of Complex III (Fig. 46a, pages 95–96), which is detected by the Amplex Red assay (after the conversion of O₂^{•-} to H₂O₂ catalyzed by CuZnSOD) but not by the MitoSOX Red assay. Hence, MitoSOX Red is sensitive enough to detect the decrease of Complex-I mediated inward O₂^{•-} production that is effectively masked for Amplex Red detection (despite the presence of MnSOD converting O₂^{•-} to H₂O₂) by the burst of O₂^{•-} release into the intermembrane space (Figs. 8, 46a, pages 20, 95–96).

When no rotenone is present (Fig. 46b, pages 95–96), an equilibrium shift of the Q-cycle, owing to the competition between MitoQ₁₀ and the coenzyme Q, favors the oxidized form of CoQ to predominate. The concomitant elevated NADH/NAD⁺ ratio and electron flux led to higher Complex I-mediated O₂^{•-} production [101] in comparison to intact respiratory chain in the absence of MitoQ₁₀. Furthermore, the possibility that MitoQ₁₀ accesses also the internal Q_i site of Complex III, competing for this site with the native CoQ, might not be excluded. In this case further retardation of the Q-cycle would analogously increase O₂^{•-} production at the Q_i site. The suggested hypothetical scheme is corroborated also by the observed involvement of complexes II (Fig. 28, page 63) and III (Fig. 27, page 62) in the mechanism of MitoQ₁₀ action. We support the notion that TTFA (Complex II inhibitor) interrupts the alternative electron transfer pathway brought on by MitoQ₁₀, resulting in high O₂^{•-} production (Fig. 46c, pages 95–96)

Our hypothesis provides a considerable insight into the mechanism of MitoQ₁₀ action, clearly demonstrating the conditions favoring either the pro-oxidant or anti-oxidant effects of MitoQ₁₀, and explaining why different research groups arrived to contradictory conclusions about the possible antioxidant properties of MitoQ₁₀. The observation that MitoQ₁₀ raises O₂^{•-} production in intact mitochondria has important consequences on the potential use of MitoQ₁₀ as a therapeutic. Mitochondria-targeted antioxidants, such as MitoQ₁₀ or SkQ1, may efficiently prevent or treat oxidative stress-related ailments upon restricting their effect only to tissues from which oxidative stress emanates.

5.3 ● The Role of Mitochondrial Phospholipases in Concert with Uncoupling in Feedback Down-regulation of Oxidative Stress

Our results demonstrate the orchestrated action of mitochondrial phospholipase iPLA₂ and the uncoupling protein 2 (UCP2) in their common physiological function to downregulate reactive oxygen species formation. Oxidative stress-initiated lipid peroxidation, occurring within the inner and/or outer mitochondrial membranes, gives rise to phospholipid hydroperoxides (PLOOHs) [71–72]. PLOOHs may serve as substrates for the mitochondrial Ca²⁺-insensitive isoform of PLA₂, iPLA₂, releasing fatty acid hydroperoxides (FAOOHs). In turn, FAOOHs have the ability to act as cycling substrates for UCP2-mediated uncoupling [45]. Mild uncoupling would represent the last step of a hypothetical feedback regulatory loop leading to the direct attenuation of oxidative stress, *i.e.* lowered O₂^{•-} production by Complex I and Complex III. However oxidative stress may also originate from external sources, *e.g.* from the reaction of cytochrome P450 [274] or NADHP oxidase [275]. In this case the capacity of antioxidant systems is likely relayed to the external source of reactive species production, which is made possible due to the relieved demand for intramitochondrial O₂^{•-} detoxification [4, 276].

Mitochondrial iPLA₂ (Ca²⁺-insensitive phospholipase A₂) isoforms were reportedly found in liver [75], heart [74, 139] and brain [277]. In liver mitochondria, the participation of phospholipase A₂ in the removal of aberrant mitochondria has been suggested to occur as part of an autolysis process [75]. The β and γ isoforms, iPLA₂β [74] and iPLA₂γ [139], identified in heart mitochondria, were both shown to be sensitive to bromoenol lactone (BEL), respectively. The role of iPLA₂γ, which contains an N-terminal mitochondrial targeting sequence, was proposed to be implicated in the integration of respiration with uncoupling protein-mediated thermogenesis [139]. The localization of heart iPLA₂β has been ascribed to the outer face of the inner mitochondrial membrane [74], whereas iPLA₂ of the brain, which is also sensitive to inhibition by BEL, is rather embedded in the outer mitochondrial membrane [277]. Guidarelli *et al.* have shown that inhibition of Complex III by peroxynitrite (ONOO⁻) in PC12 pheochromocytoma cells is followed by

superoxide-mediated stimulation of phospholipase A₂, which he claims is to be calcium-dependent mtPLA₂ isoform, showing inhibitor specificity profile towards cPLA₂ [160]. A 100 kDa splice variant of human cytosolic β isoform phospholipase, cPLA₂β3, was described in lung, spleen, and ovary cells constitutively attached to the mitochondrial membrane [278]. Liver mtPLA₂ was reported to be activated by O₂^{•-} as well [161].

Our work provides supporting data for a hypothetical feedback attenuation of lipoperoxidation by its products, *i.e.* hydroperoxy fatty acids (FAOOHs), which are released by Ca²⁺-insensitive mitochondrial phospholipase A₂. The evidences can be summarized as follows:

Succinate-driven respiration of isolated lung mitochondria was stimulated by low doses of *tert*-butyl hydroperoxide (TBHP), which is an agent enabling to stimulate lipid peroxidation in the presence of minute amounts of free endogenous iron or transient metals, see Fig. 33 (*page 71*). The observed respiration increase was fully inhibited by BSA (Fig. 34, *page 73*), indicating the participation of free fatty acids, most likely hydroperoxy FAs, and by bromoenol lactone (BEL), a specific inhibitor of phospholipases iPLA₂, see Figs. 35–36 (*pages 74–75*). It shows that the observed uncoupling definitively depends on the cleavage off FAOOHs from PLOOHs formed during the lipid peroxidation chain reaction. Respiration was further partially inhibited by GTP, an inhibitor of UCP2 (Fig. 37, *page 76*). The TBHP-dependent increase in the respiratory rate was not observed in lung mitochondria isolated from UCP2-KO mice (Fig. 38, *page 77*), definitively proving the UCP2 participation. Parallel detection of H₂O₂ by Amplex Red revealed that indeed the mitochondrial H₂O₂ production (even if measured on a background of nonspecific ROS burst due to TBHP addition) was diminished (Fig. 39, *page 79*), when compared to the situation when either iPLA₂ is blocked by BEL or free FAOOHs are removed by BSA. Thus, BSA and BEL accelerated mitochondrial H₂O₂ production under the given experimental conditions. In conclusion, we demonstrate for the first time that mitochondrial UCP2 and iPLA₂ act in concert in the attenuation of the oxidative stress when activated by ongoing lipoperoxidation.

Under physiological conditions mitochondrial iPLA₂ participates in part in the repair of peroxidative damage inflicted to mitochondrial membranes through a remodeling

mechanism *via* a deacylation-reacylation cycle [279]. One can point out another aspect of the physiological role of mitochondrial phospholipase A₂ in relation to apoptosis. Originally, only participation in apoptotic cell death induction has been considered, *e.g.* the brain mitochondrial iPLA₂ has been implicated in apoptosis due to its activation by reactive oxygen species upon BAX and tBID treatment [280]. Albeit the pro-apoptotic role of mitochondrial iPLA₂ has been repeatedly reported [74, 160, 280], we expect that this could be possible only upon high-extent activation of mitochondrial iPLA₂. Nevertheless, in recent years more physiological roles of prosurvival character has been revealed for mitochondrial phospholipase A₂. For example, silencing of mtPLA₂ led to apoptosis, therefore a protective function of mitochondrial iPLA₂ has been proposed [158, 279, 281]. Furthermore, mitochondrial iPLA₂ was even implicated in the protection of mitochondrial function from the oxidative damage upon apoptotic induction [279].

Similarly, we may speculate about the role of UCP2 in the initial stage of apoptosis. Overexpression of UCP2 in HepG2 cells was previously shown to diminish oxidative damage and to prevent apoptosis [282]. From our point of view, physiological levels of FAOOHs and their respective lysophospholipid counterparts are not sufficient enough to trigger apoptotic response or to initiate the formation of pro-apoptotic pores in the inner or outer mitochondrial membranes. Two factors, the activity of UCP2 and the extent of oxidative stress might govern the delicate balance between condemning cells to death or staying alive. Once the capacity of UCP2 for reactive species attenuation is challenged at certain threshold by the overwhelming peroxidative stress, above which mitochondrial phospholipases, such as iPLA₂, generate excessive amounts of lysophospholipids to initiate cytochrome *c* release and the onset of apoptosis.

In contrast to our hypothesis, Brand *et al.* proposed that 4-hydroxynonenal (HNE) is the lipoperoxidation metabolite for UCP2 activation rather than free FAOOHs. This group claims that aldehydic lipid peroxidation end-products, such as HNE, are able to modify mitochondrial uncoupling proteins, converting them into active protonophores [137, 283–285]. Note that in this model UCP2 acts as a pure proton transporter, which is in total contrast to fatty acid cycling mechanism [45], proposed by us, based on the fact that UCP2 belongs to the family of anion transporters, *i.e.* mitochondrial anion carrier proteins (MACPs) [3]. The feedback attenuation of mitochondrial O₂^{•-} production by activation of

UCP2-mediated mild uncoupling is common to both models, only the activating species differ, resulting from different stages of lipoperoxidation. Unlike fatty acid hydroperoxides (FAOOHs), which can be considered as early products of lipid peroxidation, HNE and related alkenals are nearly terminal products of lipoperoxidation, emerging from a self-propagating chain of free radical reactions occurring within the PUFA side chains still covalently bound to the glycerophospholipid backbone [286–288]. Hence UCP2 activation by HNE is a phospholipase-independent process. Although reactive aldehydes, many of which are cytotoxic, take part in various signaling pathways [289], our work brings forth another piece of evidence for UCP2 activation mediated by FAOOHs, well upstream of the peroxidation cascade leading to HNE.

The mechanism by which superoxide or other downstream reactive oxygen species activate mitochondrial phospholipases A₂ however remains unclear [160, 280]. An indirect activation could conceivably stem from a preferential PLA₂ specificity to cleave hydroperoxy phospholipids (PLOOHs) rather than intact glycerophospholipids, unaffected by lipoperoxidation [133]. In the literature it has been assumed that it was superoxide itself which was directly activating mtPLA₂. Apparently, a direct activation would involve interaction between mitochondrial PLA₂ and reactive oxygen species. The source of the superoxide burst could be either peroxynitrite which causes inhibition of Complex III and promotes elevated superoxide formation [139]. Also conditions such as hypoxia (see chapter 5.4, *page 102*) and the inhibition of cytochrome *c* oxidase (Complex IV) by •NO, *etc.*, may raise the mitochondrial production of superoxide.

Collectively, the number of mtPLA₂, their specificity, as well as the exact mechanism of mtPLA₂ regulation is yet to be established. Our results demonstrate the presence of iPLA₂ in lung mitochondria and underscore the straightforward mechanism of mtPLA₂-mediated fatty acid hydroperoxides release to stimulate UCP2-dependent attenuation of reactive oxygen species [290–291].

5.4 Implementation of Physiological Normoxia Conditions as a Real Experimental Model

Oxidative metabolism gives higher yield of energy production than anaerobic metabolism. However, oxygen utilization occurs on behalf of side reactions leading to the production of reactive oxygen metabolites, which if in excess, destroy cellular constituents. In this light, oxygen is perceived as a reactive and toxic compound for living organisms [292]. It was not for no reason that organisms adapted to increasing levels of oxygen in the atmosphere during evolution by developing antioxidant mechanisms of varied nature [293]. For instance upon exposure to oxygen, *Escherichia coli* induces the expression of enzymes essential for aerobic respiration, such as components of the Krebs cycle and terminal oxidase complexes, in parallel with simultaneous induction of antioxidant enzymes MnSOD and catalase [294]. Mitochondria, which probably evolved from an early aerobic parasite of anaerobic cells, are the cornerstone of aerobic metabolism [295].

Experiments with cell cultures are routinely performed at an air atmosphere ($\sim 21\% \text{ O}_2$) because of its convenience and ease of use. However, these conditions in terms of oxygen concentration are far away from what is going on the level of tissues and organs [195], referred here to as physiological normoxia ($\sim 5\% \text{ O}_2$ for liver). Moreover, under certain pathological circumstances (ischemic disorders, diabetes, atherosclerosis, etc.) [195], when the demand for O_2 by the respiratory chain exceeds its supply, oxygen levels may temporarily drop even beyond a tissue-specific threshold level and attain the state of physiological hypoxia ($< 5\% \text{ O}_2$ for liver) [200]. We may speculate, to what extent the commonly employed hyperoxic conditions for cultivation of tissues and cells affect the biochemistry and physiology of the cell.

We attempted to simulate these transient changes, mediated presumably by hypoxia-inducible factor (HIF) [199], by transferring hepatocellular carcinoma HepG2 cells (cultivated at atmospheric O_2) to 5% for the period of three days, and quantified basic respiratory parameters (Figs. 40–43, pages 82–85). Furthermore, we have applied

variations between the oxidative phosphorylation and glycolytic metabolism extent of the cells. The correctness of our model is supported by the fact that OXPHOS cells, with active oxidative phosphorylation machinery, adapted more efficiently to tissue normoxia than cells utilizing glycolysis as the main energy source, GLC5 and GLC25 cells (Figs. 40–41, pages 82–83). On this basis, we may assume that similar adaptations occur during transfer from physiological normoxia to hypoxia *in vivo*. These results can be compared to those observed by Chandel *et al.*, who reported a reversible suppression of respiration during prolonged hypoxia in hepatocytes suggesting an oxygen sensing role of cytochrome *c* oxidase (Complex IV) [296]. However, to prove the direct involvement of HIF or cytochrome *c* oxidase in our studies would require further investigation.

The observed differences in the capacities of HepG2 cells to adapt to low oxygen levels might be related their carcinogenicity [297]. Stem cells and embryonic cells, in one period before passage through the fallopian tube during ontogenesis, largely employ glycolysis as the main source of energy. This allows replication of mitochondrial DNA to cease in order to dilute mtDNA among mitochondria. Later on, during cell differentiation and organ/tissue maturation oxidative metabolism prevails. From the perspective of the balance between glycolysis and oxidative phosphorylation, tumorigenesis could be viewed as a reversal back to the fetal bioenergetic status. The original Warburg's hypothesis [298] of assuming glycolytic only cancer cells was recently challenged by biochemical studies that revealed the existence of a wide class of tumors where ATP is produced more in a higher extent by mitochondrial oxidative phosphorylation rather than solely by glycolysis [299]. Hence, a survey of these studies showed that various tumors produce a significant part of their ATP (> 80%) by the mitochondrion [300].

Altogether, embryonic and tumor cells, as well as cells deficient of respiratory substrates, undergoing slow respiration at the edge of non-phosphorylating state 4 share an increased tolerance to hypoxia due to their diminished demand for oxygen. On the other hand, differentiated and metabolically active cells rely on instant adaptation mechanisms to survive. The ratio between the extent of oxidative phosphorylation and glycolysis governs these specific adaptations, so as the homeostasis of reactive oxygen species and related redox regulations.

We should also highlight the important function of pyruvate at the metabolic junction between glycolysis and oxidative phosphorylation, which is well suited for the cell's need to regulate these interconnected anaerobic and O₂-dependent energy metabolism pathways, respectively [301]. Such regulation undoubtedly includes pyruvate-mediated stabilization of HIF1 α [238–239]. Similar function has been attributed to all α -ketoglutarate structural analogs, such as Krebs cycle intermediates succinate, fumarate, and oxalacetate.

Recently emerging knowledge states that the morphology of mitochondrial network and of cristae internal structure depends on the bioenergetic activity of mitochondria and *vice versa* [302]. In similar way, the relationship between the extent of oxidative phosphorylation *vs.* glycolysis and mitochondria-derived production of reactive oxygen species has to be carefully considered. Under physiological conditions, the basic presumption predicts proportional dependence of increasing O₂^{•-} formation with higher magnitude of respiration coupled to oxidative phosphorylation.

My colleague, RNDr. Lydie Plecítá-Hlavatá, Ph.D. tried to seek correlations in addition to respiration, also among the extent of oxidative phosphorylation, O₂^{•-} production, and concomitant variations in the morphology of mitochondrial reticulum after three-day adaptation of HepG2 cells to 5% oxygen. She has found that upon such normoxic adaptation, OXPHOS cells drastically reduce mitochondrial superoxide production down to 8% with accompanying thinning of mitochondrial reticulum tubules (Dr. Lydie Plecítá-Hlavatá, unpublished).





Added together with my results, we show that HepG2 cells, forced to oxidative phosphorylation (OXPHOS cells), adapt slowly but more efficiently to physiological normoxia than their glycolytic counterparts (GLC5 and GLC25 HepG2 cells). Such adaptation corresponded with highly repressed mitochondrial O₂^{•-} production on the background of efficient oxidative phosphorylation and ongoing dynamic changes of mitochondrial reticulum.

6 SUMMARY OF FINDINGS

6.1 Characterization of a Novel Inhibitor of Proton Pumping by Mitochondrial Complex I

Uncoupling attenuates Complex I-derived superoxide production by accelerating electron flux and proton pumping by Complex I (Fig. 45, *pages 89–90*). However, under circumstances leading to hampered proton pumping pathway within Complex I, *e.g.* due to aberrant mutations of mtDNA encoding either ND2, ND4 or ND5 H⁺-pumping subunit, therapeutic strategy based simply on uncoupling would fail. Uncoupling means either the use of a chemical uncoupler, such as FCCP, or a physiological uncoupling mediated by uncoupling protein 2 (UCP2). Experimentally, hydrophobic amiloride EIPA mimicks the model of disabled H⁺-pumping.

I have participated in this project by demonstrating that EIPA is a real inhibitor of Complex I H⁺-pumping based on the following observations:

-  Glutamate and malate, Complex I substrates, stimulate H⁺-pumping sensitive to inhibition by stigmatellin (Fig. 13, *page 43*) and FCCP (Fig. 14, *page 44*) in isolated rat liver mitochondria respiring in state 4.
-  EIPA prevents glutamate and malate-stimulated H⁺-pumping when added before the substrates (Fig. 15, *page 45*).
-  Glutamate and malate-induced H⁺-pumping is repressed by matrix acidification stimulated by EIPA added before (Fig. 16, *page 46*) or after rotenone (Fig. 17, *page 47*).
-  EIPA is able to induce matrix acidification even in the presence of glutamate, malate, and monensin irrespectively of the Na⁺ ions present (Fig. 18, *page 48*).

- EIPA dose responses for Complex I H⁺-pumping inhibition yielded IC₅₀ values of 27 μM (Fig. 20, *page 51*) and ~ 140 μM EIPA when added before and after glutamate and malate, respectively.
- In isolated rat liver mitochondria respiring in state 3, EIPA abolished glutamate and malate-stimulated H⁺-pumping after the addition of substrates (Fig. 19, *page 49*) with the IC₅₀ of 50 μM (Fig. 20, *page 51*).
- EIPA does not affect glutamate and malate-driven state 4 respiration within the concentration range required for H⁺-pumping inhibition (Fig. 20, *page 51*).

6.2 ● The Mechanism of Action of Mitochondrial Matrix-targeted Ubiquinone MitoQ₁₀

Based on the results of experiments with EIPA, we were trying to search an agent, which would be beneficial in treatment of oxidative stress arising from mtDNA mutations in segments encoding H⁺-pumping subunits of Complex I. Note that chemical uncoupler is ineffective in preventing such an oxidative stress, see chapter 6.1 (*page 105*). So we tried to test the antioxidant developed by Murphy's group, MitoQ₁₀. However, MitoQ₁₀ showed to be an effective antioxidant only when the rate of superoxide formation is high due to the electron flow retardation within Complex I, *e.g.* induced by rotenone. In this case, MitoQ₁₀ serves as an electron acceptor prior to the Q-site occupied by rotenone and the oxidized form is regenerated *via* the reverse mode of action of Complex II (Fig. 46, *pages 95–96*). The principal advantage of MitoQ₁₀ over antioxidant drugs based on uncoupling is that it preserves its antioxidant properties even when proton pumping by Complex I is obstructed. Nevertheless, due to the pro-oxidant properties of MitoQ₁₀, a targeted delivery to the pathological tissue would have to be part of the therapeutic strategy.

I have contributed in elucidating the antioxidant mechanism of MitoQ₁₀ by showing that:

- MitoQ₁₀ accelerates respiration of both, HepG2 glycolysis-dependent GLC25 cells and HepG2 oxidative phosphorylation-dependent OXPHOS cells, on average 1.5-fold (Fig. 21, *page 55*, Table 4, *pages 53–54*).
- The accelerated level accounts for ~ 60% of uncoupled respiration (Fig. 22, *page 56*, Table 4, *pages 53–54*).
- MitoQ₁₀ restores rotenone-suppressed respiration to 67% and 45% of state 3 respiration in GLC and OXPHOS cells, respectively (Fig. 23, *page 57*, Table 4, *pages 53–54*).
- A negligible effect on respiratory acceleration was shown for DecylTPP, a negative control (Figs. 24–25, *pages 58–59*, Table 4, *pages 53–54*).
- MitoQ₁₀ dose responses for respiratory acceleration yielded AC₅₀ values of 0.6 nM and 0.6 nM in GLC25 cells (Fig. 25, *page 59*, Table 4, *pages 53–54*); and 1.1 nM and 0.9 nM in OXPHOS cells (Fig. 26, *page 60*, Table 4, *pages 53–54*); in the absence or presence of rotenone, respectively.
- Respiration increase induced by MitoQ₁₀ requires complexes II (Fig. 28, *page 63*, Table 4, *pages 53–54*) and III (Fig. 27, *page 62*).
- Rotenone slightly accelerated H₂O₂ production in rat liver mitochondria respiring in state 3 (Fig. 29, *page 65*).
- In mitochondria isolated from GLC25 cells respiring on glutamate, malate, and succinate, MitoQ₁₀ induced a 1.37-fold increase in state 3 respiration with the AC₅₀ of 1 nM, and a 1.4-fold increase in state 3 rotenone-inhibited respiration with the AC₅₀ of 0.7 nM (Fig. 32, *page 69*).

6.3 ● Mitochondrial Phospholipase iPLA₂-Dependent Regulation of Uncoupling Protein 2

It has been concluded before, that uncoupling fails to diminish oxidative stress resulting from aberrant parts of mtDNA encoding H⁺-pumping subunits of Complex I, see chapter 6.1 (*page 105*). We resolved this situation by suggesting the use of MitoQ₁₀ antioxidant for this purpose, see chapter 6.2 (*page 106*). Hence, we have drawn our further attention to the mechanisms by which physiological uncoupling, mediated by the ubiquitous uncoupling protein 2, is regulated in order to counteract oxidative stress. Here we focused on oxidative stress associated with lipid peroxidation. In experiments, lipoperoxidation was simulated by low amounts of *tert*-butyl hydroperoxide (TBHP). Activation of mitochondrial phospholipase iPLA₂ by mild oxidative stress can provide free fatty acid hydroperoxides (FAOOH) as the cycling substrates for UCP2 that initiates mild uncoupling leading to the attenuation of ROS production and the concomitant oxidative stress. Hence certain feedback inhibition of lipid peroxidation would occur.

The orchestrated action of UCP2 and iPLA₂ in feedback down-regulation of reactive oxygen species production can be deduced from the following observations:

- Succinate-supported was stimulated by low concentrations of TBHP in isolated rat lung mitochondria (Fig. 33, *page 71*).
- The observed respiration increase was fully inhibited by BSA, indicating the participation of free fatty acids (Fig. 34, *page 73*), blocked by bromoenol lactone (BEL), a specific inhibitor of phospholipases iPLA₂ (Figs. 35–36, *pages 74–75*), and partially inhibited by GTP, an inhibitor of UCP2 (Fig. 37, *page 76*).
- The TBHP-dependent increase in respiratory rate was not observed in lung mitochondria isolated from UCP2-KO mice. (Fig. 38, *page 77*).
- Mitochondrial H₂O₂ production was accelerated by BSA and BEL (Fig. 39, *page 79*).

6.4 ● The Elevation of State 4 Respiration upon Adaptation to Physiological Normoxia


The amount of superoxide production depends also on the actual effective concentration of oxygen in the cell. Cell and tissue cultures are artificially grown at an air atmosphere as a standard laboratory practice. Both reasons motivated us to look at what is going on at the level of *in vivo* intracellular oxygen concentration. We measured respiratory parameters of HepG2 cells after a three-day adaptation to 5% O₂ and compared them to the controls. Moreover, we distinguished three different metabolic conditions with regard to the content of glycolysis *vs.* oxidative phosphorylation. We found that, cells with lower oxidative phosphorylation content adapt less efficiently to the conditions of physiological normoxia as observed from the decline of their respiration. Furthermore, state 3/state 4 respiratory control ratio analysis indicates that OXPHOS cells contain higher proportion of phosphorylating mitochondria than glycolytic cells. This is in agreement with the presumption that OXPHOS cells utilize efficient oxidative phosphorylation tightly coupled to mitochondrial respiration. High-amplitudes of uncoupled state *vs.* state 4 were observed for all metabolic conditions independently of the O₂ level during adaptation with the exception of GLC5 cells adapted to 5% O₂. Hence, glycolytic normoglycemic cells adapt to 5% oxygen by elevated state 4 respiration.


The results are summarized as follows:


- Respiration of cells cultivated in 5 mM (GLC5) and 25 mM (GLC25) glucose decreased by 55% and 61%, respectively after a 3-day adaptation to 5% oxygen (Figs. 40–41, *pages 82–83*).
- Respiration of cells cultivated in galactose and glutamine, relying predominantly on oxidative phosphorylation (OXPHOS cells), decreased only by 15% after 3-day adaptation to 5% oxygen (Figs. 40–41, *pages 82–83*).
- OXPHOS cells elicited significantly higher respiratory state 3/state 4 control ratio than glycolytic cells GLC5 and GLC25 (Fig. 42, *page 84*).


- GLC5 cells showed significant decrease of uncoupled state/state 4 respiratory control ratio upon a three-day adaptation to 5% O₂ (Fig. 43, *page 85*).
- Instant adaptation of HepG2 cells did not show any influence on their endogenous respiration (Figs. 40–41, 44, *pages 82–83, 87*).

7 CONCLUSIONS

 Accelerated electron flux and concomitant proton pumping within Complex I by uncoupler or uncoupling proteins, which attenuate Complex I-derived superoxide production, cannot be in effect when proton pumping is blocked. In experiments, this block was simulated by EIPA. EIPA is indeed an effective inhibitor of proton pumping mediated by Complex I. Hence, uncoupling *per se* can diminish ROS production but not the one resulting from damage of mtDNA linked to impairment of the proton pumping pathway.

 MitoQ₁₀ exerts its antioxidant action by bypassing electron block on Complex I *via* an alternative electron transfer pathway involving Complex II acting in the reverse mode. Unlike uncoupling, MitoQ₁₀ is able to possibly cure diseases and aging symptoms coming from oxidative stress due to the impairment of Complex I proton pumping subunits, *i.e.* those coded by oxidatively damaged mtDNA. However a targeted delivery to the pathological tissue would have to be ensured.

 Oxidative stress attenuation by UCP2-dependent uncoupling is initiated upon the activation of mitochondrial phospholipase iPLA₂ as a feedback regulatory response to increased lipoperoxidation.

 Cells with high oxidative phosphorylation content adapt to more efficient oxidative phosphorylation under conditions of physiological normoxia, whereas glycolytic normoglycemic cells adapt to physiological normoxia by elevated state 4 respiration.

8 REFERENCES

- [1] Dlasková, A., Hlavatá, L., Ježek, J., Ježek, P.: *Int. J. Biochem. Cell Biol.* **40**, 2098–2109 (2008) <http://dx.doi.org/10.1016/j.biocel.2008.02.007>
- [2] Plecítá-Hlavatá, L., Ježek, J., Ježek, P.: *Int. J. Biochem. Cell Biol.* **41**, 1697–1707 (2009) <http://dx.doi.org/10.1016/j.biocel.2009.02.015>
- [3] Ježek, P., Ježek, J.: *FEBS Lett.* **534**, 15–25 (2003) [http://dx.doi.org/10.1016/S0014-5793\(02\)03779-1](http://dx.doi.org/10.1016/S0014-5793(02)03779-1)
- [4] Ježek, P., Hlavatá, L.: *Int. J. Biochem. Cell Biol.* **37**, 2478–2503 (2005)
- [5] Raha, S., Robinson, B.H.: *Trends Biochem. Sci.* **25**, 502–508 (2000)
- [6] Wallace, D.C.: *Science* **283**, 1482–1488 (1999)
- [7] St-Pierre, J., Buckingham, J.A., Roebuck, S.J., Brand, M.D.: *J. Biol. Chem.* **277**, 44784–44790 (2002)
- [8] Boveris, A., Chance, B.: *Biochem. J.* **134**, 707–716 (1973)
- [9] Liu, S.S.: *Biosci. Rep.* **17**, 259–272 (1997)
- [10] Turens, J.F.: *J. Physiol.* **552**, 335–344 (2003)
- [11] <http://www.genome.jp/kegg/pathway.html>
- [12] De Grey, A.D.N.J.: *DNA Cell Biol.* **21**, 251–257 (2002)
- [13] Rebrin, I., Sohal, R.S.: *Adv. Drug Deliv. Rev.* **60**, 1545–1552 (2008)
- [14] Fernández-Checa, J.C.: *Biochem. Biophys. Res. Commun.* **304**, 471–479 (2003)
- [15] Feissner, R.F., Skalska, J., Gaum, W.E., Sheu, S.S.: *Front. Biosci.* **14**, 1197–1218 (2009)
- [16] Archer, S.L., Gomberg-Maitland, M., Maitland, M.L., Rich, S., Garcia, J.G., Weir, E.K.: *Am. J. Physiol. Heart Circ. Physiol.* **294**, H570–H578 (2008)
- [17] Ott, M., Gogvadze, V., Orrenius, S., Zhivotovsky, B.: *Apoptosis* **12**, 913–922 (2007)
- [18] Klimova, T., Chandel, N.S.: *Cell Death Differ.* **200815**, 660–666 (2008)
- [19] Valko, M., Morris, H., Cronin, M.T.: *Curr. Med. Chem.* **12**, 1161–1208 (2005)
- [20] Hiona, A., Leeuwenburgh, C.: *Exp. Gerontol.* **43**, 24–33 (2008)
- [21] Kakkar, P., Singh, B.K.: *Mol. Cell. Biochem.* **305**, 235–253 (2007)

- [22] Mancuso, M., Coppedè, F., Murri, L., Siciliano, G.: *Antioxid. Redox Signal.* **9**, 1631–1646 (2007)
- [23] Lambert, A.J., Brand, M.D.: *Aging Cell* **6**, 417–420 (2007)
- [24] Skulachev, V.P.: *Biochemistry Mosc.* **62**, 1191–1195 (1997)
- [25] Gruber, J., Schaffer, S., Halliwell, B.: *Front. Biosci.* **13**, 6554–6579 (2008)
- [26] Finsterer, J.: *VASA* **36**, 229–240 (2007)
- [27] Fridlyand, L.E., Philipson, L.H.: *Curr. Diabetes Rev.* **2**, 241–259 (2006)
- [28] Ballinger, S.W.: *Free Radic. Biol. Med.* **38**, 1278–1295 (2005)
- [29] Mantena, S.K., King, A.L., Andringa, K.K., Eccleston, H.B., Bailey, S.M.: *Free Radic. Biol. Med.* **44**, 1259–1272 (2008)
- [30] Lin, M.T., Beal, M.F.: *Nature* **443**, 787–795 (2006)
- [31] Reeve, A.K., Krishnan, K.J., Turnbull, D.M.: *Biotechnol. J.* **3**, 750–756 (2008)
- [32] Schapira, A.H.: *Lancet Neurol.* **7**, 97–109 (2008)
- [33] Votyakova, T.V., Reynolds, I.J.: *J. Neurochem.* **79**, 266–277 (2001)
- [34] Bossy-Wetzell, E., Barsoum, M.J., Godzik, A., Schwarzenbacher, R., Lipton, S.A.: *Curr. Opin. Cell Biol.* **15**, 706–716 (2003)
- [35] Hu, J., de Souza-Pinto, N.C., Haraguchi, K., Hogue, B.A., Jaruga, P., Greenberg, M.M., Dizdaroglu, M., Bohr, V.A.: *J. Biol. Chem.* **280**, 40544–40551 (2005)
- [36] Wong, L.J.: *Muscle Nerve* **36**, 279–293 (2007)
- [37] Zhadanov, S.I., Grechanina, E.Y., Grechanina, Y.B., Gusar, V.A., Fedoseeva, N.P., Lebon, S., Münnich, A., Schurr, T.G.: *Mitochondrion* **7**, 260–266 (2007)
- [38] <http://www.mrc-mbu.cam.ac.uk/research>
- [39] Zhang, H., Osyczka, A., Dutton, P.L., Moser, C.C.: *Biochim. Biophys. Acta* **1767**, 883–887 (2007)
- [40] Lambert, A.J., Brand, M.D.: *J. Biol. Chem.* **279**, 39414–39420 (2004)
- [41] Dröse, S., Brandt, U.: *J. Biol. Chem.* **283**, 21649–21654 (2008)
- [42] Cape, J.L., Bowman, M.K., Kramer, D.M.: *Proc. Natl. Acad. Sci. U.S.A.* **104**, 7887–7892 (2007)
- [43] Brand, M.D., Affourtit, C., Esteves, T.C., Green, K., Lambert, A.J., Miwa, S., Pakay, J.L., Parker, N.: *Free Radic. Biol. Med.* **37**, 755–767 (2004)
- [44] Arsenijevic, D., Onuma, H., Pecqueur, C., Raimbault, S., Manning, B.S., Miroux, B., Couplan, E., Alves-Guerra, M.C., Gubern, M., Surwit, R., Bouillaud, F., Richard, D., Collins, S., Ricquier, D.: *Nat. Genet.* **26**, 435–439 (2000)

- [45] Jabůrek, M., Miyamoto, S., Di Mascio, P., Garlid, K.D., Ježek, P.: *J. Biol. Chem.* 279, 53097–53102 (2004)
- [46] Růžička, M., Škobisová, E., Dlasková, A., Šantorová, J., Smolková, K., Špaček, T., Žáčková, M., Modrianský, M., Ježek, P.: *Int. J. Biochem. Cell Biol.* 37, 809–821 (2005)
- [47] Nègre-Salvayre, A., Hirtz, C., Carrera, G., Cazenave, R., Troly, M., Salvayere, R., Penicaud, L., Caisteila, L.A.: *FASEB J.* 11, 809–815 (1997)
- [48] Horimoto, M., Fulop, P., Derdak, Z., Wands, J.R., Baffy, G.: *Hepatology* 39, 386–392 (2004)
- [49] Miwa, S., Brand, M.D.: *Biochem. Soc. Trans.* 31, 1300–1301 (2003)
- [50] Rousset, S., Alves-Guerra, M.C., Mozo, J., Miroux, B., Cassard-Doulicier, A.M., Bouillaud, F., Ricquier, D.: *Diabetes* 53, S130–S135 (2004)
- [51] Kadenbach, B.: *Biochim. Biophys. Acta* 1604, 77–94 (2003)
- [52] Skulachev, V.P.: *Aging Cell* 3, 17–19 (2004)
- [53] Lambert, A.J., Brand, M.D.: *Biochem. J.* 382, 511–517 (2004)
- [54] Muller, F.L., Liu, Y., Van Remmen, H.: *J. Biol. Chem.* 279, 49064–49073 (2004)
- [55] Xu, X., Arriaga, E.A.: *Free Radic. Biol. Med.* 46, 905–913 (2009)
- [56] Korshunov, S.S., Skulachev, V.P., Starkov, A.A.: *FEBS Lett.* 416, 15–18 (1997)
- [57] Starkov, A.A., Fiskum, G.: *J. Neurochem.* 86, 1101–1107 (2003)
- [58] Liu, Y., Fiskum, G., Schubert, D.: *J. Neurochem.* 80, 780–787 (2002)
- [59] Grivennikova, V.G., Vinogradov, A.D.: *Biochim. Biophys. Acta* 1757, 553–561 (2006)
- [60] Tahara, E.B., Navarete, F.D., Kowaltowski, A.J.: *Free Radic. Biol. Med.* 46, 1283–1297 (2009)
- [61] Lacza, Z., Pankotai, E., Busija, D.W.: *Front. Biosci.* 14, 4436–4443 (2009)
- [62] Afanas'ev, I.: *Front. Biosci.* 14, 3899–3912 (2009)
- [63] Liaudet, L., Vassalli, G., Pacher, P.: *Front. Biosci.* 14, 4809–4814 (2009)
- [64] Cooper, C.E., Brown, G.C.: *J. Bioenerg. Biomembr.* 40, 533–539 (2008)
- [65] Ghafourifar, P., Cadenas, E.: *Trends Pharmacol. Sci.* 26, 190–195 (2005)
- [66] Galkin, A., Higgs, A., Moncada, S.: *Essays Biochem.* 43, 29–42 (2007)
- [67] Finocchietto, P., Barreyro, F., Holod, S., Peralta, J., Franco, M.C., Méndez, C., Converso, D.P., Estévez, A., Carreras, M.C., Poderoso, J.J.: *PLoS ONE* 3, e1749 (2008)

- [68] Radi, Z.A.: *Toxicol. Pathol.* 37, 34–46 (2009)
- [69] Maccarrone, M., Melino, G., Finazzi-Agrò, A.: *Cell Death Differ.* 8, 776–784 (2001)
- [70] Yamamoto, S.: *Biochim. Biophys. Acta* 1128, 117–131 (1992)
- [71] Niki, E., Yoshida, Y., Saito, Y., Noguchi, N.: *Biochem. Biophys. Res. Commun.* 338, 668–676 (2005)
- [72] Uchida, K.: *Curr. Atheroscler. Rep.* 9, 216–221 (2007)
- [73] Spiteller, G.: *Prostaglandins Leukot. Essent. Fatty Acids* 67, 151–162 (2002)
- [74] Williams, S.D., Gottlieb, R.A.: *Biochem. J.* 362, 23–32 (2002)
- [75] Broekemeier, K.M., Iben, J.R., LeVan, E.G., Crouser, E.D., Pfeiffer, D.R.: *Biochemistry* 41, 7771–7780 (2002)
- [76] Zickermann, V., Kerscher, S., Zwicker, K., Tocilescu, M.A., Radermacher, M., Brandt, U.: *Biochim. Biophys. Acta* 1787, 574–583 (2009)
- [77] Lenaz, G., Baracca, A., Fato, R., Genova, M.L., Solaini, G.: *Antioxid. Redox Signal.* 8, 417–437 (2006)
- [78] Lenaz, G., Fato, R., Formiggini, G., Genova, M.L.: *Mitochondrion* 78, S8–S33 (2007)
- [79] Yagi, T., Matsuno-Yagi, A.: *Biochemistry* 42, 2266–2274 (2003)
- [80] Brandt, U.: *Annu. Rev. Biochem.* 75, 69–92 (2006)
- [81] Galkin, A., Dröese, S., Brandt, U.: *Biochim. Biophys. Acta* 1757, 1575–1581 (2006)
- [82] Degli Esposti, M.: *Biochim. Biophys. Acta* 1364, 222–235 (1998)
- [83] Fendel, U., Tocilescu, M.A., Kerscher, S., Brandt, U.: *Biochim. Biophys. Acta* 1777, 660–665 (2008)
- [84] Lindell, S.D., Ort, O., Lümmer, P., Klein, R.: *Bioorg. Med. Chem. Lett.* 14, 511–514 (2004)
- [85] Okun, J.G., Lümmer, P., Brandt, U.: *J. Biol. Chem.* 274, 2625–2630 (1999)
- [86] Lümmer P.: *Biochim. Biophys. Acta* 1364, 287–296 (1998)
- [87] Lenaz, G., Baracca, A., Fato, R., Genova, M.L., Solaini, G.: *Ital. J. Biochem.* 55, 232–253 (2006)
- [88] King, M.S., Sharpley, M.S., Hirst, J.: *Biochemistry* 48, 2053–2062 (2009)
- [89] http://www.biocenter.helsinki.fi/bi/hbg/research_Complex_I.html

- [90] Yakovlev, G., Reda, T., Hirst, J.: *Proc. Natl. Acad. Sci. U.S.A.* 104, 12720–12725 (2007)
- [91] Mathiesen, C., Hägerhäll, C.: *Biochim. Biophys. Acta* 1556, 121–132 (2002)
- [92] Sazanov, L.A., Hinchliffe, P.: *Science* 311, 1430–1436 (2006)
- [93] Morgan, D.J., Sazanov, L.A.: *Biochim. Biophys. Acta* 1777, 711–718 (2008)
- [94] Baranova, E.A., Holt, P.J., Sazanov, L.A.: *J. Mol. Biol.* 366, 140–154 (2007)
- [95] Sazanov, L.A.: *Biochemistry* 46, 2275–2288 (2007)
- [96] Yano, T.: *Mol. Aspects Med.* 23, 345–368 (2002)
- [97] <http://www.ncbi.nlm.nih.gov/unigene>
- [98] Kushnareva, Y., Murphy, A.N., Andreyev, A.: *Biochem. J.* 368, 545–553 (2002)
- [99] Genova, M.L., Ventura, B., Giuliano, G., Bovina, C., Formiggini, G., Parenti Castelli G., Lenaz, G.: *FEBS Lett.* 505, 364–368 (2001)
- [100] Galkin, A., Brandt, U.: *J. Biol. Chem.* 280, 30129–30135 (2005)
- [101] Kussmaul, L., Hirst, J.: *Proc. Natl. Acad. Sci. U.S.A.* 103, 7607–7612 (2006)
- [102] Ohnishi, S.T., Ohnishi, T., Muranaka, S., Fujita, H., Kimura, H., Uemura, K., Yoshida, K., Utsumi, K.: *J. Bioenerg. Biomembr.* 37, 1–15 (2005)
- [103] Magnitsky, S., Touloukhonova, L., Yano, T., Sled, V.D., Hägerhäll, C., Grivennikova, V.G., Burbaev, D.S., Vinogradov, A.D., Ohnishi, T.: *J. Bioenerg. Biomembr.* 34, 193–207 (2002)
- [104] Ohnishi, T., Salerno, J.C.: *FEBS Lett.* 579, 4555–4561 (2005)
- [105] Tocilescu, M.A., Fendel, U., Zwicker, K., Kerscher, S., Brandt, U.: *J. Biol. Chem.* 282, 29514–29520 (2007)
- [106] Brandt, U., Kerscher, S., Dröse, S., Zwicker, K., Zickermann, V.: *FEBS Lett.* 545, 9–17 (2003)
- [107] Hamamoto, T., Hashimoto, M., Hino, M., Kitada, M., Seto, Y., Kudo, T., Horikoshi, K.: *Mol. Microbiol.* 14, 939–946 (1994)
- [108] Nakamaru-Ogiso, E., Seo, B.B., Yagi, T., Matsuno-Yagi, A.: *FEBS Lett.* 549, 43–46 (2003)
- [109] Gemperli, A.C., Schaffitzel, C., Jakob, C., Steuber, J.: *Arch. Microbiol.* 188, 509–521 (2007)
- [110] Nakamaru-Ogiso, E., Sakamoto, K., Matsuno-Yagi, A., Myioshi, H., Yagi, T.: *Biochemistry* 42, 746–754 (2003)

- [111] Kadenbach, B., Ramzan, R., Wen, L., Vogt, S.: *Biochim. Biophys. Acta* in press (2009) <http://dx.doi.org/10.1016/j.bbagen.2009.04.019>
- [112] Bourges, I., Ramus, C., Mousson de Camaret, B., Beugnot, R., Remacle, C., Cardol, P., Hofhaus, G., Issartel, J.P.: *Biochem. J.* **383**, 491–499 (2004)
- [113] Chomyn, A., Attardi, G.: *Biochem. Biophys. Res. Commun.* **304**, 519–529 (2003)
- [114] Dlasková, A., Hlavatá, L., Ježek, P.: *Int. J. Biochem. Cell Biol.* **40**, 1792–1805 (2008)
- [115] Muller, F.L., Lustgarten, M.S., Jang, Y., Richardson, A., Van Remmen, H.: *Free Radic. Biol. Med.* **43**, 477–503 (2007)
- [116] Bai, Y., Hu, P., Park, J.S., Deng, J.H., Song, X., Chomyn, A., Yagi, T., Attardi, G.: *Ann. N. Y. Acad. Sci.* **1011**, 272–283 (2004)
- [117] Adlam, V.J., Harrison, J.C., Porteous, C.M., James, A.M., Smith, R.A., Murphy, M.P., Sammut, I.A.: *FASEB J.* **19**, 1088–1095 (2005)
- [118] Armstrong, J.S.: *Antioxid. Redox Signal.* **10**, 575–578 (2008)
- [119] Camello-Almaraz, M.C., Pozo, M.J., Murphy, M.P., Camello, P.J.: *J. Cell. Physiol.* **206**, 487–494 (2006)
- [120] Cochemé, H.M., Kelso, G.F., James, A.M., Ross, M.F., Trnka, J., Mahendiran, T., Asin-Cayuela, J., Blaikie, F.H., Manas, A.R., Porteous, C.M., Adlam, V.J., Smith, R.A., Murphy, M.P.: *Mitochondrion* **7**, S94–S102 (2007)
- [121] Reddy, P.H.: *J. Biomed. Biotechnol.* **31372**, 1–13 (2006)
- [122] Tauskela, J.S.: *IDrugs* **10**, 399–412 (2007)
- [123] Doughan, A.K., Dikalov, S.I.: *Antioxid. Redox Signal.* **9**, 1825–1836 (2007)
- [124] James, A.M., Cochemé, H.M., Smith, R.A., Murphy, M.P.: *J. Biol. Chem.* **280**, 21295–21312 (2005)
- [125] O'Malley, Y., Fink, B.D., Ross, N.C., Prisinzano, T.E., Sivitz, W.I.: *J. Biol. Chem.* **281**, 39766–39775 (2006)
- [126] Adlam, V.J., Harrison, J.C., Porteous, C.M., James, A.M., Smith, R.A., Murphy, M.P., Sammut, I.A.: *FASEB J.* **19**, 1088–1095 (2005)
- [127] James, A.M., Cochemé, H.M., Murphy, M.P.: *Mech. Ageing Dev.* **126**, 982–986 (2005)
- [128] Asin-Cayuela, J., Manas, A.R., James, A.M., Smith, R.A., Murphy, M.P.: *FEBS Lett.* **571**, 9–16 (2004)

- [129] James, A.M., Sharpley, M.S., Manas, A.R., Frerman, F.E., Hirst, J., Smith, R.A., Murphy, M.P.: *J. Biol. Chem.* 282, 14708–14718 (2007)
- [130] Kelso, G.F., Porteous, C.M., Coulter, C.V., Hughes, G., Porteous, W.K., Ledgerwood, E.C., Smith, R.A., Murphy, M.P.: *J. Biol. Chem.* 276, 4588–4596 (2001)
- [131] Kelso, G.F., Porteous, C.M., Hughes, G., Ledgerwood, E.C., Gane, A.M., Smith, R.A., Murphy, M.P.: *Ann. N. Y. Acad. Sci.* 959, 263–274 (2002)
- [132] Ramirez, F., Jain, M.K.: *Proteins* 9, 229–239 (1991)
- [133] van Kuijk, F.J.G.M, Sevanian, A., Handelman, G.J., Dratz E.A.: *Trends Biochem. Sci.* 12, 31–34 (1987)
- [134] Burke, J.E., Dennis, E.A.: *Cardiovasc. Drugs Ther.* 23, 49–59 (2009)
- [135] Žáčková, M., Škobisová, E., Urbánková, E., Ježek, P.: *J. Biol. Chem.* 278, 20761–20769 (2003)
- [136] Beck, V., Jabůrek, M., Demina, T., Rupprecht, A., Porter, R.K., Ježek, P., Pohl, E.E.: *FASEB J.* 21, 1137–1144 (2007)
- [137] Echtay, K.S., Esteves, T.C., Pakay, J.L., Jekabsons, M.B., Lambert, A.J., Portero-Otín, M., Pamplona, R., Vidal-Puig, A.J., Wang, S., Roebuck, S.J., Brand, M.D.: *EMBO J.* 22, 4103–4110 (2003)
- [138] Murphy, M.P., Echtay, K.S., Blaikie, F.H., Asin-Cayuela, J., Cochemé, H.M., Green, K., Buckingham, J., Taylor, E.R., Hurrell, F., Hughes, G., Miwa, S., Cooper, C.E., Svistunenko, D.A., Smith, R.A., Brand, M.: *J. Biol. Chem.* 278, 48534–48545 (2003)
- [139] Mancuso, D.J., Jenkins, C.M., Sims, H.F., Cohen, J.M., Yang, J., Gross, R.W.: *Eur. J. Biochem.* 271, 4709–4724 (2004)
- [140] Nanda, B.L., Nataraju, A., Rajesh, R., Rangappa, K.S., Shekar, M.A., Vishwanath, B.S.: *Curr. Top. Med. Chem.* 7, 765–777 (2007)
- [141] Khanapure, S.P., Garvey, D.S., Janero, D.R., Letts, L.G.: *Curr. Top. Med. Chem.* 7, 311–340 (2007)
- [142] Lambeau, G., Gelb, M.H.: *Annu. Rev. Biochem.* 77, 495–520 (2008)
- [143] Farooqui, A.A., Litsky, M.L., Farooqui, T., Horrocks, L.A.: *Brain Res. Bull.* 49, 139–153 (1999)
- [144] O'Donnell, V.B., Maskrey, B., Taylor, G.W.: *Methods Mol. Biol.* 462, 5–23 (2009)
- [145] Harizi, H., Corcuff, J.B., Gualde, N.: *Trends Mol. Med.* 14, 461–469 (2008)

- [146] Burke, J.E., Dennis, E.A.: *J. Lipid Res.* 50, S237–S242 (2009)
- [147] Six, D.A., Dennis, E.A.: *Biochim. Biophys. Acta* 1488, 1–19 (2000)
- [148] Boyanovsky, B.B., Webb, N.R.: *Cardiovasc. Drugs Ther.* 23, 61–72 (2009)
- [149] Jönsson-Rylander, A.C., Lundin, S., Rosengren, B., Pettersson, C., Hurt-Camejo, E.: *Curr. Atheroscler. Rep.* 10, 252–259 (2008)
- [150] Koenig, W., Khuseyinova, N.: *Cardiovasc. Drugs Ther.* 23, 85–92 (2009)
- [151] Rosenson, R.S.: *Cardiovasc. Drugs Ther.* 23, 93–101 (2009)
- [152] Kinsey, G.R., McHowat, J., Beckett, C.S., Schnellmann, R.G.: *Am. J. Physiol. Renal Physiol.* 292, F853–F860 (2007)
- [153] Stewart, A., Ghosh, M., Spencer, D.M., Leslie, C.C.: *J. Biol. Chem.* 277, 29526–29536 (2002)
- [154] Tucker, D.E., Stewart, A., Nallan, L., Bendale, P., Ghomashchi, F., Gelb, M.H., Leslie, C.C.: *J. Lipid Res.* 46, 2122–2133 (2005)
- [155] Larsson Forsell, P.K., Kennedy, B.P., Claesson, H.E.: *Eur. J. Biochem.* 262, 575–585 (1999)
- [156] Cedars, A., Jenkins, C.M., Mancuso, D.J., Gross, R.W.: *J. Cardiovasc. Pharmacol.* 53, 277–289 (2009)
- [157] Jenkins, C.M., Cedars, A., Gross, R.W.: *Cardiovasc. Res.* 82, 240–249 (2009)
- [158] Mancuso, D.J., Sims, H.F., Han, X., Jenkins, C.M., Guan, S.P., Yang, K., Moon, S.H., Pietka, T., Abumrad, N.A., Schlesinger, P.H., Gross, R.W.: *J. Biol. Chem.* 282, 34611–34622 (2007)
- [159] Martín, C., Martínez, R., Navarro, R., Ruiz-Sanz, J.I., Lacort, M., Ruiz-Larrea, M.B.: *Biochem. Pharmacol.* 62, 705–712 (2001)
- [160] Guidarelli, A., Cantoni, O.: *Biochem. J.* 366, 307–314 (2002)
- [161] Madesh, M., Balasubramanian, K.A.: *Arch. Biochem. Biophys.* 346, 187–192 (1997)
- [162] Caro, A.A., Cederbaum, A.I.: *Arch. Biochem. Biophys.* 457, 252–263 (2007)
- [163] Almeida, T., Cunha, R.A., Ribeiro, J.A.: *Brain Res.* 826, 104–111 (1999)
- [164] Arrington, D.D., Van Vleet, T.R., Schnellmann, R.G.: *Am. J. Physiol., Cell Physiol.* 291, C1159–C1171 (2006)
- [165] Krauss, S., Zhang, C.Y., Lowell, B.B.: *Nat. Rev. Mol. Cell Biol.* 6, 248–261 (2005)
- [166] Boss, O., Samec, S., Paoloni-Giacobino, A., Rossier, C., Dulloo, A., Seydoux, J., Muzzin, P., Giacobino, J.P.: *FEBS Lett.* 408, 39–42 (1997)

- [167] Mao, W., Yu, X.X., Zhong, A., Li, W., Brush, J., Sherwood, S.W., Adams, S.H., Pan, G.: *FEBS Lett.* **443**, 326–330 (1999)
- [168] Sanchis, D., Fleury, C., Chomiki, N., Gubern, M., Huang, Q., Neverova, M., Grégoire, F., Easlick, J., Raimbault, S., Lévi-Meyrueis, C., Miroux, B., Collins, S., Seldin, M., Richard, D., Warden, C., Bouillaud, F., Ricquier, D.: *J. Biol. Chem.* **273**, 34611–34615 (1998)
- [169] Vercesi, A.E., Martins, I.S., Silva, M.A.P., Leite, H.M.F., Cuccovia, I.M., Chaimovich, H.: *Nature* **375**, 24–24 (1995)
- [170] Laloi, M., Klein, M., Riesmeier, J.W., Muller-Rober, B., Fleury, C., Bouillaud, F., Ricquier, D.: *Nature* **389**, 135–136 (1997)
- [171] Garlid, K.D., Jabůrek, M., Ježek, P.: *FEBS Lett.* **438**, 10–14 (1998)
- [172] Jabůrek, M., Vařecha, M., Gimeno, R.E., Dembski, M., Ježek, P., Zhang, M., Burn, P., Tartaglia, L.A., Garlid, K.D.: *J. Biol. Chem.* **274**, 26003–26007 (1999)
- [173] Skulachev, V.P.: *Biochim. Biophys. Acta* **1363**, 100–124 (1998)
- [174] Alán, L., Smolková, K., Kronusová, E., Šantorová, J., Ježek, P.: *J. Bioenerg. Biomembr.* **41**, 71–78 (2009)
- [175] Fleury, C., Neverova, M., Collins, S., Raimbault, S., Champigny, O., Levi-Meyrueis, C., Bouillaud, F., Seldin, M.F., Surwit, R.S., Ricquier, D., Warden, C.H.: *Nat. Genet.* **15**, 269–272 (1997)
- [176] Gimeno, R.E., Dembski, M., Weng, X., Deng, N., Shyjan, A.W., Gimeno, C.J., Iris, F., Ellis, S.J., Woolf, E.A., Tartaglia, L.A.: *Diabetes* **46**, 900–906 (1997)
- [177] Pecqueur, C., Alves-Guerra, M.C., Gelly, C., Levi-Meyrueis, C., Couplan, E., Collins, S., Ricquier, D., Bouillaud, F., Miroux, B.: *J. Biol. Chem.* **276**, 8705–8712 (2001)
- [178] Zamzami, N., Hirsch, T., Dallaporta, B., Petit, P.X., Kroemer, G.: *J. Bioenerg. Biomembr.* **29**, 185–193 (1997)
- [179] Nedergaard, J., Ricquier, D., Kozak, L.P.: *EMBO Rep.* **6**, 917–921 (2005)
- [180] Zhang, C.Y., Parton, L.E., Ye, C.P., Krauss, S., Shen, R., Lin, C.T., Porco, J.A. Jr, Lowell, B.B.: *Cell Metab.* **3**, 417–427 (2006)
- [181] Wu, Z., Zhang, J., Zhao, B.: *Antioxid. Redox Signal.* in press (2009)
<http://dx.doi.org/10.1089/ARS.2009.2427>
- [182] Ježek, P., Žáčková, M., Růžička, M., Škobisová, E., Jabůrek, M.: *Physiol. Res.* **53**, S199–S211 (2004)

- [183] Cannon, B., Shabalina, I.G., Kramarova, T.V., Petrovic, N., Nedergaard, J.: *Biochim. Biophys. Acta.* 1757, 449–458 (2006)
- [184] Couplan, E., Gonzales-Barroso, M., Alves-Guerra, M.C., Ricquier, D., Goubern, M., Bouillaud, F.: *J. Biol. Chem.* 277, 26268–26275 (2002)
- [185] Ježek, P.: *Int. J. Biochem. Cell Biol.* 34, 1190–1206 (2002)
- [186] Erlanson-Albertsson C.: *Acta Physiol. Scand.* 178, 405–412 (2003)
- [187] Hagen, T., Zhang, C.Y., Vianna, C.R., Lowell, B.B.: *Biochemistry* 39, 5845–5851 (2000)
- [188] Nedergaard, J., Cannon, B.: *Exp. Physiol.* 88, 65–84 (2003)
- [189] Duval, C., Nègre-Salvayre, A., Doglio, A., Salvayre, R., Pénicaud, L., Casteilla, L.: *Biochem. Cell Biol.* 80, 757–764 (2002)
- [190] Blanc, J., Alves-Guerra, M.C., Esposito, B., Rousset, S., Gourdy, P., Ricquier, D., Tedgui, A., Miroux, B., Mallat, Z.: *Circulation* 107, 388–390 (2003)
- [191] Mattiasson, G., Shamloo, M., Gido, G., Mathi, K., Tomasevic, G., Yi, S., Warden, C.H., Castilho, R.F., Melcher, T., Gonzalez-Zulueta, M., Nikolich, K., Wieloch, T.: *Nat. Med.* 9, 1062–1068 (2003)
- [192] Beck., V., Jabůrek, M., Breen, E.P., Porter, R.K., Ježek, P., Pohl, E.E.: *Biochim. Biophys. Acta* 1757, 474–479 (2006)
- [193] Jabůrek, M., Garlid, K.D.: *J. Biol. Chem.* 278, 25825–25831 (2003)
- [194] Forman, H.J., Fukuto, J.M., Miller, T., Zhang, H., Rinna, A., Levy, S.: *Arch. Biochem. Biophys.* 477, 183–195 (2008)
- [195] Brahimi-Horn, M., Pouysségur, J.: *FEBS Lett.* 581, 3582–3591 (2007)
- [196] Folkman, J., Hahnfeltdt, P., Hlatky, L.: *Nat. Rev. Mol. Cell Biol.* 1, 76–79 (2000)
- [197] Brooks, A.J., Eastwood, J., Beckingham, I.J., and Girling, K.J.: *Br. J. Anaesth.* 92, 735–737 (2004)
- [198] Towler, M.C., Hardie, D.G.: *Circ. Res.* 100, 328–341 (2007)
- [199] Taylor, C.T.: *Biochem. J.* 409, 19–26 (2008)
- [200] Jiang, B.H., Semenza, G.L., Bauer, C., Marti, H.H.: *Am. J. Physiol.* 271, C1172–C1180 (1996)
- [201] Lee., M., Hwang, J.T., Lee, H.J., Jung, S.N., Kang, I., Chi, S.G., Kim, S.S., Ha, J.: *Biol. Chem.* 278, 39653–39661 (2003)
- [202] Lu, H., Forbes, R.A., Verma, A.: *J. Biol. Chem.* 277, 23111–23115 (2002)
- [203] Kietzmann, T., Goerlach, A.: *Semin. Cell Dev. Biol.* 16, 474–486 (2005)

- [204] Semenza, G.L.: *Biochem. J.* 405, 1–9 (2007)
- [205] Ward, J.P.: *Biochim. Biophys. Acta* 1777, 1–14 (2008)
- [206] Gu, Y.Z., Moran, S.M., Hogenesch, J.B., Wartman, L., Bradfield, C.A.: *Gene Expr.* 7, 205–213 (1998)
- [207] Hu, C.J., Wang, L.Y., Chodosh, L.A., Keith, B., Simon, M.C.: *Mol. Cell. Biol.* 23, 9361–9374 (2003)
- [208] Tian, H., McKnight, S.L., Russel, D.W.: *Genes Dev.* 11, 72–82 (1997)
- [209] Wang, G.L., Semenza, G.L.: *J. Biol. Chem.* 270, 1230–1237 (1995)
- [210] Semenza, G.L., Nejfelt, M.K., Chi, S.M., Antonarakis, S.E.: *Proc. Natl. Acad. Sci. U.S.A.* 88, 5680–5684 (1991)
- [211] Semenza, G.L., Wang, G.L.: *Mol. Cell. Biol.* 12, 5447–5454 (1992)
- [212] Semenza, G.L., Roth, P.H., Fang, H.M., Wang, G.L.: *J. Biol. Chem.* 269, 23757–23763 (1994)
- [213] Sowter, H.M., Raval, R.R., Moore, J.W., Ratcliffe, P.J., Harris, A.L.: *Cancer Res.* 63, 6130–6134 (2003)
- [214] Talks, K.L., Turley, H., Gatter, K.C., Maxwell, P.H., Pugh, C.W., Ratcliffe, P.J., Harris, A.L.: *Am. J. Pathol.* 157, 411–421 (2000)
- [215] Wang, G.L., Jiang, B.H., Rue, E.A., Semenza, G.L.: *Proc. Natl. Acad. Sci. U.S.A.* 92, 5510–5514 (1995)
- [216] Ebert, B.L., Bunn, H.F.: *Mol. Cell. Biol.* 18, 4089–4096 (1998)
- [217] Dames, S.A., Martinez-Yamout, M., De Guzman, R.N., Dyson, H.J., Wright, P.E.: *Proc. Natl. Acad. Sci. U.S.A.* 99, 5271–5276 (2002)
- [218] Freedman, S.J., Sun, Z.Y., Poy, F., Kung, A.L., Livingston, D.M., Wagner, G., Eck, M.J.: *Proc. Natl. Acad. Sci. U.S.A.* 99, 5367–5372 (2002)
- [219] http://www.fibrogen.com/hif_biology
- [220] Feldser, D., Agani, F., Iyer, N.V., Pak, B., Ferreira, G., Semenza, G.L.: *Cancer Res.* 59, 3915–3918 (1999)
- [221] Krishnamachary, B., Berg-Dixon, S., Kelly, B., Agani, F., Feldser, D., Ferreira, G., Iyer, N., LaRusch, J., Pak, B., Taghavi, P., Semenza, G.L.: *Cancer Res.* 63, 1138–1143 (2003)
- [222] Ivan, M., Kondo, K., Yang, H., Kim, W., Valiando, J., Ohh, M., Salic, A., Asara, J.M., Lane, W.S., Kaelin, W.G. Jr.: *Science* 292, 464–468 (2001)

- [223] Jaakkola, P., Mole, D.R., Tian, Y.M., Wilson, M.I., Gielbert, J., Gaskell, S.J., von Kriegsheim, A., Hebestreit, H.F., Mukherji, M., Schofield, C.J., Maxwell, P.H., Pugh, C.W., Ratcliffe, P.J.: *Science* 292, 468–472 (2001)
- [224] Maxwell, P.H., Wiesener, M.S., Chang, G.W., Clifford, S.C., Vaux, E.C., Cockman, M.E., Wykoff, C.C., Pugh, C.W., Maher, E.R., Ratcliffe, P.J.: *Nature* 399, 271–275 (1999)
- [225] Bruick, R.K., McKnight, S.L.: *Science* 294, 1337–1340 (2001)
- [226] Epstein, A.C., Gleadle, J.M., McNeill, L.A., Hewitson, K.S., O'Rourke, J., Mole, D.R., Mukherji, M., Metzen, E., Wilson, M.I., Dhanda, A., Tian, Y.M., Masson, N., Hamilton, D.L., Jaakkola, P., Barstead, R., Hodgkin, J., Maxwell, P.H., Pugh, C.W., Schofield, C.J., Ratcliffe, P.J.: *Cell* 107, 43–54 (2001)
- [227] Ivan, M., Haberberger, T., Gervasi, D.C., Michelson, K.S., Günzler, V., Kondo, K., Yang, H., Sorokina, I., Conaway, R.C., Conaway, J.W., Kaelin, W.G. Jr.: *Proc. Natl. Acad. Sci. U.S.A.* 99, 13459–13464 (2002)
- [228] Schofield, C.J., Zhang, Z.: *Curr. Opin. Struct. Biol.* 9, 722–731 (1999)
- [229] Kondo, K., Klco, J., Nakamura, E., Lechpammer, M., Kaelin, W.G. Jr.: *Cancer Cell* 1, 237–246 (2002)
- [230] Maranchie, J.K., Vasselli, J.R., Riss, J., Bonifacino, J.S., Linehan, W.M., Klausner, R.D.: *Cancer Cell* 1, 247–255 (2002)
- [231] Bell, E.L., Klimova, T.A., Eisenbart, J., Moraes, C.T., Murphy, M.P., Budinger, G.R., Chandel, N.S.: *J. Cell Biol.* 177, 1029–1036 (2007)
- [232] Chandel, N.S., Maltepe, E., Goldwasser, E., Mathieu, C.E., Simon, M.C., Schumacker, P.T.: *Proc. Natl. Acad. Sci. U.S.A.* 95, 11715–11720 (1998)
- [233] Gerald, D., Berra, E., Frapart, Y.M., Chan, D.A., Giaccia, A.J., Mansuy, D., Pouyssegur, J., Yaniv, M., Mechta-Grigoriou, F.: *Cell* 118, 781–794 (2004)
- [234] Lando, D., Peet, D.J., Gorman, J.J., Whelan, D.A., Whitelaw, M.L., Bruick, R.K.: *Genes Dev.* 16, 1466–1471 (2002)
- [235] Lando, D., Peet, D.J., Whelan, D.A., Gorman, J.J., Whitelaw, M.L.: *Science* 295, 858–861 (2002)
- [236] Lisy, K., Peet, D.J.: *Cell Death Differ.* 15, 642–649 (2008)
- [237] Mahon, P.C., Hirota, K., Semenza, G.L.: *Genes Dev.* 15, 2675–2686 (2001)
- [238] Dalgard, C.L., Lu, H., Mohyeldin, A., Verma, A.: *Biochem. J.* 380, 419–424 (2004)

- [239] Lu, H., Dalgard, C.L., Mohyeldin, A., McFate, T., Tait, A.S., Verma, A.: *J. Biol. Chem.* 280, 41928–41939 (2005)
- [240] Isaacs, J.S., Jung, Y.J., Mole, D.R., Lee, S., Torres-Cabala, C., Chung, Y.L., Merino, M., Trepel, J., Zbar, B., Toro, J., Ratcliffe, P.J., Linehan, W.M., Neckers, L.: *Cancer Cell* 8, 143–153 (2005)
- [241] Selak, M.A., Armour, S.M., MacKenzie, E.D., Boulahbel, H., Watson, D.G., Mansfield, K.D., Pan, Y., Simon, M.C., Thompson, C.B., Gottlieb, E.: *Cancer Cell* 7, 77–85 (2005)
- [242] Carbia-Nagashima, A., Gerez, J., Perez-Castro, C.: *Cell* 131, 309–323 (2007)
- [243] Denko, N.C.: *Nat. Rev. Cancer* 8, 705–713 (2008)
- [244] Richard, D.E., Berra, E., Pouyssegur, J.: *J. Biochem.* 275, 26765–26771 (2000)
- [245] Zezler, E., Levy, Y., Kahana, C., Shilo, B.Z., Tubistcin, M., Cohen, B.: *EMBO J.* 17, 5085–5094 (1998)
- [246] Hagen, T., Taylor, C.T., Lam, F., Moncada, S.: *Science* 302, 1975–1978 (2003)
- [247] Semenza, G.L.: *Nat. Rev. Cancer* 3, 721–732 (2003)
- [248] Wenger, R.H., Stiehl, D.P., Camenish, G.: *Sci. STKE* 306, re12 (2005)
- [249] Iyer, N.V., Kotch, L.E., Agani, F., Leung, S.W., Laughner, E., Wenger, R.H., Gassmann, M., Gearhart, J.D., Lawler, A.M., Yu, A.Y., Semenza, G.L.: *Genes Dev.* 12, 149–162 (1998)
- [250] Seagroves, T.N., Ryan, H.E., Lu, H., Wouters, B.G., Knapp, M., Thibault, P., Laderoute, K., Johnson, R.S.: *Mol. Cell. Biol.* 21, 3436–3444 (2001)
- [251] Maxwell, P.H., Dachs, G.U., Gleadle, J.M., Nicholls, L.G., Harris, A.L., Stratford, I.J., Hankinson, O., Pugh, C.W., Ratcliffe, P.J.: *Proc. Natl. Acad. Sci. U.S.A.* 94, 8104–8109 (1997)
- [252] Kaluz, S., Kaluzová, M., Stanbridge, E.J.: *Clinica Chim Acta* 395, 6–13 (2008)
- [253] Ullah, M.S., Davies, A.J., Halestrap, A.P.: *J. Biol. Chem.* 281, 9030–9037 (2006)
- [254] Hogeboom, G.H., Schneider, W.C., Pallade, G.E.: *J. Biol. Chem.* 172, 619–635 (1948)
- [255] Smith, P.K., Krohn, R.I., Hermanson, G.T., Mallia, A.K., Gartner, F.H., Provenzano, M.D., Fujimoto, E.K., Goeke, N.M., Olson, B.J., Klenk, D.C.: *Anal. Biochem.* 150, 76–85 (1985)
- [256] Bogenhagen, D., Clayton, D.A.: *J. Biol. Chem.* 249, 7991–7995 (1974)
- [257] Reiss, O.K.: *J. Cell Biol.* 30, 45–57 (1966)

- [258] Zhou, M., Diwu, Z., Panchuk-Voloshina, N., Haugland, R.P.: *Anal. Biochem.* 253, 162–168 (1997)
- [259] Gyulkhandanyan, A.V., Pennefather, P.S.: *J. Neurochem.* 90, 405–421 (2004)
- [260] Gnaiger, E.: Polarographic Oxygen Sensors, the Oxygraph, and High-Resolution Respirometry to Assess Mitochondrial Function, in *Drug-Induced Mitochondrial Dysfunction*, (Dykens, J.A., Will, Y., ed.) John Wiley & Sons, Inc., pp. 327–352 (2008)
- [261] Hotta, Y., Ishikawa, N., Ohashi, N., Matsui, K.: *Mol. Cell. Biochem.* 219, 83–90 (2001)
- [262] Vunjak-Novakovic, G., Ian Freshney, R.: *Culture of Cells for Tissue Engineering*. John Wiley & Sons, Inc. (2006)
- [263] Ingledew, W.J., Ohnishi, T.: *Biochem. J.* 164, 617–620 (1977)
- [264] Ross, M.F., Prime, T.A., Abakumova, I., James, A.M., Porteous, C.M., Smith, R.A., Murphy, M.P.: *Biochem. J.* 411, 633–645 (2008)
- [265] Jekabsons, M.B., Echtay, K.S., Brand, M.D.: *Biochem. J.* 366, 565–571 (2002)
- [266] Mitchell, P., Moyle, J.: *Nature* 213, 137–139 (1967)
- [267] Yano, T., Dunham, W.R., Ohnishi, T.: *Biochemistry* 44, 1744–1754 (2005)
- [268] Garlid, K.D., Shariat-Madar, Z., Nath, S., Ježek, P.: *J. Biol. Chem.* 266, 6518–6523 (1991)
- [269] Sato, A., Nakada, K., Hayashi, J.: *Biochim. Biophys. Acta* 1763, 473–481 (2006)
- [270] Chan, D.C.: *Cell* 125, 1241–1252 (2006)
- [271] Brand, M.D., Esteves, T.C.: *Cell Metab.* 2, 85–93 (2005)
- [272] Sullivan, P.G., Springer, J.E., Hall, E.D., Scheff, S.W.: *J. Bioenerg. Biomembr.* 36, 353–356 (2004)
- [273] Antonenko, Y.N., Roginsky, V.A., Pashkovskaya, A.A., Rokitskaya, T.I., Kotova, E.A., Zaspá, A.A., Chernyak, B.V., Skulachev, V.P.: *J. Membr. Biol.* 222, 141–149 (2008)
- [274] Myasoedova, K.N.: *Biochemistry Mosc.* 73, 965–969 (2008)
- [275] Arruda, M.A., Barja-Fidalgo, C.: *Front. Biosci.* 14, 4546–4556 (2009)
- [276] Johnson, F., Giulivi, C.: *Mol. Aspects Med.* 26, 340–352 (2005)
- [277] Macchioni, L., Corazzi, L., Nardicchi, V., Mannucci, R., Arcuri, C., Porcellati, S., Sposini, T., Donato, R., Goracci, G.: *J. Biol. Chem.* 279, 37860–37869 (2004)

- [278] Ghosh, M., Loper, R., Gelb, M.H., Leslie, C.C.: *J. Biol. Chem.* 281, 16615–16624 (2006)
- [279] Seleznev, K., Zhao, C., Zhang, X.H., Song, K., Ma, Z.A.: *J. Biol. Chem.* 281, 22275–22288 (2006)
- [280] Brustovetsky, T., Antonsson, B., Jemmerson, R., Dubinski, J.M., Brustovetsky, N.: *J. Neurochem.* 94, 980–994 (2005)
- [281] Kinsey, G.R., Blum, J.L., Covington, M.D., Cummings, B.S., McHowat, J., Schnellmann, R.G.: *J. Lipid Res.* 49, 1477–1487 (2008)
- [282] Collins, P., Jones, C., Choudhury, S., Damelin, L., Hodgson, H.: *Liver Int.* 25, 880–887 (2005)
- [283] Parker, N., Vidal-Puig, A., Brand, M.D.: *Biosci. Rep.* 28, 83–88 (2008)
- [284] Echtay, K.S., Brand, M.D.: *Redox Rep.* 12, 26–29 (2007)
- [285] Echtay, K.S., Pakay, J.L., Esteves, T.C., Brand, M.D.: *Biofactors* 24, 119–130 (2005)
- [286] Dwivedi, S., Sharma, A., Patrick, B., Sharma, R., Awasthi, Y.C.: *Redox Rep.* 12, 4–10 (2007)
- [287] Dianzani, M.U.: *Mol. Aspects Med.* 24, 263–272 (2003)
- [288] Esterbauer, H., Schaur, R.J., Zollner, H.: *Free Radic. Biol. Med.* 11, 81–128 (1991)
- [289] Catalá, A.: *Chem. Phys. Lipids* 157, 1–11 (2009)
- [290] Nubel, T., Ricquier, D.: *Horm. Res.* 65, 300–310 (2006)
- [291] Mattiasson, G., Sullivan, P.G.: *Antioxid. Redox Signal.* 8, 1–38 (2006)
- [292] Gilbert, D.L.: *Physiologist* 39, 9–34 (1965)
- [293] Gilbert, D.L., Colton, C.A.: *Reactive Oxygen Species in Biological Systems* (Gilbert, D.L, Colton, C.A., ed.), Kluwer Academic/Plenum Publishers, New York, U.S.A. (1999)
- [294] Iuchi, S., Weiner, L.: *J. Biochem.* 120, 1055–1063 (1996)
- [295] Cohen, P.J.: *Int. Anesthesiol. Clin.* 19, 9–19 (1981)
- [296] Chandel, N.S., Budinger, G.R., Choe, S.H., Schumacker, P.T.: *J. Biol. Chem.* 272, 18808–18816 (1997)
- [297] Bellance, N., Lestienne, P., Rossignol, R.: *Front. Biosci.* 14, 4015–4034 (2009)
- [298] Warburg, O.: *Metabolism of Tumors*, Arnold Constable Ltd., London (1930)
- [299] Moreno-Sánchez, R., Rodríguez-Enríquez, S., Marín-Hernández, A., Saavedra, E.: *FEBS J.* 274, 1393–1418 (2007)

- [300] Zu, X.L., Guppy, M.: *Biochem. Biophys. Res. Commun.* 313, 459–465 (2004)
- [301] Christofk, H.R., Vander Heiden, M.G., Harris, M.H., Ramanathan, A., Gerszten, R.E., Wei, R., Fleming, M.D., Schreiber, S.L., Cantley, L.C.: *Nature* 452, 230–233 (2008)
- [302] Plecítá-Hlavatá, L., Lessard, M., Šantorová, J., Bewersdorf, J., Ježek, P.: *Biochim. Biophys. Acta* 1777, 834–846 (2008)